TU Clausthal

Clausthal University of Technology

CONTROL OF FRICTION-INDUCED TORSIONAL VIBRATIONS IN DRILLING

Doctoral Thesis

to be awarded the degree
Doctor of Engineering (Dr.-Ing.)

Submitted by
Farooq Kifayat Ullah
from Dir, Munjai
Approved by the
Faculty of Mathematics/Computer Science
and Mechanical Engineering
Clausthal University of Technology

Date of oral examination: 21.02.2019

DEAN: Prof. Dr.-Ing. Volker Wesling
SUPERVISOR: Prof. Dr.-Ing. Christian Bohn
REVIEWER: Prof. Dr.-Ing. Christian Rembe

Dedicated to the loving memory of Engr. Kifayatullah Amirzada.
1946 – 1998

ABSTRACT

The thesis deals with the control of torsional oscillations in drill strings. Self excited torsional oscillations occur due to friction and complex coupling between the torsional, axial and lateral drill string dynamics. The focus of this work is on the control of friction-induced torsional oscillations in the drill string. In this work the torsional oscillations caused by the Stribeck effect of friction are studied using an experimental setup that is designed and built for the purpose. The experimental setup is a scaled model of a 150m long drill string bottom hole assembly. A nonlinear finite dimensional two degree of freedom model is used to mathematically model and simulate the drill string. The system identification of the experimental drill string setup is undertaken using the trust region reflective nonlinear least square algorithm. Extensive validations of the model using the estimated parameters are performed. It is observed that the identified model reproduces the measured response with some error. The variable nature of friction makes exact system identification unlikely. To overcome this adaptive and robust backstepping control algorithms are devised for the drill string torsional oscillation control. Furthermore, to be able to implement the control algorithms in the experimental setup where all the states are not available for feedback, observer based nonlinear controllers have been developed. A tuning function based adaptive observer backstepping control algorithm is first evaluated but is not robust to the measurement noise therefore a robust nonlinear observer based control algorithm known as dynamic surface control is devised. The closed loop stability of the dynamic surface control algorithm and designed observer is proven. The combination of the dynamic surface control with the observer used is to the best of the author's knowledge novel contribution to the drill string control literature. The dynamic surface control was successful in attenuating torsional oscillations due to stick slip in the experimental setup and also avoids exciting higher frequency vibrations in the setup.

ACKNOWLEDGEMENTS

First of all thanks be to Allah. I would like to thank my mother Naheed Kifayat Ullah for encouraging and supporting me through out my education and life. I would also like to acknowledge the support of my brothers Jameel, Majid and sister Amna for their support.

Special thanks to my wife Asma for her understanding and support during very difficult times in Clausthal.

This work would not have been possible with out support and guidance of my supervisor Christian Bohn and mentor Franklyn Duarte. I would also like to mension the support of Professor Joachim Oppelt especially during final stages of the PhD. I would also like to thank Professor Christian Rembe for agreeing to be my second examiner.

I would like to thank the DAAD and Higher education commission (HEC) Pakistan for financially supporting me through the UESTP DAAD scholarship. My experience in Germany was enriched due to the friends I met during the DAAD language program at the Goethe Institute Göttingen.

CONTENTS

LIST OF FIGURES

LIST OF TABLES

LISTINGS

CLF	Control Lyapunov function
DB	Drill bit
DSC	Dynamic surface control
FFT	Fast fourier transform
RPM	Revolutions per minute
TD	Top drive
PI	Proportional Integral
PID	Proportional Integral Derivative
LFTO	Low frequency torsional oscillations
HFTO	High frequency torsional oscillations
MSS	Multiple sliding surface
MWD	Measurement while drilling
PSD	Power spectral density

α	A positive constant	-
$\alpha(.)$	A positive definite scalar function. constant	-
$\alpha_1(x_1, z_1)$	Virtual function	-
$\alpha_2(x_1, x_2, z_1, z_2)$	Virtual function	-
$\boldsymbol{A}_0$	Observer error system matrix (dimension 3 by 3)	-
b_1	Constant parameter of the friction model	-
c_1	Tuning constant	-
c_2	Tuning constant	-
c_3	Tuning constant	-
c_r	Viscous damping constant top drive	$\mathrm{Nm/rads}^{-1}$
c_b	Viscous damping constant drill bit	$\mathrm{Nm/rads}^{-1}$
d_1	A positive constant used for controller tuning	-
d_2	A positive constant used for controller tuning	-
δ	A positive constant	-
Δf_1	Function that represents uncertainty	-

ϵ	A positive constant	-
η_2	Filter error in Chapter 6	-
η_3	Filter error in Chapter 6	-
$\boldsymbol{\epsilon}$	Vector of obserever errors	-
$f(x)$	Nonlinear function	-
$g(x)$	Nonlinear function	-
γ_b	Constant coefficient that determines slope of Stribeck curve	-
γ_1	Adaptation gain	-
G	Shear modulus	$\mathrm{kgm^{-1}s^{-2}}$
I	Area moment of inertia	$\mathrm{m^4}$
J_1	Moment of inertia top drive	$\mathrm{kgm^2}$
J_2	Moment of inertia drill bit	$\mathrm{kgm^2}$
k_t	Drill string stiffness	Nm/rad
μ_cb	Coefficient of coulomb friction	-
μ_sb	Coefficient of static friction	-
p_1	A parameter	-
p_2	A parameter	-
p_3	A parameter	-
$\boldsymbol{\phi}(y)$	A column vector of nonlinear functions (dimension 3 by 1)	-
ϕ_1	A nonlinear functions	-
ϕ_2	A nonlinear functions	-
$\boldsymbol{P}_0$	Positive definite matrix (dimension 3 by 3)	-
$\boldsymbol{\phi}(x_1)$	Vector of nonlinear functions of x_1	-
R_b	Radius of bit	m
ρ_1	Known nonlinear function	
S_1	Error variable known as sliding surface	-
S_2	Error variable known as sliding surface	-
S_3	Error variable known as sliding surface	-

T_{fu}	Friction torque at top drive	Nm
T_{fb}	Friction drill bit	Nm
T_{m}	Input torque	Nm
θ_1	Top drive angular displacement	rad
θ_2	Drill bit angular displacement	rad
$\boldsymbol{\theta}_{\mathrm{p}}$	Drill string parameter vector (dimension 3 by 1)	-
$\boldsymbol{\theta}$	Regression parameter vector (dimension p by 1)	-
τ_1	Filter time constant in Chapter 6	-
τ_2	Filter time constant in Chapter 6	-
u	Input variable	-
$V(\boldsymbol{x}, t)$	Lyapunov function	-
W_{ob}	Weight on bit	N
ω_{d}	Desired Velocity	rads^{-1}
x_1	Drill bit speed	rads^{-1}
x_2	Angular displacement between top and bottom of drill string	rad
x_3	Top drive speed	rads^{-1}
$\hat{x}_2$	Estimated value of x_2	rad
$\tilde{x}_2$	Error in the estimated value of x_2	rad
$\boldsymbol{x}$	State space vector (dimension 3 by 1)	-
ξ	Function that is used to represent virtual control input	-
$\boldsymbol{\xi}_0$	State vector of filter states	-
ξ_{01}	State variable of filter	-
ξ_{02}	State variable of filter	-
ξ_{03}	State variable of filter	-
$\boldsymbol{\xi}_1$	State vector of filter states	-
ξ_{11}	State variable of filter	-
ξ_{12}	State variable of filter	-
ξ_{13}	State variable of filter	-
z_1	Error variable	-
z_2	Error variable	-
z_3	Error variable	-

Part I

PRELIMINARIES AND MOTIVATION

The thesis has been divided in to two parts. The first part introduces the problem of torsional oscillations in drill strings. In this part the relevant literature regarding control and modelling approaches is first reviewed. The experimental setup designed to evaluate control algorithms is also described in this part of the thesis.

1 INTRODUCTION

Torsional oscillations are a common problem in rotating systems such as turbines for electricity generation, roller mills for steel, windmills and rotary drilling. In drill strings torsional oscillations were first experimentally studied by Finnie and Bailey (1960) . Crude oil or gas is a necessary raw material in chemical industries, fertilizers, plastics and for energy production. It is a finite resource formed naturally as a result of geological and biological processes taking place over a span of millions of years. As a finite resource its production was predicted to peak and then decline as explained by "Hubert Theory" (Brandt 2007), but improvement in extraction technologies have enabled access to petroleum resources that were previously inaccessible thus delaying the production decline. The petroleum industry has brought the cost of discovery and production down, partly by increasing automation. The driller has two main goals:

1. Maximize the rate of penetration (ROP) to complete the drilling process as quickly as possible to reduce costs.
2. Operate the drill string in a region where the vibrations are minimum.

To better understand the problems and challenges in mitigating drill string vibrations in the proceeding sections the drilling system is described, different types of vibrations of the drill string are described and contribution of this thesis towards this purpose is described.

1.1 DRILL STRING

Drill string refers to part of the drill rig that transfers torque, mud and cuttings from surface to the bottom drill bit. The drill rig shown in Figure 1 consists of the the following main components:

1. The top drive usually consists of an electric motor, for example, three phase synchronous motor, gearing and the rotary table.
2. The Kelly is a polygonal tubing that connects the drill string to the rotary table and allows vertical movement of the drill string.
3. The drill pipe is made of 9m long steel pipes and can have different diameters and thickness. Sections of drill pipes are screwed together to form the main body of the drill string.
4. The bottom hole assembly (BHA) is the lower part of the drill string that consists of heavy pipes called drill collars, stabilizers, data logging sensors, rotary

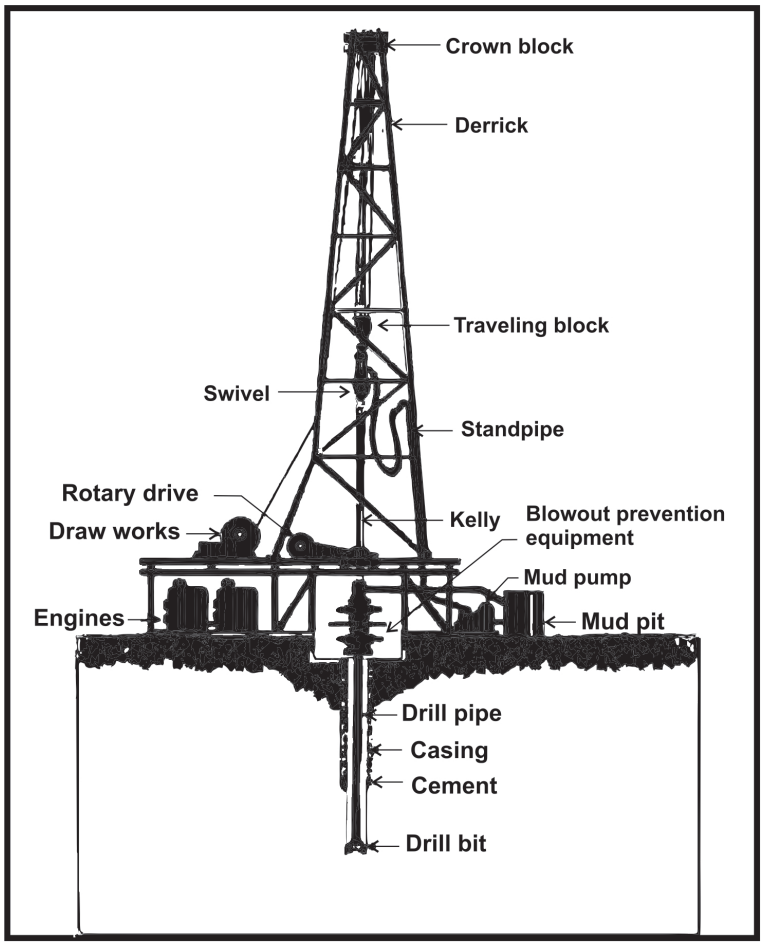

Figure 1: Drill string illustration modified from Kamooly (2012).

steerable tools and the drill bit. This section of the drill string is under compression and applies weight to the drill bit. The BHA is designed such that the drill pipe connecting it at the upper end experiences no compression, i.e. zero axial load or small tension. The point along the BHA at which the axial load is zero is called the neutral point (Spanos et al. 2003).

5. The drill collar is a section of thick heavy pipes used in the BHA.

6. A drill string will normally have three stabilizers to keep the drill string concentric in the bore hole, to avoid BHA bending and buckling and the stabilizers also prevent the drill from drilling a parallel bore hole besides the original bore hole which is a phenomenon known as side tracking.

7. The drill bit cuts the formation. Based on cutting mechanism there are two types of drill bits:
   a) Roller cutter bits that work by crushing the formation.
   b) Fixed cutter bits which are mostly polycrystalline diamond cutter (PDC) bits that work by scraping the formation. The PDC bits provide a higher

rate of penetration but are rapidly damaged when they encounter hard formations.

8. A mud pump circulates drilling mud to lubricate and cool the drill bit. It also transfers the cuttings from down hole to the surface and the hydrostatic pressure of the drilling mud stabilizes the bore hole (Spanos et al. 2003).

9. Some drill strings can be equipped with down hole mud motors that increase the angular speed of the drill bit and provide an increased rate of penetration.

1.2 VIBRATIONS OF THE DRILL STRING

The exploratory well may be several kilometers deep and the outer diameter of the drill string ranges from 3.5 to 6.625in (Jansen and Steen 1995). The drill string structure therefore has low stiffness. Therefore it is prone to vibrations. The main types of vibration and their causes are given below.

1.2.1 *Torsional Vibrations:*

A major problem when drilling wells is the failure of the drill string or the drill bit. These failures are costly and time consuming. One of the major reasons for these failures is self excited torsional oscillation of the drill string. Furthermore, torsional oscillations also reduce the rate of penetration (ROP). Therefore attenuating torsional oscillations in drill strings has attracted much interest from the research community.

Torsional vibrations can be of two types namely torsional oscillations caused by stick slip and high frequency torsional oscillations. Both types of vibrations are described in sections given below.

1.2.1.1 *Torsional oscillations due to stick slip*

Torsional oscillations are imposed on the drill string due to the stick-slip phenomenon caused by friction, such vibrations have a frequency between 0.1 and 5Hz. During limit cycles caused by friction the bit is stuck, this causes the friction forces at the bit rock interface to build up. When the friction force becomes greater than the sticktion force the drill bit slips and the stored energy is released. During stick slip the bit may accelerate and reach angular speeds several orders of magnitude larger than the top drive angular velocity .

Leine (1997) documents efforts that measured data from drill strings using special down hole sensors during four decades ranging from 1960's to 1990's in a chronological order. The common thread in these efforts was the observation of low frequency torsional oscillations that are more likely to occur at lower bit speeds than at higher bit speeds. They depend on the type of drill bit used and its mode of operation which can be either crushing or shearing. The torsional oscillations decrease the rate

of penetration and cause wear of drill string. Data from field measurements show that there is a decrease in the torque on bit with increasing bit velocity. According to Leine (1997), the first realization that the possible cause of torsional oscillations was stick-slip due to friction was in Belokobyl'skii and Prokopov (1982).

1.2.1.2 *High Frequency Torsional Oscillations*

Recently development of better downhole recording tools that can measure at a higher sampling frequency have lead to the discovery of high frequency torsional oscillations (HFTO) not related to stick slip. These vibrations are due to torsional resonance of the bottom hole assembly. Warren and Oster (1998) first reported PDC bit damage due to torsional resonance of drill collars by analyzing down hole data from 19 wells. By analyzing data from measurement while drilling instruments, Oueslati et al. (2013) found higher levels of down hole high frequency vibrations particularly when a mud motor is used in the BHA. Oueslati et al. (2013) also studied the effect of changing drilling parameters on HFTO and concluded that in order to avoid the HFTO the drill either has to be operated with low weight on bit which decreases the rate of penetration or the drill string has to be operated at high RPM which will excite other forms of vibrations, such as, backward whirl. Therefore it is unpractical to mitigate the HFTO by changing operating parameters such as WOB and RPM alone.

The HFTO are confined to the bottom hole assembly because they are attenuated before reaching the top end of the drill string. Therefore high frequency torsional oscillations are hard to detect using surface measurements.

Jain et al. (2014) used data from down hole measuring devices to analyze the drill string torsional vibrations and concluded that the HFTO do not damage the bit. But (Zhang et al. 2017) studied the effect of HFTO on the BHA in shale formations and found that the HFTO cause fatigue cracks in drill collars of the BHA. Chen et al. (2006) report that HFTO also cause rotary steerable component failure in directional drilling.

It becomes clear that although the high frequency torsional oscillations are localized to the BHA but since the BHA consists of the relatively more expensive components that constitute the drill string therefore high frequency torsional oscillations cannot be ignored. In the next section the lateral drill string vibrations are briefly described.

1.2.2 *Lateral Vibrations*

Vibrations of the drill string perpendicular to the axis of rotation can occur as the drill string behaves as a beam. Lateral vibrations in rotational dynamic systems are caused by mass imbalance. In drill strings the phenomenon is complicated, but factors that contribute to lateral vibrations include the mass imbalance of the drill collars, con-

tact of the drill string with the bore hole, stabilizer friction and nonlinear influence of the drilling fluid (Jansen 1991). Two related phenomenon of forward whirl and backward whirl also occur along with lateral vibrations. Forward whirl is caused by mass imbalance of the drill string. During forward whirl the axis of rotation of the drill string rotates in the direction of rotation. During Backward whirl the axis of rotation of the drill string rotates in opposite direction of the drill string rotation. Forward whirl is caused by stabilizer friction (Jansen 1991; Brett, Warren, and Behr 1989).

1.2.3 *Axial Vibrations*

The drill string undergoes high frequency axial vibrations that may cause bit bounce. This is a condition in which the drill bit looses contact with the ground. Axial vibrations occur more frequently in roller cone bits. Current thinking also attributes the reduction of bit torque with increasing speed to the complex coupling between axial and torsional vibrations (Richard, Germay and Detournay 2007).

1.3 STATE OF THE ART IN CONTROL OF DRILL STRING TORSIONAL OSCILLATIONS

Attenuating torsional oscillations in drill strings has attracted much interest from the research community. One objective is to extend the operational range of speeds at which the drill bit can be rotated without inducing limit cycles caused by the stick slip. The second aim is to design robust control systems that may not require extensive on site tuning for different drill string setups and also not require tuning due to change in drilling conditions (Runia, Dwars, and Stulemeijer 2013). Torsional oscillations of a drill string can be controlled either by active or passive measures but only active control methods are discussed here because the focus is limited to active control. Dong and Chen (2016) have reviewed literature that utilize passive control for drill strings. The literature review below is organized on the basis of type of control approach used. A chronologically organized literature review can be found in Table 1 on page 12.

LINEAR CONTROL: Most of the controllers that have been tested in full scale drill rigs and are currently used to control torsional oscillations are linear controllers. Therefore the research on linear control of drill string torsional oscillations is reviewed first.

Jansen and Steen (1995) used a 2 degree of freedom (DOF) lumped parameter model of the drill string and controlled the flow of energy in the top drive motor in such a way that it behaves like an active tuned vibration damper with band-pass characteristics. It reduces the angular velocity threshold of oscillation free operation.

The soft torque rotary (STR) controller developed by Shell is the predominant controller used in real drilling setups but it is effective in attenuating the first torsional oscillation mode and has to be expertly tuned for each drilling rig where it is employed (Runia, Dwars and Stulemeijer 2013).

Nessjoen et al. (2011) describe a tuned PI controller, developed by National-Oilwell Varco, that is based on modelling the drill string as a transmission line for torsional waves. The controller is tested in the field and is comercially available as a controller named SoftSpeed (Shor, Pryor, and Van Oort 2014).

One of the early active control strategies involved modelling the drill string as a transmission line for torsional waves using a simple pendulum model. Torque feedback and impedance matching are used to dampen the torsional oscillations in the drill string (Halsey, Kyllingstad and Kylling 1988).

Serrarens et al. (1998) developed and evaluated a robust H_∞-controller to attenuate the torsional oscillations in a scaled experimental setup. Vromen (2015) reports modelling an offshore drill rig deeper than 6000m using an 18 degree of freedom (DOF) finite element model which is reduced using model reduction techniques to a 4 DOF model hence a 4 DOF scaled drill rig is used to analyze controller robustness with respect to multiple modes of torsional oscillations. Soft torque controller and full state feedback H_∞ control are evaluated. The H_∞ controller was able to better attenuate stick slip torsional oscillations but with a small steady state velocity error as compared to the soft torque controller.

Karkoub et al. (2010) developed a robust μ-synthesis approach. The approach was simulated and simulations were robust to model uncertainty and noise.

Harris, Açıkmese, and Oort (2014) developed an linear matrix inequality (LMI) based disturbance rejection controller to attenuate the torsional oscillations in the drill string and simulation results showed good performance.

Pehlivantürk, Chen and Oort (2017) developed a sophisticated 35 DOF experimental drill rig to evaluate performance of proportional integral (PI) control that utilizes downhole feedback.

NONLINEAR CONTROL: Apart from linear control solutions a large body of work seeks to expand the operational working region by using nonlinear control methods. Nonlinear control methods allow the use of not only torque but also weight on bit as the manipulated control variables.

D-OSKIL: Canudas-de-Wit et al. (2005) designed a nonlinear controller that uses the WOB to attenuate the torsional oscillations of the drill string. It is named drilling oscillation killer mechanism (D-OSKIL). A separate control loop to control the angu-

lar velocity of top drive in conjunction with a band pass filter that isolates the oscillations which are then controlled by nonlinearly varying the WoB within a range of values. Stability is analyzed based on passivity. The controller was experimentally tested and attenuated torsional oscillations in an experimental drill string setup (Lu, Dumon and Wit 2009).

SLIDING MODE CONTROL: Work on full state feedback sliding mode controllers that may provide guidance to drill rig operators on optimal values of control inputs has been undertaken in Navarro-López and Licéaga-Castro (2009). Where the sliding mode apprach is used to provide drilling guidance. A discontinuous friction model with stribeck effect is considered. Recently the above full state feedback sliding mode control approach has been extended by Liu (2014) where enhanced robustness to weight on bit, in simulations is reported. Ghasemi and Song (2017) developed a sliding mode control approach assuming full state feedback for a multi degree of freedom (MDOF) drill string model where the velocity weakening is modelled using coupling between axial and torsional dynamics via bit rock interface (Germay et al. 2009) with good simulation results. A full state feedback sliding mode approach has been evaluated on an experimental setup by Vaziri, Kapitaniak, and Wiercigroch (2018). The control approach was successful in attenuating the torsional oscillations of the drill string experimental setup.

BACKSTEPPING BASED CONTROL: Work on nonlinear backstepping approach for drill string torsional oscillation attenuation that uses a lumped parameter model is described in (Abdulgalil and Siguerdidjane 2005), the backstepping approach uses one of the states as a virtual control function. In Kabziński (2017) an adaptive backstepping approach called adaptive command filtered backstepping is proposed and simulations show reduction in torsional oscillations and a better transient response as compared to previous work in Ullah, Duarte and Bohn (2016a). The backstepping control approaches have not been tested experimentally in laboratory or the field. In this thesis a backstepping based nonlinear control approach is validated experimentally.

DISCONTIUOUS CONTROL FOR SYSTEM MODELLED AS DIFFERENTIAL INCLUSIONS: In De Bruin et al. (2009) and Doris (2007) friction at bit is modelled using a set valued law and for the drill string modelled as a differential inclusion. A Popov-like criterion is utilized for output feedback control. The control approach is tested in simulations and on an experimental setup.

HYBRID CONTROL: Navarro-López and Carter (2011) interprets the discontinuous dynamic system as a hybrid automation problem and proposes a hybrid control method. Due to complexities of drilling the approach is presented as a way to give guidance to drillers on parameter selection for drilling so as to avoid torsional oscillations.

ADAPTIVE CONTROL STRATEGIES: Pavković, Deur, and Lisac (2011) use a 2 DOF model of the drill string to devise a PI controller that uses estimated torque feedback. An auto tuning procedure based on the Kalman filter is also devised and the controller is tested in a real drilling rig where it proved effective in damping the dominant torsional oscillation but was in some cases sensitive to modelling errors. Bu and Dykstra (2014) uses indirect adaptive swapping based backsteping control to control the stick slip. Majeed et al. (2013) use model identification to identify a Box-Jenkins model for a laboratory drill string setup and devise an adaptive controller.

CONTROL OF DRILLSTRING MODELLED USING PARTIAL DIFFERENTIAL EQUATIONS: Infinite dimensional models that better capture drill string dynamics described using one dimensional wave equations with negatively damped boundary condition at drill bit and Neumann actuation at top drive have been utilized in Bresch-Pietri and Krstic (2014). Bresch-Pietri and Krstic (2014) transform the wave equations in to a cascade of two transport equations with one ODE that represents the drill bit dynamics. A predictor based adaptive control law is devised. Bekiaris-Liberis and Krstic (2013) devise a method to stabilize a PDE-ODE cascade system, for the ODE a state feedback control law should be known. Similarly control approaches based on neutral type retarded models have also been developed in Saldivar et al. (2011).

1.4 CONTRIBUTION

The main contribution is to evaluate nonlinear control for attenuation of torsional oscillations in drill string. Most of the literature on nonlinear control applied to torsional oscillation attenuation is limited to simulation studies and considers full state feedback control. This thesis attempts to close this gap in the literature.

1. A drill string experimental setup is designed and built to evaluate control algorithms. Previous parameter estimation approaches used nonlinear least squares approach using position data from top drive and drill bit. The nonlinear least squares parameter estimation used in this work uses only angular velocity data from the drill bit and input torque, to estimate the parameters of the experimental setup.

2. Since only top velocity and bit velocity is measured an observer is designed to obtain the unmeasured state. Furthermore, as the separation principle is not valid in nonlinear control the closed loop stability is ensured and observer error is considered in controller stability analysis.

3. Observer based output feedback nonlinear controllers are designed. Full state feedback backstepping control, adaptive tuning function based backstepping control and finally a robust dynamic surface controller are designed and evaluated on the experimental drill string setup. Experimental evaluation of nonlinear controllers helps test assumptions that are made during design and reveals

weakness of the assumptions. Validity of assumptions related to friction could not be evaluated in simulation based studies. As in practice the mathematical model used for control design will suffer from modelling errors and the measured outputs have noise.

4. Measurements on the experimental setup indicate that stiff speed control causes high frequency torsional oscillations that can be attenuated using the dynamic surface control.

1.5 ORGANIZATION OF THIS THESIS

In the next chapter modelling of the drill string torsional dynamics is discussed. In chapter 3 the experimental setup built to validate control algorithms is described and parameter identification is discussed. In chapter 4 the backstepping control is introduced and its application to a drill string is presented. In chapter 5 adaptive observer based backstepping algorithms are evaluated for application in the drill string. Chapter 6 presents a robust observer based dynamic surface control algorithm that is evaluated using the experimental setup. A summary and prospects for possible future research are presented in chapter 7.

Table 1: Literature on active control of torsional oscillations.

AUTHOR	CONTROL METHOD	APPLICATION
Halsey, Kyllingstad, and Kylling (1988)	Linear PI control, transmission line model.	Field tests.
Jansen and Steen (1995)	Linear control, tuned active vibration damper using lumped element model.	Field tests.
Serrarens et al. (1998)	Linear H_∞ control using lumped element model.	Scaled experimental setup.
Abdulgalil and Siguerdidjane (2005)	Backstepping control using a lumped element model.	Simulations.
Canudas-de-Wit et al. (2005)	Nonlinear control using passive stabilization.	Simulations.
Doris (2007)	Nonlinear control using a Popov-like criterion, system modelled as a differential inclusion.	Scaled experimental setup.
Lu, Dumon and Wit (2009)	Nonlinear control using passive stabilization.	Scaled experimental setup.
Navarro-López and Licéaga-Castro (2009)	Nonlinear sliding mode control.	Simulations.
De Bruin et al. (2009)	Nonlinear control using a Popov-like criterion, system modelled as a differential inclusion.	Scaled experimental setup.
Karkoub et al. (2010)	Linear μ-synthesis approach using lumped element model.	Simulations.
Nessjoen et al. (2011)	Linear PI control, transmission line model used.	Field tests.
Navarro-López and Carter (2011)	Sliding mode control using hybrid model.	Simulations.
Pavković, Deur, and Lisac (2011)	Linear PI control incorporating Kalman filter for torque estimation, lumped model used.	Field tests.

Table continued on next page

AUTHOR	CONTROL METHOD	APPLICATION
Saldivar et al. (2011)	Linear infinite dimensional control, using single dimensional wave equation model.	Simulations.
Majeed et al. (2013)	Adaptive control using Box-Jenkins model.	Scaled experimental setup.
Bekiaris-Liberis and Krstic (2013)	Linear infinite dimensional backstepping, using single dimensional wave equation model.	Analytic study.
Bresch-Pietri and Krstic (2014)	Adaptive backstepping control, using single dimensional wave equation model.	Simulations.
Liu (2014)	Nonlinear sliding mode control, using lumped element models.	Simulations.
Harris, Açıkmese, and Oort (2014)	LMI based disturbance rejection control, using lumped element model.	Simulations.
Bu and Dykstra (2014)	Indirect adaptive backstepping control, using lumped element model.	Simulations.
Vromen (2015)	Linear H_∞ control and soft torque control.	Scaled experimental setup.
Ullah, Duarte and Bohn (2016a)	Robust backstepping control, using lumped element model.	Simulations.
Kabziński (2017)	Adaptive control using command filtered backstepping.	Simulations.
Pehlivantürk, Chen and Oort (2017)	Linear PI control.	Scaled experimental setup.
Ghasemi and Song (2017)	Nonlinear sliding mode control, coupled torsional and axial lumped element model used.	Simulations.
Vaziri, Kapitaniak, and Wiercigroch (2018)	Nonlinear sliding mode control, 2 DOF model.	Scaled experimental setup.

2

CONTROL ORIENTED MODELLING OF TORSIONAL DRILL STRING DYNAMICS

Root causes of torsional oscillations in drill strings are phenomena that occur at the drill bit and rock interface. Two plausible explanations found in drilling literature are drill bit friction particularly the Stribeck effect and the alternative explanation is the coupling between the axial and torsional dynamics of the drill string that lead to a stribeck-like effect, i.e weakening of torque on bit as bit speed increases. The drill string is usually modelled using lumped parameter models or distributed parameter models. Figure 2 shows a block diagram that classifies the mathematical models that are commonly used in the literature oriented towards torsional oscillation control. In the present work a finite dimensional two degree of freedom model with the friction modelled using a static continuous friction law is used. This chapter describes the model used and also other approaches to modelling torsional dynamics of the drill string.

In the first section the finite dimensional torsional dynamic models are described. The second section, describes alternative drill string torsional dynamic models. The third section, describes the distributed parameter models. In the last section challenges that have to be overcome to control the torsional oscillations in a drill string are described.

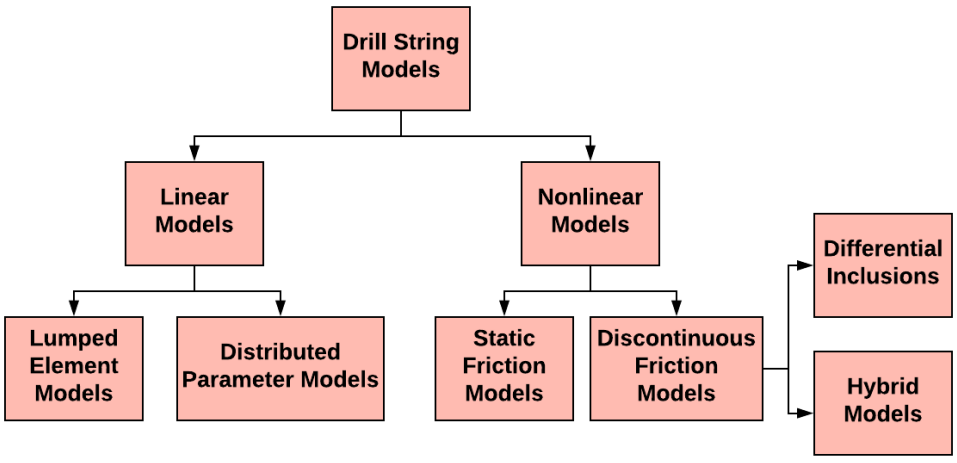

Figure 2: Drill string models.

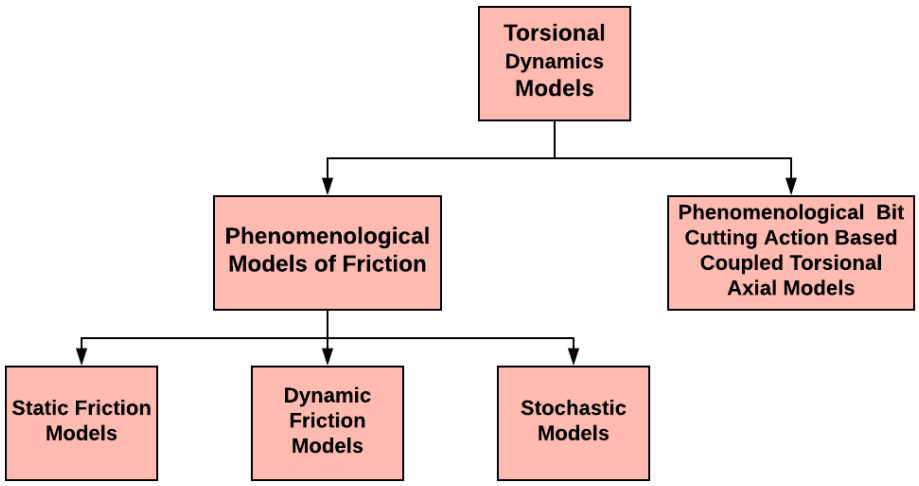

Figure 3: Models that explain torsional oscillations and stick slip.

2.1 LUMPED ELEMENT MODELS

Lumped dashpot models are often used to model the drill string. In most of the control oriented literature the drill string is modelled as a finite dimensional system where at least one and at the most four degrees of freedom are considered. The drill string model is expressed as a system of ordinary differential equations. The difference between various lumped parameter drill string models stems from how friction at drill bit is modelled. Figure 3 classifies torsional dynamic models according to the way friction is modelled. The system shown in Figure 4a can be represented by

$$\boldsymbol{J}\ddot{\boldsymbol{\theta}} + \boldsymbol{C}\dot{\boldsymbol{\theta}} + \boldsymbol{K}\boldsymbol{\theta} + \boldsymbol{f}(\dot{\boldsymbol{\theta}}) = \boldsymbol{u}, \tag{2.1}$$

where $\boldsymbol{J} \in \mathbb{R}^M$ is the inertia matrix, $\boldsymbol{\theta} \in \mathbb{R}^M$ is the angular displacement vector, $\boldsymbol{C} \in \mathbb{R}^{M\times M}$ is the damping matrix, $\boldsymbol{K} \in \mathbb{R}^{M\times M}$ is the stifness matrix, $\boldsymbol{f}(\dot{\boldsymbol{\theta}}) : \mathbb{R}^M \to \mathbb{R}^M$ is the friction torque vector function and $\boldsymbol{u} \in \mathbb{R}^M$ is the input torque vector. The lumped element model assumes that the drill string is perfectly vertical, ignores the lateral bit motion, viscous damping represents the effect of drilling mud and mud flow is not turbulent (Navarro-López and Suárez 2004).

The most prevalent finite dimensional lumped element model is the 2 DOF model. The 2 DOF model has been used in this work to model the experimental setup therefore it is explained in detail in the following section.

2.1.1 *Two degree of freedom model*

In most of experimental work the drill string is modeled using a lumped parameter model shown in Figure 4b having 2 DOF. Such low order models offer physical

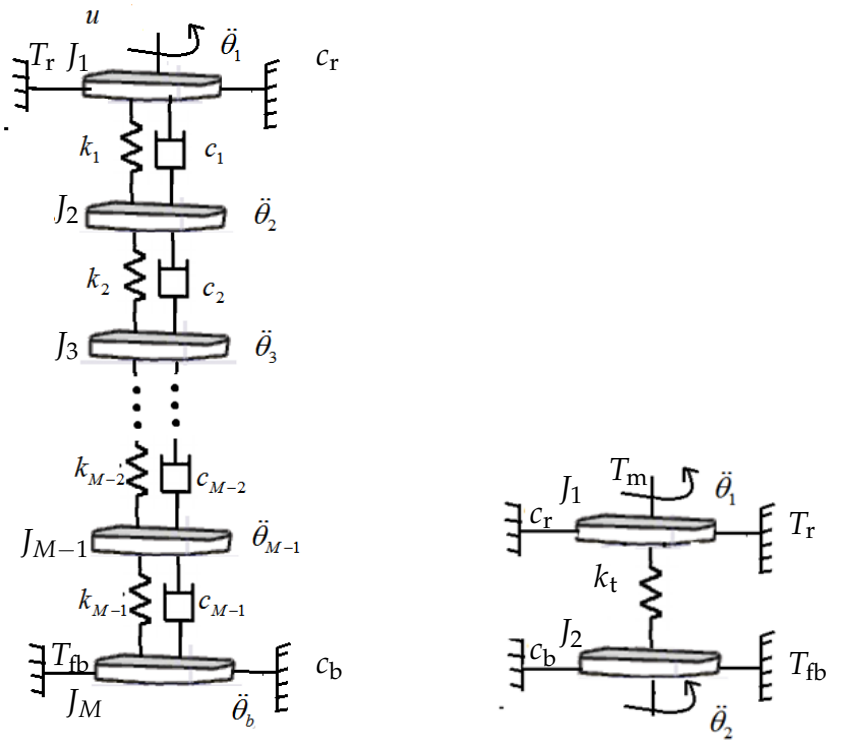

(a) MDOF model.

(b) Two Degree of freedom model which neglects drill string damping.

Figure 4: Lumped Drill string models.

insight and reduce the complexity of controler, observer design and have been used in field tests (Doris 2007; Jansen and Steen 1995; Pavković, Deur, and Lisac 2011).

The top drive system is modeled by an inertial mass J_1 and the lower drill bit is modeled by an inertial mass J_2, the drill string is modeled by a massless spring with stiffness k_t. The linear friction effect at the upper drive system and at the lower drive system is modeled by dampers c_r and c_b respectively. The angular velocity of top drive is given by $\dot{\theta}_1$ and the angular velocities of bit is represented by $\dot{\theta}_2$, T_{fb} is the torque due to friction at the bit also called torque on bit. Similarly frictional torque at top drive can be represented by T_r. The input torque from the motor or actuator is T_m.

From the torque balance equations derived using free body diagrams of forces on moment of inertias J_1 and J_2 the equations for a 2 DOF model are

$$J_1\ddot{\theta}_1 + c_r\dot{\theta}_1 + k_t(\theta_1 - \theta_2) + T_r(\dot{\theta}_1) = T_m, \tag{2.2}$$

and

$$J_2\ddot{\theta}_2 + c_b\dot{\theta}_2 - k_t(\theta_1 - \theta_2) + T_{fb}(\dot{\theta}_2) = 0, \tag{2.3}$$

where equation 2.2 represents the dynamics of the top drive and part of drill string and equation 2.3 represents the dynamics of the drill bit. The state variables for the system are chosen as,

$$\mathbf{x} = \begin{bmatrix} x_1 \\ x_2 \\ x_3 \end{bmatrix} = \begin{bmatrix} \dot{\theta}_2 \\ \theta_2 - \theta_1 \\ \dot{\theta}_1 \end{bmatrix}. \tag{2.4}$$

In matrix notation the system given by equation 2.2 and equation 2.3 using state variables given in equation 2.4 can be written as

$$\dot{\mathbf{x}} = \begin{bmatrix} -\frac{c_b}{J_2} & \frac{k_t}{J_2} & 0 \\ -1 & 0 & 1 \\ 0 & -\frac{k_t}{J_1} & -\frac{c_r}{J_1} \end{bmatrix} \begin{bmatrix} x_1 \\ x_2 \\ x_3 \end{bmatrix} + \begin{bmatrix} \frac{-T_{fb}(x_1)}{J_2} \\ 0 \\ \frac{-T_r(x_3)}{J_1} + \frac{T_m}{J_1} \end{bmatrix}. \tag{2.5}$$

The model can be further classified according to how the friction is modelled. The next section describes the different ways friction can be modelled.

2.1.2 *Choice of Friction model*

The way friction is modelled determines how the lumped model is described mathematically. Two types of deterministic friction models can be found in the literature namely static friction models and dynamic friction models.

Tribology explains the origin of friction as arising due to roughness of surfaces, even smooth surfaces have microscopic protrusions known as asperities, when two surfaces slide on each other these asperities interlock and give rise to friction (Armstrong-Hélouvry, Dupont, and De Wit 1994). Since the surface roughness is random, stochastic models of friction are also used.

In most of the literature on torsional oscillation control of the drill string, deterministic models are used. Therefore the deterministic models of friction are described in the proceeding sections.

2.1.2.1 *Static Friction models*

A static model of friction can either be continuous or discontinuous described as follows:

1. The friction may be approximated using a continuous model which leads to continuous time state space equations for which well developed control techniques exist. Continuous friction models are continuous approximations of "Classic models" (Olsson et al. 1998; Armstrong-Hélouvry, Dupont, and De Wit 1994: 1096) of friction. Such continuous approximations have been used in control oriented literature for drill strings as well as for other mechanical motion

systems where friction cannot be ignored (Abdulgalil and Siguerdidjane 2005). When the friction is approximated by a smooth function this ensures that equation 2.5 is smooth and admits a continuously differentiable unique solution. Such an approximate model is easy to simulate using commonly available programs like Simulink. The frictional torque on bit is modelled as

$$T_{\mathrm{fb}}(\dot{\theta}_2) = W_{\mathrm{ob}} \cdot R_{\mathrm{b}} \cdot (\mu_{\mathrm{cb}} + (\mu_{\mathrm{sb}} - \mu_{\mathrm{cb}})\mathrm{e}^{-\gamma_{\mathrm{b}}|\dot{\theta}_2|}) \tanh(\alpha\dot{\theta}_2), \tag{2.6}$$

where $\dot{\theta}_2$ is the bit angular velocity, W_{ob} is the weight on bit, R_{b} is the radius of the bit, μ_{cb} and μ_{sb} are the friction coefficients, γ_{b} is a parameter that determines the stribeck effect and α determines the steepness of the tanh function that approximates the sign function. The equation 2.6 above models the static friction and also takes into account the Stribeck effect which is the decrease in friction as speed increases as seen in Figure 5. An additional term to account for viscous friction is sometimes added in equation 2.6. Otherwise the damping parameter c_{b} in equation 2.5 accounts for this phenomenon. The model is designed in some cases only for the velocity greater than or equal to zero. This means the drill string is assumed to stick and slip but no reversal in direction is allowed. So the torque on bit can be expressed as

$$T_{\mathrm{fb}}(\dot{\theta}_2) = W_{\mathrm{ob}} \cdot R_{\mathrm{b}} \cdot (\mu_{\mathrm{cb}} + (\mu_{\mathrm{sb}} - \mu_{\mathrm{cb}}) \exp^{-\gamma_{\mathrm{b}}\dot{\theta}_2}) \tanh(\alpha\dot{\theta}_2). \tag{2.7}$$

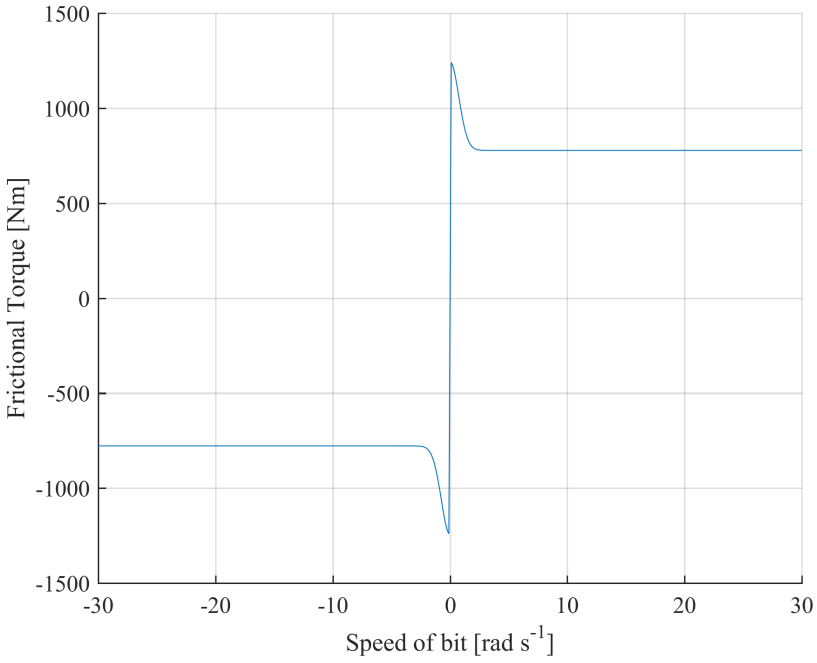

Figure 5: Continuous Model of Friction.

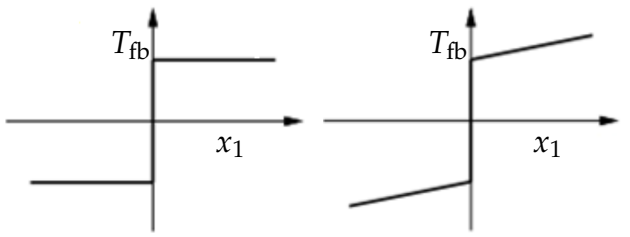

(a) Amonton-Coulomb friction law.

(b) Amonton-Coulomb friction law with viscous component.

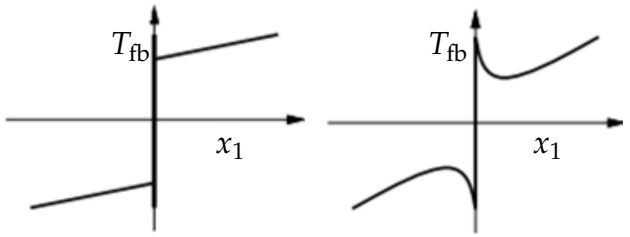

(c) Amonton-Coulomb friction law with stiction.

(d) Amonton-Coulomb friction law with viscous Stribeck effect.

Figure 6: Set valued Friction models where $x_1 = \dot{\theta}_2$.

2. The second type of static friction models are called set valued friction models. If the friction is modelled using a set valued discontinuous function then the system is represented by a Fillipov type differential equation with discontinuous right hand side and a differential inclusion is obtained. The other possibility in the discontinuous case is to use Utkin's equivalent control method and design a sliding mode controller. Similarly hybrid modelling is also used. The Amonton-Coulomb friction law is a set valued friction law. The torque on bit in this model is given by,

$$T_{fb} = T_c \text{sign}(\dot{\theta}_2), \tag{2.8}$$

where $T_c = \mu_c W_{ob}$. This is an ideal relay model and the value at $\dot{\theta}_2 = 0$ can be any value between $-T_c$ and $+T_c$. A viscous friction term $T_{\dot{\theta}_2} = \mu \dot{\theta}_2^{\beta}$ can be added to equation 2.8 in order to model the viscous effects of mud. The effects of stiction can also be considered. The stiction effect implies that the friction required to move the bit is greater at zero velocity and as soon as the body starts moving the force decreases to the sliding frictional torque. Similarly Stribeck effect can also be modelled as shown in Figure 6. If T_s is the stiction torque the set valued model can be written as

$$T_{fb} = \begin{cases} T_c \text{sign}(\dot{\theta}_2), & \text{if } \dot{\theta}_2 \neq 0, \\ [-T_s, T_s], & \text{if } \dot{\theta}_2 = 0. \end{cases} \tag{2.9}$$

The set valued frictional torque given in equation 2.9 can take any value in the set $[-T_s, T_s]$ when bit velocity is zero. This leads to nonuniqueness of the solution (Leine 2000: 12) of equation 2.5. The system represented by equation 2.5 and equation 2.9 can now generally be represented as

$$\dot{x} = f(x) \in \begin{cases} f_-(x), & \text{if } \dot{\theta}_2 < 0, \\ f_+(x), & \text{if } \dot{\theta}_2 > 0. \end{cases} \tag{2.10}$$

The solution of equation 2.10 is defined in the Fillipov sense (Leine 2000) where the system of differential equations with discontinuous right hand side is first represented in the form of a convex differential inclusion to avoid the problem of nonexistence of unique solutions. The differential inclusion is

$$\dot{x} = f(x) \in \begin{cases} f_-(x), & \text{if } \dot{\theta}_2 < 0, \\ \overline{co}\{f_-(x), f_+(x)\}, & \text{if } \dot{\theta}_2 = 0, \\ f_+(x), & \text{if } \dot{\theta}_2 > 0, \end{cases} \tag{2.11}$$

where $\overline{co}\{f_-(x), f_+(x)\} = \{(1-q)f_-(x) + qf_+(x) \ \forall \ q \in [0,1]\}$ is a convex set and q is a constant. Uppersemicontinuity of equation 2.11 guarantees existence of solutions (Leine 2000: 13). Simulation involves dividing the state space into several subspaces in which different ODE's are valid and switching between them. The main disadvantage is that as the number of switching surfaces increases the logical complexity also increases (Viguié et al. 2009; Leine 2000). The Fillipov type systems discussed here present difficulties in simulation on the sliding surface and zero crossing detection (Navarro-López and Carter 2011). Navarro-López (2009) has introduced hybrid dynamic models for the torsional dynamics of the drill string which provide a convenient framework that can handle multiple discontinuity surfaces.

2.1.2.2 *Dynamic Friction models*

The so called Lugre Model is a dynamic model of friction that includes the Stribeck effect and can be used to model stick slip. The Lugre model employs a hidden state z called the internal friction state which can be visualized as bristle deflection in a bristle model of surface contacts (Astrom and Canudas-De-Wit 2008). The differential equation that describes the model is

$$\frac{dz}{dt} = v - \sigma_0 \frac{|\dot{\theta}_2|}{g(\dot{\theta}_2)} z, \tag{2.12}$$

and the torque due to friction is

$$T_{fb} = \sigma_0 z + \sigma_1 \dot{z} + f(\dot{\theta}_2), \tag{2.13}$$

where σ_0 is a stifness constant and σ_1 is a damping constant. The function $g(\dot{\theta}_2)$ models the Stribeck effect and can be expressed as

$$g(\dot{\theta}_2) = W_{ob} \cdot R_b \cdot (\mu_{cb} + (\mu_{sb} - \mu_{cb})e^{-\gamma_b|\dot{\theta}_2|}). \tag{2.14}$$

Similarly the function $f(\dot{\theta}_2)$ is also a velocity dependent term that models viscous damping and can be expressed as

$$f(\dot{\theta}_2) = \sigma_v\dot{\theta}_2, \tag{2.15}$$

where σ_v is the damping constant.

2.2 COUPLED AXIAL AND TORSIONAL DYNAMIC MODELS VIA BIT ROCK INTERFACE

Richard, Germay, and Detournay (2007) presented an alternative explanation for the stick slip phenomenon. In their hypothesis the axial vibrations are responsible for the reduction in torque as speed increases causing the stick slip phenomenon. The drill string is modelled in Richard, Germay, and Detournay (2007) so that the axial and torsional oscillations are coupled at the bit rock interface. The model may replace the friction oriented explanation of self excited stick slip oscillations in drill strings. Germay et al. (2009) numerically analyzed a simplified 1 DOF coupled axial and torsional model of the drill string in which the frictional torque on bit depends on present and past values of axial vibrations. A separation of time scales analysis to separately analyze the fast axial and the slow torsional dynamics were used to get analytical and simulation results which identify loss of contact due to axial vibrations as the reason for decrease in torque on bit with increasing speed which leads to stick slip. Currently efforts to verify the theory using experimental studies are being pursued by Wiercigroch et al. (2017). Experimental results did not support the assertion that drill bit causes periodic axial vibration but Wiercigroch et al. (2017) postulate that irregularly spaced blades of the drill bit may be responsible for the self excited torsional oscillations. Further studies are needed in this direction.

2.3 DISTRIBUTED PARAMETER MODELS

Developing control algorithms for infinite dimensional systems is a developing area of theoretical research with torsional oscillation control of the drill string as one of the possible applications. The drill string can be modelled as a string so the torsional oscillations can be described using d'Alembert's one dimensional wave equation. This approach is the most popular infinite dimensional model used in control oriented literature (Saldivar et al. 2016; Zhao 2017; Aarsnes and Wouw 2018). The wave equation is classified as a hyperbolic PDE and mathematically represented as

$$GJ\frac{\partial^2\phi}{\partial s^2}(s,t) - I\frac{\partial^2\phi}{\partial t^2}(s,t) = 0 \quad s \in (0,L), \tag{2.16}$$

where s is the spatial coordinate, L is the length of drill string, ϕ is the angular displacement that depends both on time and space, G is the shear modulus, J is the second moment of area, I is the inertia with $I = \rho_a J$ and ρ_a is the area density. The equation 2.16 ignores the material damping of the drill string. Substituting $\tilde{c} = \sqrt{\frac{I}{GJ}}$ in equation 2.16 the more familiar form

$$\frac{\partial^2 \phi}{\partial s^2}(s,t) = \tilde{c}^2 \frac{\partial^2 \phi}{\partial t^2}(s,t) \quad s \in (0, L), \tag{2.17}$$

is obtained. By the d'Alembert solution of equation 2.17 at any time instant the torsional oscillation of drill string can be decomposed in to two components traveling in opposite directions (Kreyszig and Norminton 1993: 553-554). The d'Alembert solution is given by

$$\phi(s,t) = a_1(s + \tilde{c}t) + a_2(s - \tilde{c}t), \tag{2.18}$$

where $a_1(s + \tilde{c}t)$ can be considered as the torsional wave traveling towards the top drive and $a_1(s - \tilde{c}t)$ is the traveling wave traveling towards the drill bit.

2.4 CONTROL CHALLENGES

The drill string is an underactuated system i.e. it has lower number of actuators[1] than degrees of freedom. The only actuator available is the top drive where as the frictional torque that is the source of self excited oscillations is at the other end. The mud motor is used to increase the velocity of the bit which increases the rate of penetration. But it is not used to control torsional oscillations of the drill rig.

The measurements from downhole require expensive data logging or measurement while drilling (MWD) tools. Current MWD tools use mud pulse telemetry where mud is used as the transmission medium. The rate at which mud pulse based MWD tools transmit measured data to the surface is 3bits/s to 10bits/s depending on the depth and mud pulse telemetry technology used (Emmerich et al. 2016). Disadvantages of mud pulse telemetry are slow data transmission rates and inability to transfer data when the mud circulation is interrupted. Wired drills that have faster transmission rates of up to 2Mbits/sec have been developed and tested in field trials (Reeves et al. 2005).

Friction is a nonlinear phenomenon which may be controlled using nonlinear control techniques. Most of the proposed algorithms assume full state feedback and assume that perfect model of the system is available, strategies for control that require the friction to be estimated or known are currently impractical due to uncertainties in the friction modelling and down hole conditions. Robust control algorithms are needed that may handle modelling uncertainties and measurement noise.

1 An actuator is the mechanism responsible for controlling or moving the system e.g. DC motor.

In linear control the controller and observer separation principle allows the design of a stable observer and stable controller separately as the eigenvalues of controller and observer are separate and this guarantees closed loop stability. Such a separation principle does not exist in nonlinear control hence the closed loop stability of observer based nonlinear control algorithms has to be ensured which makes observer based nonlinear control more complicated.

3

EXPERIMENTAL SETUP, MODEL AND PARAMETER ESTIMATION

In the previous chapter several different mathematical models that have been used in the literature to model the drill string for torsional oscillation control were presented. The mathematical models presented were derived by making some simplifying assumptions.

To check the validity of the assumptions under which the control law is derived experimental evaluation is required. Evaluating control strategies on real drill strings is costly and is further complicated by the lack of suitable measurement while drilling devices for reliable down hole measurements. An intermediate step frequently reported in the literature has been to use experimental setups (Patil and Teodoriu 2013). Such setups qualitatively reproduce the torsional oscillation phenomenon, enabling the evaluation and comparison of control approaches in the presence of real friction and measurement noise.

There is a vast amount of literature that deals with active control of torsional oscillations in drill strings. But in most of the studies, the control algorithms have only been evaluated in simulations (Zhu, Tang, and Yang 2014; Ghasemloonia, Rideout, and Butt 2015). In this work an experimental setup is designed and built to evaluate the designed controllers.

This chapter is organized such that in the first section, the experimental setup and the similitude analysis used to scale down a 150m bottom hole assembly is described. In the second section, the experimental setup undergoing stick slip is shown. In the third section the system identification used to identify the parameters of the model of the drill string is described. The summary and conclusions are given in the last section.

3.1 EXPERIMENTAL SETUP

To evaluate control algorithms an experimental setup is designed and built at the Institute of Electrical Information Technology (IEI). In this section the experimental setup, data acquisition and control components are described. The experimental setup is a scaled model of a 150m long drill string bottom hole assembly.

3.1.1 *Overview*

The setup shown in Figure 7 consists of a 4.1m long aluminium pipe with an inner diameter of 4×10^{-3}m and outer diameter of 6×10^{-3}m. This emulates a drill string. The top drive is an inertia disk connected to a Maxon servo motor. The bottom end of the drill string is connected to an inertia disk via a Magtrol TMB 304/411 torque and speed sensor capable of measuring up to 2Nm of torque. The drill string connects the top drive with the drill bit as shown in Figure 7. The lateral stiffness of the drill string is low so it is prevented from lateral movement using constraints at 6 points along the drill string.

An ESCON 50/5 servo controller from Maxon is used to interface with the servo motor. It is capable of measuring motor current and speed. It is also used for current control in experiments. The dynamics of this current control loop are faster than the drill string dynamics. Therefore, they are ignored.

The speed control loop is implemented in a Ds 1104 rapid prototyping system which also serves as the data acquisition system. To measure the top drive speed the motor is equipped with a 500counts/turn incremental encoder. The ESCON 50/5 servo controller measures the speed and generates a scaled analogue voltage output that is measured by the Ds 1104 rapid prototyping system. The bit speed is measured using the TMB 304/411 torque and speed sensor. The TMB 304/411 produces 60 pulses per revolution. The pulse to speed calculation is done using the Ds 1104 rapid prototyping system.

The experimental setup is designed and built at the Institute of Electrical and Information Technology (IEI) is designed to evaluate the control algorithms. The design uses adjustable aluminium beams so the length of the drill string can be increased or decreased with minor modifications. The experimental setup is inspired by similar drill string setup designed in Patil (2013) but has considerable modifications that make it more suitable for control oriented research.

A full scale drill string may be over 5000m in length. An exact scaled model would require a laboratory drill string one hundredth of a mm in diameter which is physically not possible. The approach used in Patil (2013) is followed and the 4.1m long laboratory drill is scaled to represent 150m long bottom hole assembly of a real drill string.

Since this dissertation focuses on control of friction-induced torsional oscillations caused by bit friction therefore the scaling of the torque on bit is of particular interest. The torque on bit of the scaled experimental setup should be the scaled version of the torque on bit experienced by the full scale drill rig. Table 2 given on page 29 compares the dimensions of a real drill string to the scaled experimental setup. Table 3 given on page 29 shows the range of torque on bit values for a full scale drill rig with a 150m

long bottom hole assembly. To find the down scaled torque required at lower disc of the experimental setup that will be equivalent to torque on bit of a 150m length bottom hole assembly the following similitude analysis is performed (Patil 2013: 61).

The length of the drill string of the experimental setup is represented by l. The full scale bottom hole assembly length is represented by L. The ratio of the experimental setup length to full scale bottom hole assembly length is given by

$$\frac{l}{L} = \frac{1}{n} \simeq \frac{1}{36}, \tag{3.1}$$

where n is the scaling factor. The torque on the lower end of the drill string is

$$T = \frac{GI}{R}, \tag{3.2}$$

where G is the shear modulus, I is the area moment of inertia and R is the outer radius of the pipe.

The ratio of torque on bit of real drill string to torque on bit of experimental setup is

$$\frac{T_{\text{real}}}{T_{\text{model}}} = \frac{\frac{G_{\text{real}} I_{\text{real}}}{R_{\text{real}}}}{\frac{G_{\text{model}} I_{\text{model}}}{R_{\text{model}}}} = \frac{G_{\text{real}} I_{\text{real}} R_{\text{model}}}{G_{\text{model}} I_{\text{model}} R_{\text{real}}}, \tag{3.3}$$

where T_{real} is used to represent torque on the real drill string at the lower end, G_{real} its shear modulus, I_{real} its polar moment of inertia and R_{real} its outer diameter. Similarly T_{model} is used to represent torque on the experimental laboratory drill string at the lower end, G_{model} its shear modulus, I_{model} its polar moment of inertia and R_{model} its outer diameter. Subsitituting values from Table 2 given on page 29 into equation 3.3 the relation

$$\frac{T_{\text{real}}}{T_{\text{model}}} = 2.4897 \times 10^7 = 36^{4.7524} = n^{4.7524}, \tag{3.4}$$

is obtained. By substituting values of T_{real} from Table 3 given on page 29 into equation 3.4 the torque on bit of the experimental setup is calculated. It nominal value of the torque on bit should be between 0 and 0.2856×10^{-3}Nm. Higher values of torque on bit will not effect controller evaluation but lower values of torque on bit may not produce the torsional oscillations.

3.1.2 *Top drive assembly*

The top drive shown in Figure 8 consists of two main components:

1. Servo motor.
2. Rotating inertia disk.

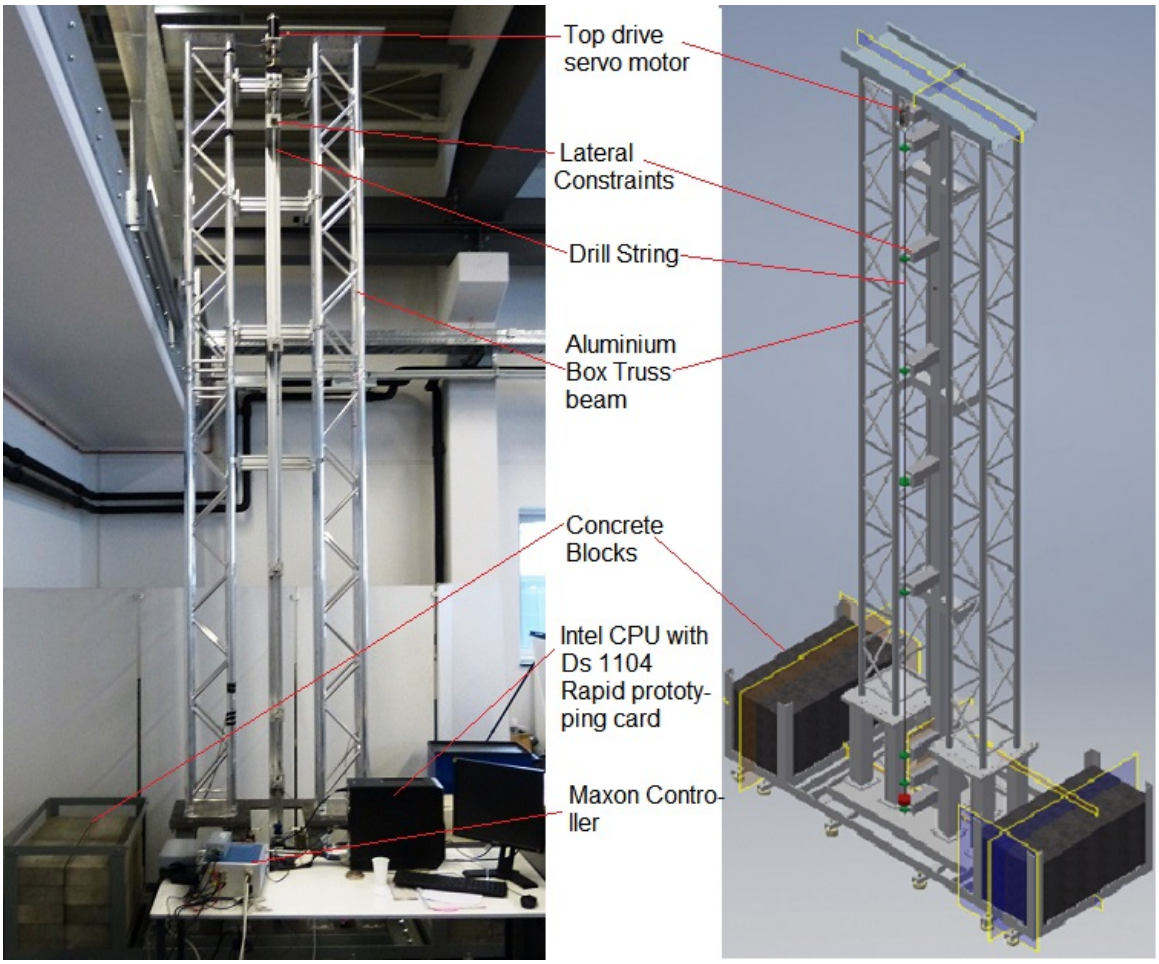

Figure 7: Experimental Setup used.

The top drive servo motor is capable of supplying 0.8Nm nominal torque at 6.8A nominal current. It has a torque constant of 0.123Nm/A. The maximum torque it can provide is 2Nm. It is connected to the rotating disc via a flexible coupling to mitigate the effects of any shaft misalignment and axial shocks that may damage the servomotor. It has a 500 counts/turn incremental HEDL 5540 encoder from Maxon. The disc models the top drive inertia. Its weight is supported by a plain bearing machined from brass, so that the motor bears no axial load. Furthermore, additional discs can be added to increase the inertia of the top drive. The drill string is connected to the lower part of the disc via a second flexible coupling.

3.1.3 *Bottom bit assembly*

The bottom bit assembly shown in Figure 9 on page 31 consists of a torque and speed sensor and a rotating inertia disk. The torque sensor used in the setup is manufactured by Magtrol and is called TMB 304. The torque sensor can measure up

Table 2: Comparison between dimensions and physical parameters of a real drill string and the experimental setup.

QUANTITIES	FULL SCALE DRILL STRING BHA	EXPERIMENTAL SETUP
Length	150m	4.1m
Inner diameter	127×10^{-3}m	4×10^{-3}m
Outer diameter	157×10^{-3}m	6×10^{-3}m
Shear modulus	7.69×10^{10}Nm	27×10^{9}Nm
Polar moment of Inertia	3.4109×10^{-5}m^4	1.021×10^{-10}m^4

Table 3: Operating parameters of a real drill string (Patil 2013).

OPERATING PARAMETERS	VALUES
Angular speed	$50 - 200$RPM
Weight on bit	$0 - 134 \times 10^{3}$N
Torque on bit	$0 - 10 \times 10^{3}$Nm

to 2Nm of torque. It has built in adjustable signal conditioning filters. Furthermore, it is used to measure the bit speed. It generates 60 digital pulses per revolution.

Figure 10 on page 31 plots the top drive torque calulated from motor current and also shows the torque measured at bit using the torque sensor. It can be seen that the torque on bit of the setup during this particular experimental run was up to 0.2Nm during the stick phase. In Figure 10 the torque applied by motor is calculated by multiplying the measured motor current with the motor torque constant of 0.123Nm/A. It can bee seen that during startup the torque applied by motor is entirely determined by the static bit friction. And at about 20s there is a decrease in Torque on bit which is due to increase in bit speed. A clear decrease in bit torque as speed increases is observed in measurements.

3.1.4 *Data acquisition and rapid prototyping*

The data acquisition and controller rapid prototyping is accomplished using two main devices:

1. Escon 50/5 servo controller from Maxon.
2. Ds 1104 controller from Dspace.

The Escon 50/5 servo controller is a 4 quadrant pulse width modulation controller capable of closed loop speed control and can also be used in current control mode.

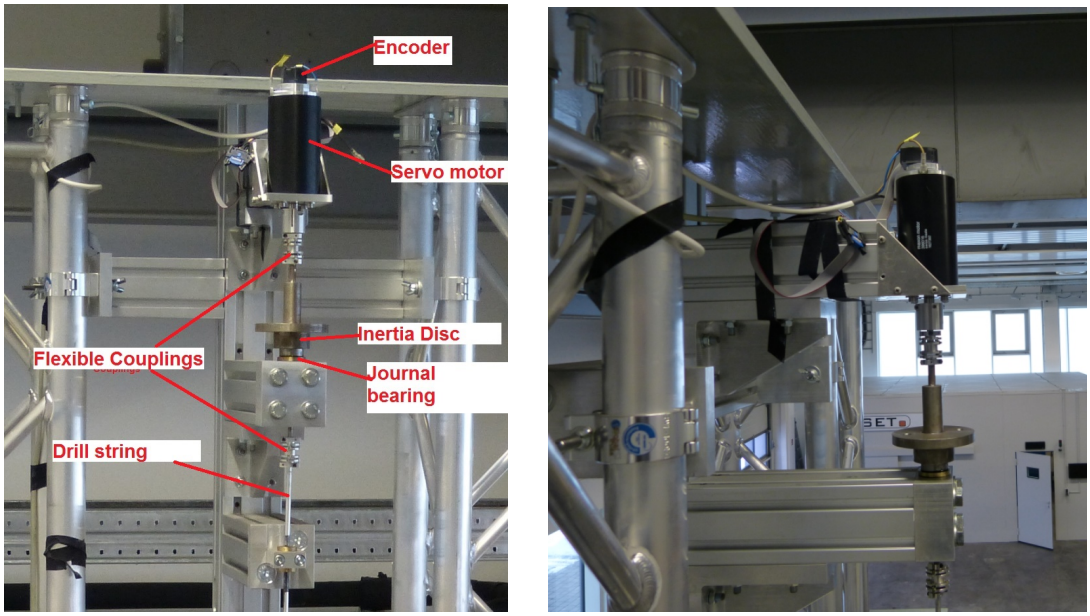

(a) Front view of the top drive showing inertia disks and supporting components.

(b) Side view of the top drive.

Figure 8: The top drive assembly.

Furthermore it can be used to measure the motor speed using signals from the encoder mounted on the motor. It has analogue output channels that can be used to provide motor speed and motor current to the Ds 1104 rapid prototyping system for control purposes. In current control mode it can be used to track a reference current that is fed to the servo motor.

For speed control it has an auto tunable PID controller. But for the setup the auto tuning failed and the built in PID controller caused large oscillations in the system. The built in PID controller behaved as a bang bang controller which saturated the input current measurement channels of the controller therefore it could not be used for system identification. Hence a PID controller was manually tuned and implemented in the Ds 1104 system and used to obtain data for parameter estimation.

The Ds 1104 R&D Controller board is a real time control system that is plugged in to the PCI slot of a computer. It is programmed using Simulink and can be used for rapid prototyping of the designed control algorithm. At the heart of the data acquisition and control system is the Ds 1104 as shown in Figure 11 on page 32, which acquires the current and top drive speed as analogue voltage signals from the ESCON 50/5 module. The TMB 304 generates 60 pulses/revolution. These pulses are input to one of the digital input channels of the Ds 1104 controller. The Ds 1104 is programmed to calculate the bit speed using the time duration between two consecutive pulses. The controller after calculating required control action feeds this to

Figure 9: Lower bit assembly.

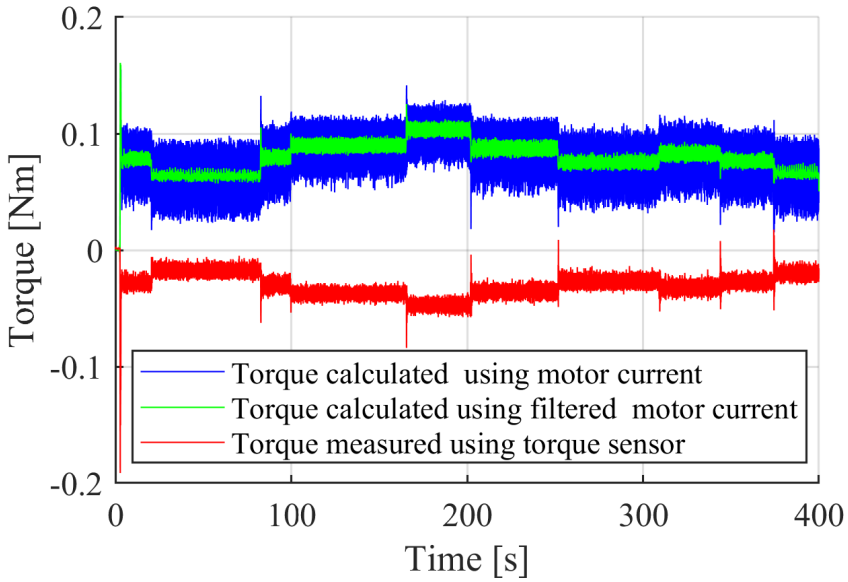

Figure 10: Torque measured at bit using torque sensor and calculated torque from measured motor current. Note that the torque calculated by measuring motor current is the total torque applied to drive the whole system including top drive and the drill bit. Where as the torque sensor measures the torque at bit.

the analogue input channel of the ESCON 50/5 module through an analogue output channel.

3.1.5 *Speed measurement and measurement errors*

A digital encoder is used to measure the angular speed. Selection of proper encoder resolution and measurement method is critical for speed control. The top drive is equipped with an optical incremental encoder called HEDL 5540. It produces 500 counts per turn To measure the angular velocity using incremental encoders two different algorithmic approaches namely frequency measurement and period measurement are used both have advantages and disadvantages. In the drill string setup the top drive speed is measured using the frequency counting method where as the bit speed is measured using period measurement.

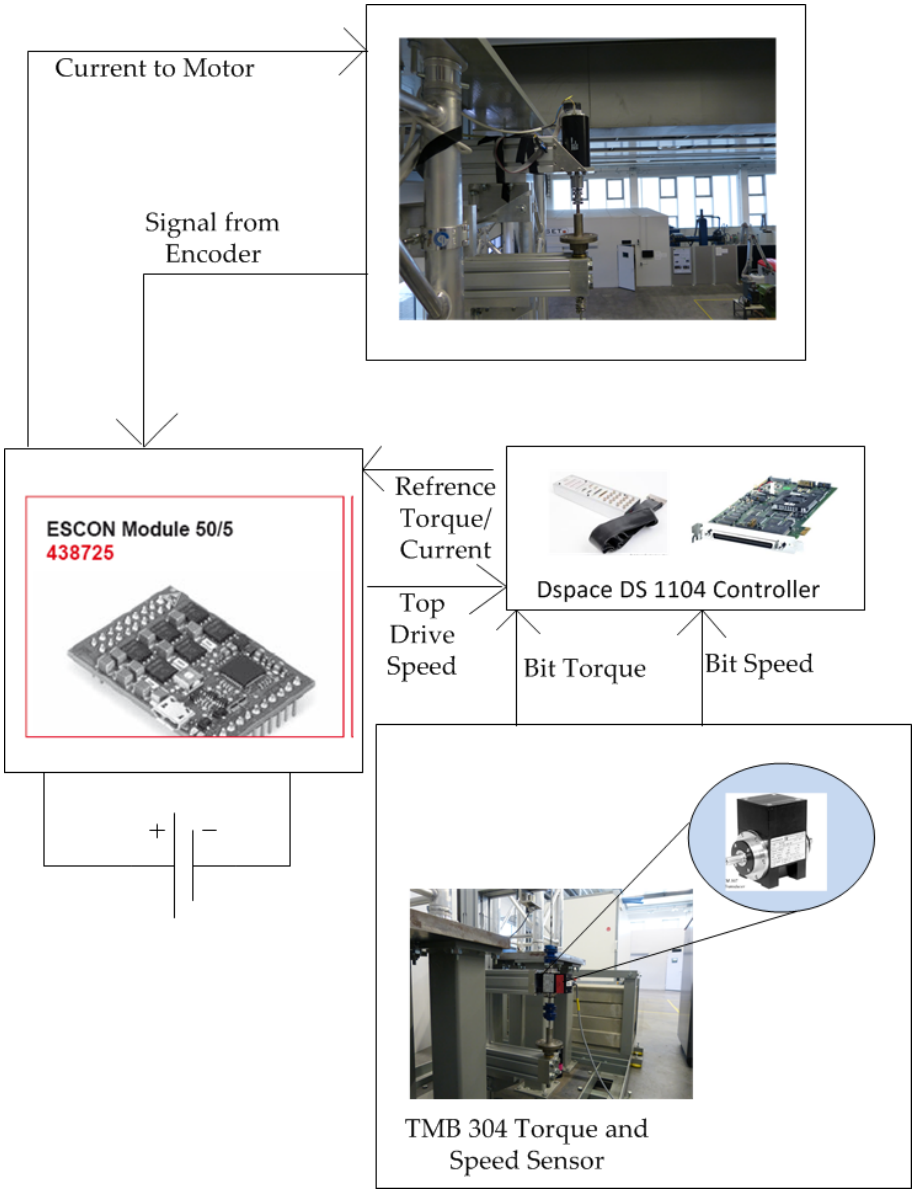

Figure 11: Data acquisition system.

In the frequency measurement method the number of pulses are counted for a constant time period T_{sc}, the speed for the duration of the time period is considered constant. If N_p is the number of counts per revolution and ΔN be the number of pulses counted during the time period or duration of counting (Petrella et al. 2007). The angular speed ω can be given by

$$\omega = \frac{d\theta}{dt} = \frac{\Delta\theta}{T_{sc}} = \frac{2\pi\Delta N}{N_p T_{sc}}. \tag{3.5}$$

The speed measurement quantization error $\Delta\omega$ is expressed as (Petrella et al. 2007)

$$\Delta\omega = \frac{2\pi}{N_p T_{sc}}. \tag{3.6}$$

Figure 12 shows the quantization error as a function of sensor resolution N_p and T_{sc}. The figure shows that using a higher resolution encoder will reduce the quantization error but this also requires a fast controller. Similarly increasing the time duration for which the pulses are measured reduces the quantization error but this will slow down the control loop. The ESCON controller from Maxon reduces the noise by using a first order low pass filter with a cutoff of 5Hz.

The errors in speed measurement using the frequency method increase at low speed. An alternative method to measure low speed is the period measurement method. This method is used to measure the bit speed using pulses from the tachometer. The speed is obtained by measuring the time duration between two pulses of the tachometer. If T_s is the sampling period of the data acquisition system then under

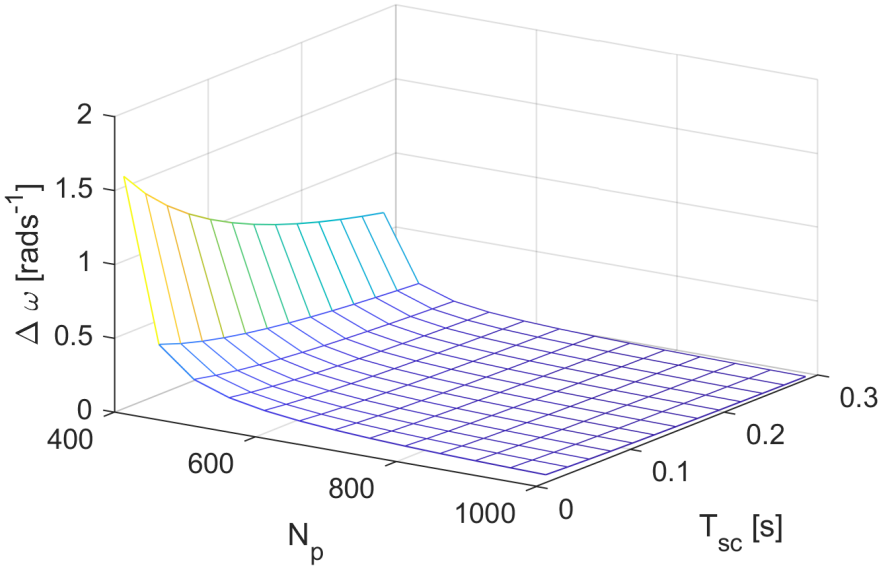

Figure 12: Speed quantization error in pure frequency measurement.

the assumption that the angular speed in between two encoder pulses is constant the following expression for angular speed is derived

$$\omega = \frac{2\pi}{N_p.n.T_s}, \tag{3.7}$$

where N_p represents the number of encoder pulses per revolution. The time period of the pulses (T_p) is a function of angular velocity ω and is calculated as

$$T_p = \frac{2\pi}{N_p.\omega}. \tag{3.8}$$

The error in speed calculation for the period measurement method depends on the ratio between the period T_p of the encoder which depends on motor speed and the time period T_s of the measurement system Petrella et al., 2007. An absolute error relationship such as given in Figure 12 for the frequency measurement method can not be given. Petrella et al. (2007) calculated a worst case percentage error (e_ω) given by

$$e_\omega = \frac{T_s}{\frac{2\pi}{N_p\omega} - T_s} \times 100. \tag{3.9}$$

The Figure 13 shows the percentage error plotted for angular velocity range of interest for the drill string. The values of $N_p = 60$ and $T_s = \frac{1}{10000}s$ are used to plot Figure 13. The value $N_p = 60$ is selected based on the bit speed sensor used during experiments. Similarly the sampling rate during experiments was 10Khz giving a sampling period of $T_s = \frac{1}{10000}s$. The advantage of using digital sensors is that no analogue to digital conversion is involved for bit speed measurement.

3.1.6 *Uncertainty in the measurement*

Uncertainty in the sensor measurement can be calculated using the guide to the expression of uncertainty in measurement (GUM) Type B method (Kirkup and Frenkel 2006). The worst case error in the measurement of time period T_p can be twice the sampling frequency of measurement. If the angular speed is constant then T_p is also constant.The speed after rearranging equation 3.8 can be written as $\omega = \frac{2\pi}{N_p T_p}$.

The maximum error in the measurement of T_p can be denoted by ΔT_p which for the worst case can be given as

$$\Delta T_p = 2 \times T_s. \tag{3.10}$$

The speed measurement error e_ω due to error in measuring T_p using the Type B Method of GUM is calculated as

$$e_\omega = \frac{\partial \omega}{\partial T_p} \Delta T_p. \tag{3.11}$$

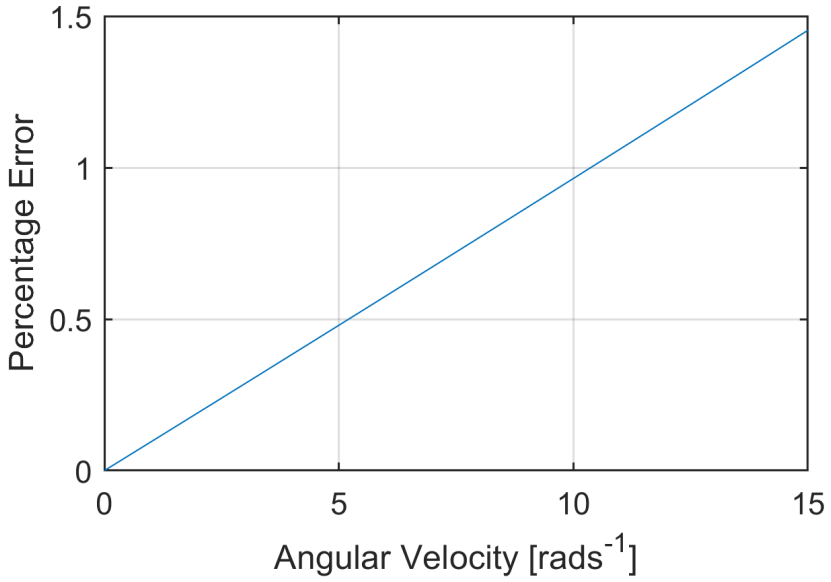

Figure 13: The percentage error plotted for a sampling frequency of 10Khz and N_p=60.

The partial derivative $\frac{\partial \omega}{\partial T_p} = -\frac{2\pi}{N_p T_p^2}$, is substituted in to equation 3.11 to obtain

$$e_\omega = -\frac{2\pi}{N_p T_p^2} \Delta T_p. \tag{3.12}$$

The error bound e_b is thus

$$e_b = \pm \frac{4\pi T_s}{N_p T_p^2} \tag{3.13}$$

Assuming a uniform probability distribution function for the uncertainty. The uncertainty in measurement can be estimated as

$$u_{\text{measurement}} = \pm \frac{e_b}{\sqrt{3}}. \tag{3.14}$$

Using equation 3.14 the uncertainty in bit speed measurement at 6rads^{-1} can be calculated to be $u_{\text{bit}} = \pm \frac{0.0688}{\sqrt{3}} \text{rads}^{-1}$.

3.2 STICK SLIP

One of the principal causes of torsional oscillations of a drill string is stick slip due to friction. The experimental setup is capable of reproducing the stick slip phenomenon. Liu et al. (2017) studied the stick slip phenomenon in an experimental setup and observed that stick slip depends on the stiffness of the drill string. A drill string with lower stiffness will exhibit more stick slip. This implies that as the drill string drills deeper the stick slip should increase. This observation is in line with studies in Patil (2013) where a factor called stick slip indicator is used to indicate the severity of the stick slip. Figure 14 shows the experimental setup used in this work undergoing stick slip. As can bee seen the drill bit measured velocity can be 4 times the top drive velocity during stick slip. The bit speed was measured using an analogue tachometer. A point to be noted about the analogue tachometer output shown in Figure 14 is that the analogue tachometer output is a noisy voltage output and will be effected by noise at low speeds where the voltage levels are very low, in other words the signal to noise ratio is low at low speeds. Therefore the speed reversal seen in Figure 14 may be due to noise.

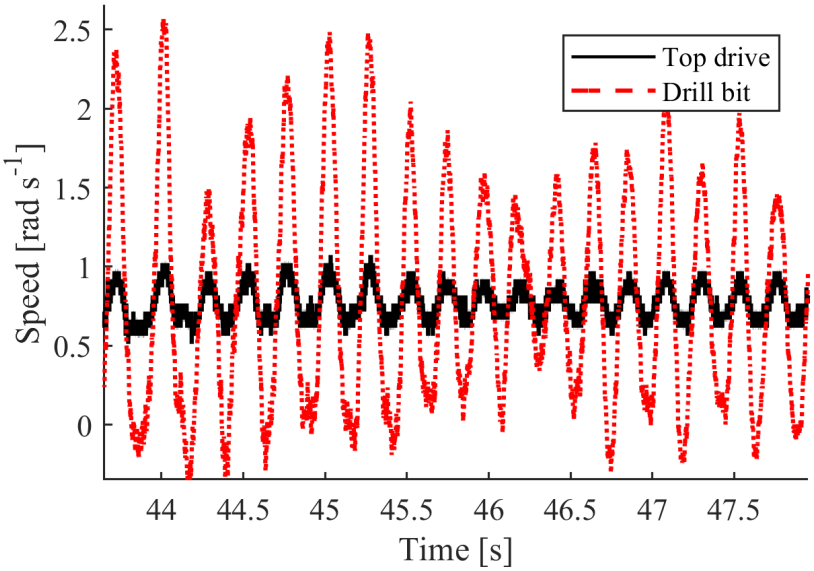

Figure 14: Experimental setup undergoing stick slip.

3.3 SYSTEM IDENTIFICATION

There are limitations on the kind of identification experiments that can be performed. The sections of the drill string pipes are screwed together in a long chain of pipes. To avoid unwinding the drill string rotation in one direction only is allowed. Similarly due to flexibility of the drill string using a zero mean pseudo random input at top drive will produce a response at the bit that is too low to be registered by the digital

tachometer. Furthermore, it may be damaging for the top drive components. The purpose of identification in this work is to design a stable regulator for drill string bit speed that minimizes the torsional oscillations of the drill string. For regulation tasks crude models often suffice (Åström and Eykhoff 1971: 125).

The drill string models derived from first principles discussed in Chapter 2 are nonlinear continuous time models. In this work the experimental setup is described by the system of differential equations given in equation 2.5 and friction represented by continuous approximation given in equation 2.6. Such first principle models that contain unknown parameters are known as grey box models (Rao and Unbehauen 2006).

Parameter estimation of experimental drill string setups that take in to account friction was first undertaken by Mihajlovic (2005). Later studies by Doris (2007) used the same technique. Mihajlovic (2005) determined the parameters of the friction model by disconnecting the drill string from the top drive and using pseudorandom input to obtain the friction parameters using the nonlinear least squares criterion to minimize the error between the measured angular displacement and simulated angular displacement. A similar identification procedure is used to estimate parameters of the friction model for the drill bit of experimental setup by isolating it.

Lu, Dumon, and Wit (2009) uses the step response data to fit a first order transfer function and finds the moment of inertia and damping for the top and bottom inertia.

In the current work nonlinear least squares criterion is used but only the bit speed and input torque are used for parameter identification. The nonlinear least squares error between actual bit speed and the simulated bit speed is minimized using the trust region reflective algorithm. Instead of a pseudo random input a multi step input is used to excite the drill string in a range of velocities. The validation is performed using multi step inputs and mulitsine inputs. The choice of speed as an output signal necessitates the use of closed loop control as the drill string can not be controlled in open loop. The input current of the motor is measured from which the torque is calculated.

3.3.1 *System model*

To model the experimental setup a two degree of freedom lumped parameter model shown in Figure 4b given on page 17 is used. The equations used to model the drill string are

$$\dot{x}_1 = -\frac{c_b}{J_2}x_1 + \frac{k_t}{J_2}x_2 - \frac{T_{fb}(x_1)}{J_2}, \tag{3.15}$$

$$\dot{x}_2 = x_3 - x_1, \tag{3.16}$$

and

$$\dot{x}_3 = -\frac{k_t}{J_1}x_2 - \frac{c_r}{J_1}x_3 - \frac{T_{fu}(x_3)}{J_1} + \frac{T_m}{J_1}. \tag{3.17}$$

The states of the system x_1, x_2 and x_3 are defined in equation 2.4. The upper bearing friction $T_{fu}(x_3)$ and lower bit friction $T_{fb}(x_1)$ are mathematically modelled using a static continuous friction model given by

$$T_{fb}(x_1) = (a_1 + b_1 e^{-\gamma_b |x_1|}) \tanh(\alpha x_1), \tag{3.18}$$

and

$$T_{fu}(x_3) = (a_2 + b_2 e^{-\gamma_{top} |x_3|}) \tanh(\alpha x_3). \tag{3.19}$$

3.3.2 *Nonlinear Least Squares*

The least square criterion $I(N)$ to be minimized for parameter estimation is given as

$$I(N) = \sum_{n=1}^{N} (y(n) - \hat{y}(n|\boldsymbol{\theta}_p))^2, \tag{3.20}$$

where $y(n)$ is the measured output, $\hat{y}(n|\boldsymbol{\theta}_p)$ is the estimated output and $\boldsymbol{\theta}_p$ is the parameter vector. The nonlinear least squares criterion is minimized using the trust region reflective algorithm of Matlab (Coleman and Li 1996).

The input is the torque applied by the motor and the output is bit speed. Some of the parameters, namely moment of inertia, stiffness of the setup to be found are physical quantities that are positive and can be approximately calculated. Similarly, the unknown damping ratios at top drive and drill bit are also positive quantities. And parameters of the friction model are positive coefficients. The optimization procedure can be sped up by bounding the parameter space. Hence upper and lower bound constraints are used in the optimization. The bounds used were between 0 and 2 for the parameters.

3.3.3 *Procedure*

The parameter estimation procedure consists of four steps:

1. `Data preprocessing:` The input current is filtered using a digital low-pass filter with cut off frequency of 5Hz. To implement the filter the filtfilt command in Matlab is used to avoid introducing any phase delay between the input and output.

2. `Inputs:` Multi step input references are used to excite the experimental setup for parameter estimation. The negative or counter clockwise rotation is avoided

as the bit speed sensor is unidirectional. It should be noted that the real drill string setup is also constrained to rotate in one direction to avoid unscrewing the drill string.

3. `Initialization:` The iterative procedure requires initialization of the parameters. For the experimental setup calculated values were used and those parameters that could not be calculated were initialized to zero.

4. `Simulation:` In each iteration the mathematical model is simulated using the updated parameters, from the model output and measured response, $I(n)$ is calculated. The stopping criterion for the procedure is based on a threshold value for change in the parameters (step size tolerance). If the change (step size) is below this threshold value the optimization iterations are stopped. A step size tolerance of 10^{-6} was used for the stopping criterion. In each experiment the states were initialized from zero.

3.3.4 *The estimated parameters*

The parameters were estimated using experiment shown in Figure 15. The identified model has acceptable fidelity in the range from 50 to 160RPM which is within the nominal RPM range for drilling. The parameters that were identified are given in Table 4.

Table 4: Parameters identified for the experimental setup.

PARAMETER	CALCULATED VALUE
J_1	0.0004kgm^2
J_2	0.0035kgm^2
c_r	0.0025Nms/rad
c_b	0.0029Nms/rad
k_t	1.0513Nm/rad
γ_b	0.7521
γ_{top}	0.1478
a_1	0.0146
b_1	0.0246
a_2	0.0125
b_2	0.0192

3.3.5 *Validation*

The identified model was validated using data from experiments that used multi step reference inputs and multi sine reference inputs. The experiments were performed over a period of several days. Validation experiments in Figure 16, Figure 17 and Figure 18 show that the identified model can reproduce the experimental step response. The ability of the model to replicate measured rotational speed is effected by the static friction. It is observed that the static friction can vary from experiment to experiment. This effects the fidelity of the model this is the reason for increased error for validation experiment shown in Figure 19. Similarly the model over estimates the speed below 4rad/sec as is apparent from validation plot of Figure 20. In Figure 21 the error is relatively large when compared to a similar validation experiment shown in Figure 22 which may be due to variation in friction of the experimental setup. The experiments are summarized in Table 5. Validation at different sampling frequencies does not effect the error. To compare the validation results mean square error between measured and simulated data is used. The mean square error is chosen because the negative and positive bias of the simulated output will not cancel out when calculating the mean as the error is squared. A drawback of the mean square error is that it is sensitive to outliers in the data, that is, a large error during the transient phase will have a larger than desired effect on the calculated mean square error value.

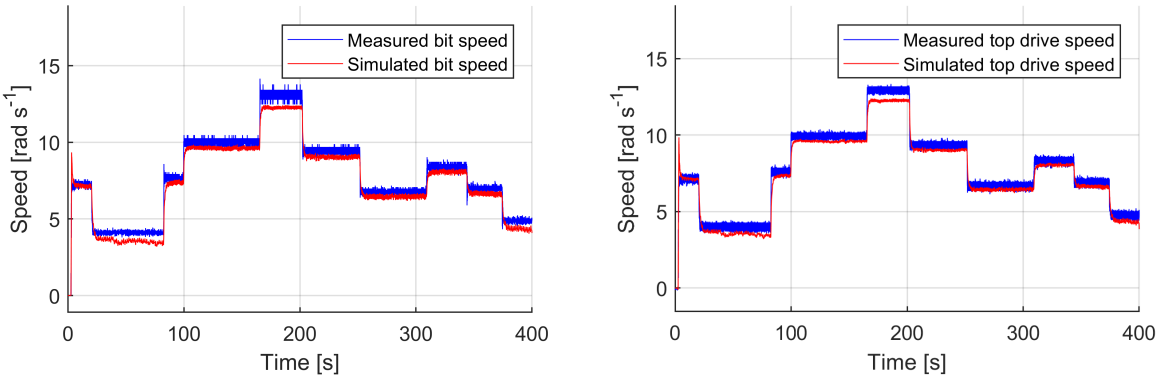

(a) Drill Bit Velocity (MSE $= 0.2695\text{rad}^2\text{s}^{-2}$). (b) Top drive velocity (MSE $= 0.1980\text{rad}^2\text{s}^{-2}$).

Figure 15: Result of least squares fit for parameter estimation of drill string.

3.4 SUMMARY AND CONCLUSIONS

To evaluate control algorithms that are designed to control the torsional oscillations of the drill string experimental evaluation is necessary. The experimental setup presented in this chapter can be used to evaluate control algorithms and parameter estimation algorithms. It may be pointed out that lateral vibrations in the drill string of the experimental setup can not be completely eliminated and hence any coupling

Table 5: Data acquisition rates and time duration of validation experiments.

DATA	SAMPLING FREQUENCY	DURATION	MEAN SQUARE ERROR (MSE) IN BIT SPEED
Figure 15	500Hz	400s	$0.2695\text{rad}^2\text{s}^{-2}$
Figure 16	500Hz	600s	$0.6180\text{rad}^2\text{s}^{-2}$
Figure 17	1000Hz	600s	$0.5468\text{rad}^2\text{s}^{-2}$
Figure 18	2000Hz	200s	$0.3250\text{rad}^2\text{s}^{-2}$
Figure 19	2000Hz	100s	$1.1307\text{rad}^2\text{s}^{-2}$
Figure 20	2000Hz	100s	$0.5508\text{rad}^2\text{s}^{-2}$
Figure 21	2000Hz	100s	$2.3348\text{rad}^2\text{s}^{-2}$
Figure 22	50Hz	2000s	$0.3520\text{rad}^2\text{s}^{-2}$

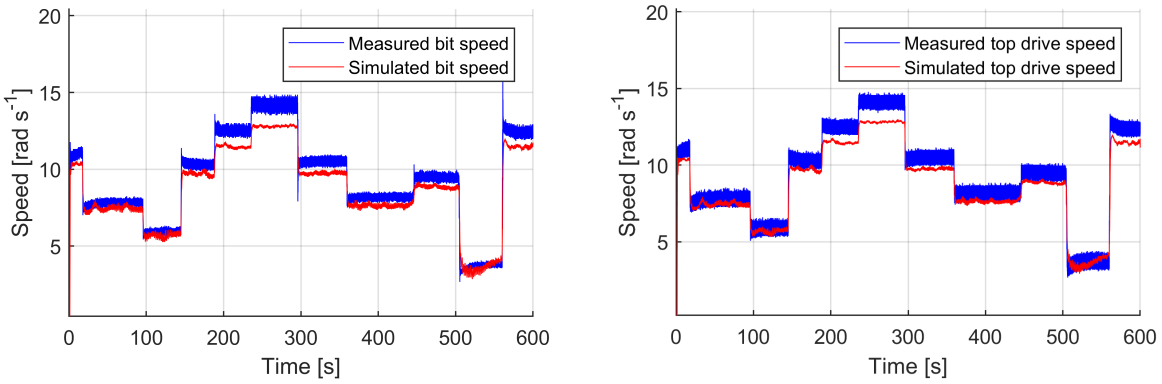

(a) Drill bit velocity (MSE $= 0.6180\text{rad}^2\text{s}^{-2}$). (b) Top drive velocity (MSE $= 0.5867\text{rad}^2\text{s}^{-2}$).

Figure 16: Result of least squares fit for parameter estimation of drill string.

between lateral and torsional dynamics is unmodeled. Another shortcoming of the experimental drill rig is that the length of the drill string does not change where as a real drill string lengthens during the drilling operation.

The parameter estimation procedure is straight forward in theory but in practice it is more challenging. Obtaining reliable input and output signals is crucial. Initial experiments by the author were not satisfactory because the input measurement channels were saturated by the PID speed controller that is built in to the ESCON 50/5 controller. During startup very high currents were produced by the improperly tuned ESCON 50/5 controller. This also lead to high torsional oscillations. This problem was masked by the low-pass filters that are built in to the ESCON 50/5 controller. To remedy the problem a better tuned PID controller was implemented in the Ds 1104 system. The unfiltered input signal was acquired and filtered offline before it was used for system identification. Many experimental drill strings use mo-

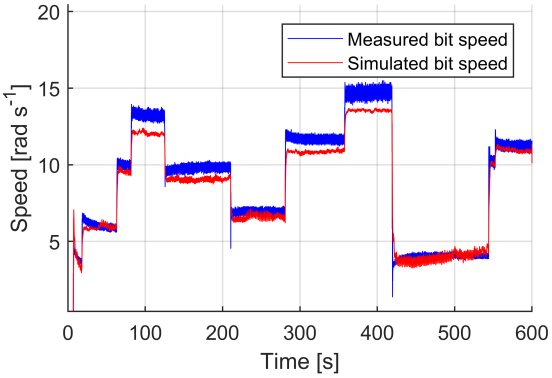

(a) Drill bit velocity (MSE $= 0.5468\text{rad}^2\text{s}^{-2}$).

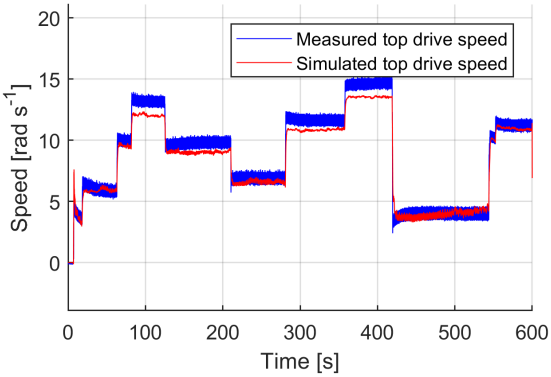

(b) Top drive velocity (MSE $= 0.5353\text{rad}^2\text{s}^{-2}$).

Figure 17: Result of a validation experiment using parameters identified for the experimental setup.

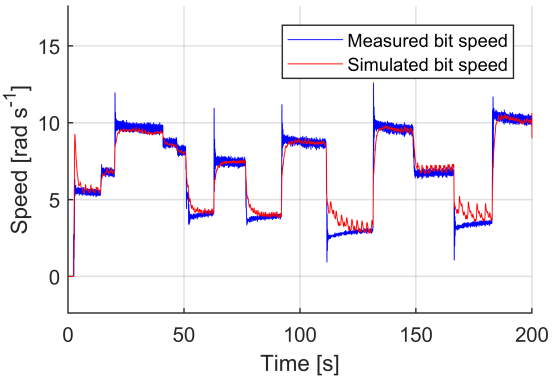

(a) Drill bit velocity (MSE $= 0.3250\text{rad}^2\text{s}^{-2}$).

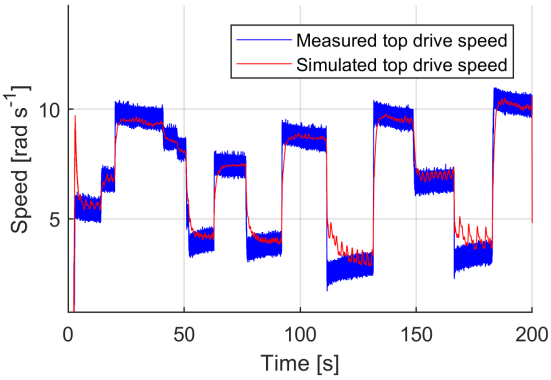

(b) Top drive velocity (MSE $= 0.4036\text{rad}^2\text{s}^{-2}$).

Figure 18: Result of a validation experiment using parameters identified for the experimental setup.

tors with built in PID controllers that may suffer from identical problems that must be addressed before carrying out a satisfactory system identification task.

The model validation results presented cover a larger operating range from 50 to 160RPM. At lower angular speeds the error between the simulated and measured speed increases. It is noticed that the identified model has high fidelity during the transient phase of the multistep inputs.

The torque on bit during multistep experiments was measured and it decreases as the angular speed is increased. To model this behaviour inclusion of the Stribeck effect in the friction model is necessary to obtain a system model that will be valid in the operating range of the drill string.

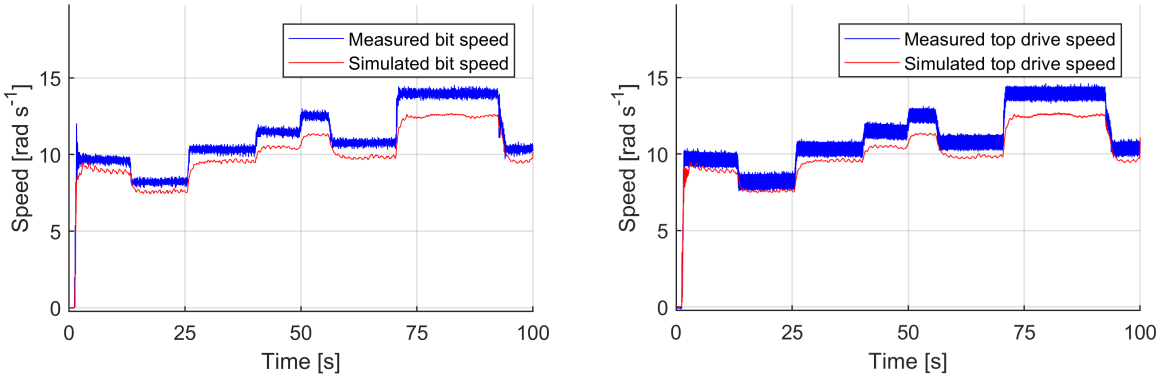

(a) Drill bit velocity (MSE $= 1.1307\text{rad}^2\text{s}^{-2}$). (b) Top drive velocity (MSE $= 1.0517\text{rad}^2\text{s}^{-2}$).

Figure 19: Result of a validation experiment using parameters identified for the experimental setup.

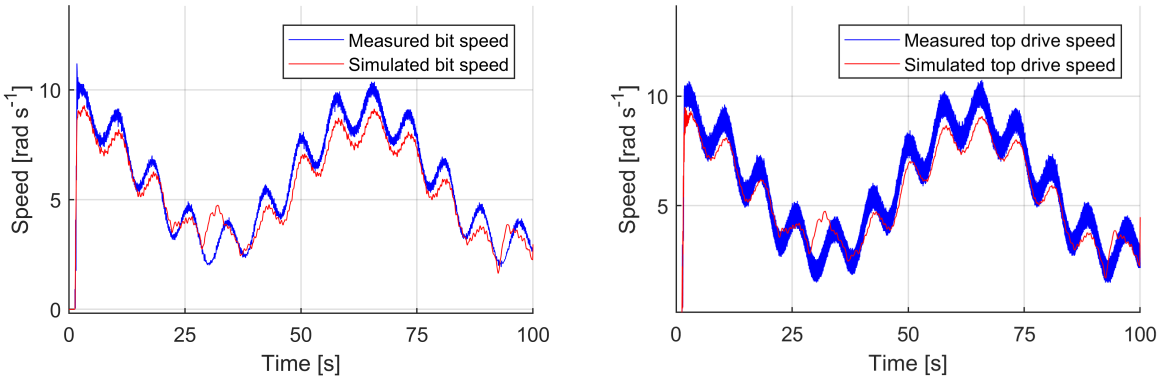

(a) Drill bit velocity (MSE $= 0.5508\text{rad}^2\text{s}^{-2}$). (b) Top drive velocity (MSE $= 0.5955\text{rad}^2\text{s}^{-2}$).

Figure 20: Result of a validation experiment using parameters identified for the experimental setup.

Experiments on the drill string show that the friction is difficult to model accurately at low speeds. It is observed from experiments carried out on the drill string that sensor noise at low speeds is more pronounced which makes the parameter estimation task difficult. Furthermore, the friction of the surface may change with change in temperature and wear and tear of the setup also effects the friction levels.

The uncertain nature of frictional torque on bit of a drill string will make model based friction compensation techniques difficult to implement in practice. To deal with the varying friction, control algorithms need to be either robust to modelling errors or be able to adapt. Therefore in the next part robust and adaptive control algorithms will be evaluated.

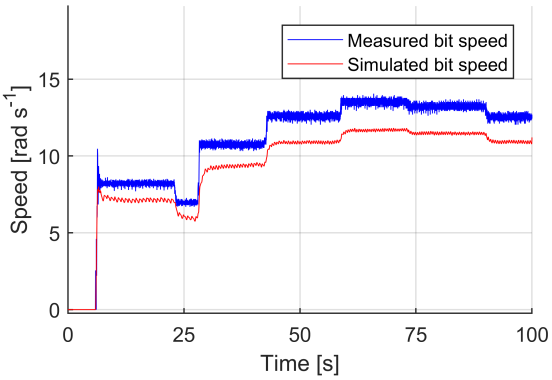

(a) Drill bit velocity (MSE $= 2.3348\text{rad}^2\text{s}^{-2}$).

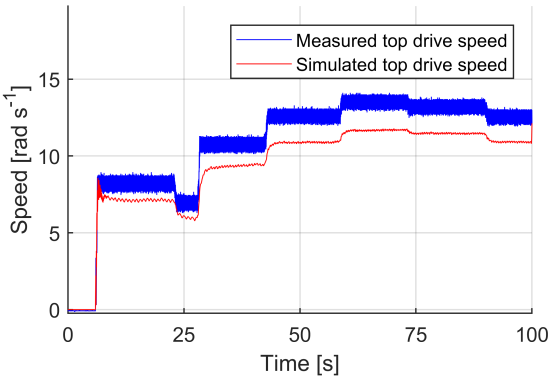

(b) Top drive velocity (MSE $= 2.2097\text{rad}^2\text{s}^{-2}$).

Figure 21: Result of a validation experiment using parameters identified for the experimental setup.

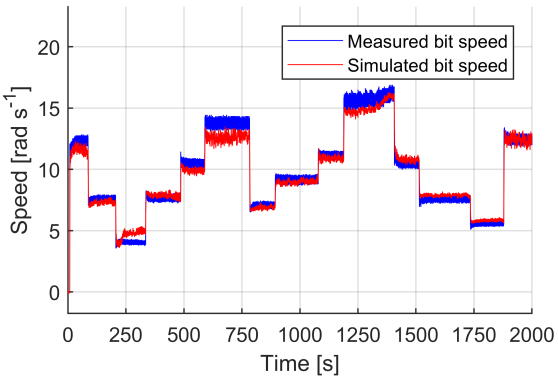

(a) Drill bit velocity (MSE $= 0.3520\text{rad}^2\text{s}^{-2}$).

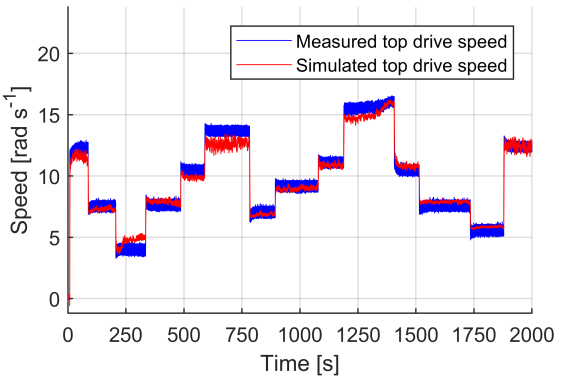

(b) Top drive velocity (MSE $= 0.3948\text{rad}^2\text{s}^{-2}$).

Figure 22: Result of a validation experiment using parameters identified for the experimental setup.

Part II

CONTROL DESIGN

This part of the thesis deals with observer based control design drill string. The backstepping approach to control torsional oscillation in a drill string is introduced in Chapter 4. A tuning function based adaptive backstepping control approach that uses a filtered observer is evaluated in chapter 5. In chapter 6 a robust dynamic surface control approach is evaluated. Summary and conclusions are presented in chapter 7. This part of this thesis thus constitutes the main contributions to control of drill string torsional vibrations.

4

FULL STATE FEEDBACK BACKSTEPPING CONTROL

In this chapter, a robust full state feedback backstepping control for attenuation of torsional oscillations in a drill string is presented on the basis of which more complex observer based adaptive and observer based robust controllers will be designed in the next chapters. In the first section, basic tools used to determine stability for nonlinear systems are discussed. In the second section, the integrator backstepping control is explained. In the third section, of this chapter, ways to make the backstepping control robust to modelling errors are presented. In the last section a robust controller designed to attenuate torsional oscillations in the drill string is presented.

4.1 NONLINEAR CONTROL

Most of the mechanical systems that have moving parts will have nonlinear behaviour caused by phenomenon such as friction. The class of nonlinear finite dimensional systems that are considered here are given by (Horacio 2003)

$$\dot{\boldsymbol{x}} = \boldsymbol{f}(\boldsymbol{x}, t, \boldsymbol{u}), \tag{4.1}$$

where $\boldsymbol{x}$ is the state variable vector, t is the time and $\boldsymbol{u}$ is the input vector. The systems studied in this chapter are restricted to a subclass of systems represented by equation 4.1 called time-invariant systems. Time-invariant systems do not depend explicitly on time. Time-invariant systems can be represented by

$$\dot{\boldsymbol{x}} = \boldsymbol{f}(\boldsymbol{x}, \boldsymbol{u}). \tag{4.2}$$

The objective pursued in this work is to stabilize in some sense the system represented by equation 4.2. To make the concept of stability clear some notions and definitions of stability will be presented in the next section.

4.1.1 *Notions of stability*

It is important to define the stability notions that will be used throughout the dissertation. Stability in the sense of Lyapunov categorizes the equilibrium point of the system as stable, asymptotically stable and uniformly stable. If the right hand side of the system in equation 4.2 is Lipschitz [1] with respect to $\boldsymbol{x} \in \mathbb{R}^n$, then it has a unique solution. Let $\boldsymbol{x_e}$ be an equilibrium point. The equilibrium point can be shifted to the origin without loss of generality. The three types of stable equilibria are defined as follows:

1 A function $\boldsymbol{f}(t, \boldsymbol{x})$ is Lipschitz if it satisfies the inequality $||\boldsymbol{f}(t, \boldsymbol{x}) - \boldsymbol{f}(t, \boldsymbol{y}) \leq L||\boldsymbol{x} - \boldsymbol{y}||$, where L is a positive constant. Any p-norm is denoted by $||\cdot||$.

1. The equillibrium point of the system is stable in the sense of Lyapunov if at initial time $t = t_0$, $\boldsymbol{x}(t_0)$ for any $\epsilon > 0$ there exists a $\delta(t_0, \epsilon) > 0$ such that any trajectory starting with in $||\boldsymbol{x}(t_0)|| < \delta$ remains confined to $||\boldsymbol{x}(t)|| < \epsilon$ for all $t > 0$. This is illustrated in Figure 23a.

2. A uniformly stable equilibrium point is a stable equilibrium point for which δ is not a function of t_0.

3. An equilibrium point $\boldsymbol{x_e} = \mathbf{0}$ is asymptotically stable if $\boldsymbol{x_e}$ is stable and furthermore the equilibrium point $\boldsymbol{x_e}$ is attractive which means any trajectory starting within $||\boldsymbol{x_0}|| < \delta$ converges to $\lim_{t\to\infty} \boldsymbol{x}(t) = \mathbf{0}$, as shown in Figure 23b.

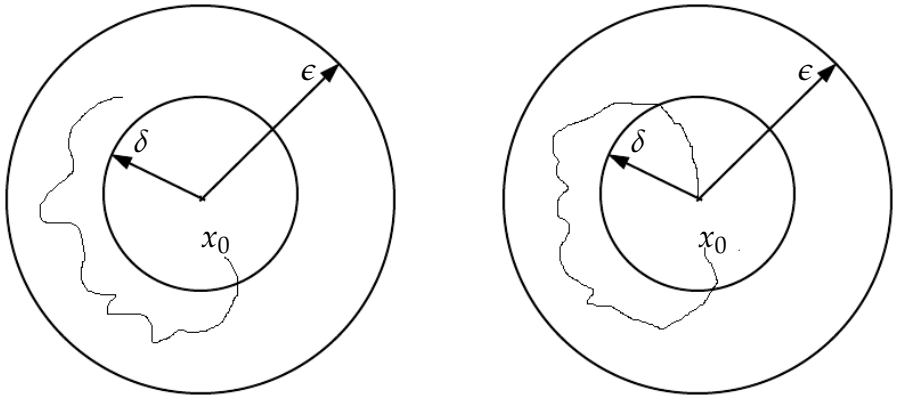

(a) Stable equillibrium point.

(b) Asymptotically stable equillibrium point.

Figure 23: Stability notions.

4.1.2 *Lyapunov's Direct Method*

The stability of a system is determined using Lyapunov's direct method in this dissertation, therefore it is briefly described here. Also known as Lyapunov's second method. To check if a system is stable the definitions given in Section 4.1.1 require solutions of the system of differential equations, but this is not possible for many problems. The Lyapunov's direct method provides a means of certifying the stability of a system without explicitly solving the differential equation. A system is stable if its energy decreases with time. The Lyapunov's second method generalized this notion of stability, i.e., stability can be proven if any scalar function $V(\boldsymbol{x})$ that satisfies certain properties can be found. To state the theorem the following five terms are defined (Hedrick and Girard 2005; Slotine and Li 1991):

1. $V(\boldsymbol{x}, t)$ is positive definite if a scalar function $\beta(.)$ exists such that $\beta(0) = 0$ and $\forall \boldsymbol{x} \neq 0, 0 < \beta(\|\boldsymbol{x}\|) < V(\boldsymbol{x}, t)$.

2. The time derivative of $V(\boldsymbol{x}, t)$ taken along the trajectories of $\dot{\boldsymbol{x}} = \boldsymbol{f}(\boldsymbol{x}, t)$ is $\dot{V}(\boldsymbol{x}, t) = \frac{\partial V}{\partial \boldsymbol{x}^T} \boldsymbol{f}(\boldsymbol{x}, t)$.
3. $\dot{V}(\boldsymbol{x}, t)$ is negative definite if $\dot{V}(\boldsymbol{x}, t) \leq -\beta(\|\boldsymbol{x}\|) < 0$.
4. $V(\boldsymbol{x}, t)$ is decrescent i.e bounded from above if $V(\boldsymbol{x}, t) < \beta(\|\boldsymbol{x}\|)$.
5. $V(\boldsymbol{x}, t)$ is radially unbounded if $V(\boldsymbol{x}, t)$ becomes infinity as $\|\boldsymbol{x}\|$ becomes infinity.

Lyapunov's direct method states that if the time derivative of $V(\boldsymbol{x}, t)$ along the system trajectories is negative definite then the equilibrium point is asymptotically stable. If it is negative semidefinite then its only stable. Furthermore, if the Lyapunov function $V(\boldsymbol{x}, t)$ is decrescent then the stability is uniform. If $V(\boldsymbol{x}, t)$ is radially unbounded the stability properties hold globally.

4.1.3 *LaSalle's Invariance Principle*

Asymptotic stability is desired but often the derivative of the Lyapunov function is not negative definite but negative semidefinite. LaSalle's invariant set theorems prove convergence of the trajectory to the largest invariant set which is the union of equilibrium points and the limit cycle of a system (Slotine and Li 1991).

4.1.4 *Control Lyapunov function (CLF)*

The Lyapunov's second method can be used to find if the equilibrium point of a system is stable. The CLF is an extension of the Lyapunov function concept. A control Lyapunov function can be used to stabilize the equillibrium point of a system using feedback. To explain this consider a system

$$\dot{\boldsymbol{x}} = \boldsymbol{f}(\boldsymbol{x}, u),\ \boldsymbol{x} \in \mathbb{R}^n,\ u \in \mathbb{R}, \boldsymbol{f}(\boldsymbol{0}, 0) = \boldsymbol{0}. \tag{4.3}$$

The goal is to find feedback $u = \alpha(\boldsymbol{x})$, such that the system described by equation 4.3 is asymptotically stable. This can be accomplished when a control Lyapunov function $V(\boldsymbol{x})$ is found, such that its derivative along the trajectories of the system represented by equation 4.3 is negative definite. If $W(\boldsymbol{x})$ is a positive definite function then then the sufficient condition for a stabilizing feedback to exist is

$$\frac{\partial V(\boldsymbol{x})}{\partial \boldsymbol{x}^T} \boldsymbol{f}(\boldsymbol{x}, \alpha(\boldsymbol{x})) \leq -W(\boldsymbol{x}) \quad \forall\, \boldsymbol{x} \in \mathbb{R}^n. \tag{4.4}$$

To further elaborate how the CLF is used a scalar system

$$\dot{x} = -x^3 + x^2 + u, \tag{4.5}$$

is considered. A control Lyapunov function for system of equation 4.5 can be chosen as $V(x) = \frac{1}{2}x^2$. A feedback linearizing input to stabilize the system of equation 4.5 about its origin is

$$u = -x^2 + x^3 - x. \tag{4.6}$$

The derivative of $V(x)$ along the trajectories of system described by equation 4.5 is

$$\dot{V}(x) = x\dot{x} = -x^4 + x^3 + x^4 - x^3 - x^2 = -x^2, \tag{4.7}$$

which is negative definite. Hence $V(x)$ is a control Lyapunov function. The system is asymptotically stabilized about the origin using designed u.

It must be noted if the term $-x^3$ is not cancelled using the input u. The Lyapunov derivative along the trajectories of the system with this term present will remain negative definite. Therefore it is not necessary to cancel this term. The control law can be made robust by avoiding unnecessary cancellation of $-x^3$ term which is stabilizing for the system and one could have used $u = -x^2 - x$.

4.2 BACKSTEPPING

Backstepping is a constructive method to develop control Lyapunov functions for feedback stabilization (Kokotović and Arcak 2001). It is applicable to systems in the strict feedback form but is explained using an integral feedback system

$$\dot{x} = f(x) + g(x)\xi, \tag{4.8}$$

and

$$\dot{\xi} = u, \tag{4.9}$$

where $f(x)$ and $g(x)$ are nonlinear functions. The states are given by x and ξ. The input is represented by u.

The system represented by equation 4.8 and equation 4.9 is called unmatched because no control action appears in equation 4.8 and the input u is separated from the equation 4.8 by an integrator. The system can be viewed as a cascade of two subsystems where the input u enters the system via an integrator as shown in Figure 24. In the first step the origin of the system $\dot{x} = f(x) + g(x)\xi$ is first stabilized by using the state $\xi = \alpha(x)$ as the so called virtual control input. This objective is realized if we can find a Lyapunov function $V(x)$ that has a derivative

$$\frac{\partial V}{\partial x}[f(x) + g(x)\alpha(x)] \leq -W(x), \tag{4.10}$$

along the trajectories of the system, where $W(x)$ is positive definite.

Since there is no input in equation 4.8, the state ξ is used as the virtual control input. To do this a virtual function $\alpha(x)$ is used. To introduce the virtual control function into equation 4.8, the term $g(x)\alpha(x)$ is added into and subtracted from equation 4.8 and the system equations

$$\dot{x} = [f(x) + g(x)\alpha(x)] + g(x)[\xi - \alpha(x)], \tag{4.11}$$

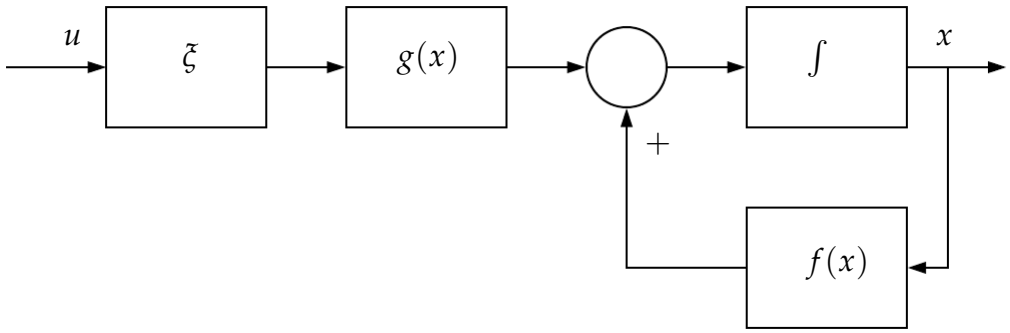

Figure 24: Integrator backstepping.

and

$$\dot{\xi} = u, \tag{4.12}$$

are obtained. The first backstepping variable defined as $z_1 = \xi - \alpha(x)$ is substituted into equation 4.11 to obtain system of equations

$$\dot{x} = [f(x) + g(x)\alpha(x)] + g(x)z_1, \tag{4.13}$$

and

$$\dot{z}_1 = u - \dot{\alpha}(x). \tag{4.14}$$

The virtual control is backstepped through an integrator as can be seen in Figure 25.

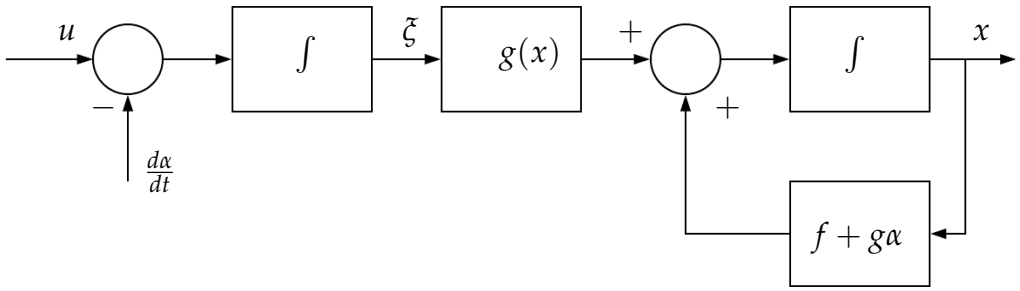

Figure 25: Shows $\dot{\alpha}$ backstepped through integrator..

Note that the derivative $\dot{\alpha}(x)$ is known. Setting $v = u - \dot{\alpha}(x)$ the equations

$$\dot{x} = [f(x) + g(x)\alpha(x)] + g(x)z_1, \tag{4.15}$$

and

$$\dot{z}_1 = v \tag{4.16}$$

are obtained. The stability of the above system represented by equation 4.15 and equation 4.16 can be checked using the Lyapunov candidate function

$$V_c(x,\xi) = V(x) + \frac{1}{2}z_1^2. \tag{4.17}$$

The derivative $\dot{V}_c(x,\xi)$ along the system represented by equation 4.15 and equation 4.16 is

$$\dot{V}_c(x,\xi) = \dot{V}(x) + z_1\dot{z}_1. \tag{4.18}$$

The equation 4.18 can be written as

$$\dot{V}_c(x,\xi) = -W(x) + \frac{\partial V}{\partial x}g(x)z_1 + z_1 v, \tag{4.19}$$

after substituting values of $\dot{V}(x)$ and $\dot{z}_1$ into equation 4.18. To make equation 4.19 negative definite in order to to stabilize the whole system about the origin the input

$$v = -\frac{\partial V}{\partial x}g(x) - kz_1, \tag{4.20}$$

is chosen where $k > 0$. The Lyapunov derivative in equation 4.19 becomes

$$\dot{V}_c(x,\xi) \leq -W(x) - kz_1^2, \tag{4.21}$$

after substituting equation 4.20 into equation 4.19. $\dot{V}_c(x,\xi)$ is negative definite. This implies that the origin $x = 0$ and $\xi = 0$ is asymptotically stable. The backstepping control algorithms can be applied to systems in a special form known as the strict feedback form described in the next section.

4.2.1 *Strict feedback form*

Backstepping is applicable in general to systems in the Strict feedback form also known as triangular form as the nonlinearity depends only on variables that are fed back (Horacio 2003) the general form is

$$\begin{aligned}
\dot{\boldsymbol{x}} &= \boldsymbol{f}(\boldsymbol{x}) + \boldsymbol{g}(\boldsymbol{x})\xi_1,\\
\dot{\xi}_1 &= f_1(\boldsymbol{x},\xi_1) + g_1(\boldsymbol{x},\xi_1)\xi_2,\\
\dot{\xi}_2 &= f_2(\boldsymbol{x},\xi_1,\xi_2) + g_2(\boldsymbol{x},\xi_1,\xi_2)\xi_3,\\
&\vdots\\
\dot{\xi}_{k-1} &= f_{k-1}(\boldsymbol{x},\xi_1,\xi_2,\cdots,\xi_{k-1}) + g_{k-1}(\boldsymbol{x},\xi_1,\xi_2,\cdots,\xi_{k-1})\xi_k,\\
&\textit{and}\\
\dot{\xi}_k &= f_k(\boldsymbol{x},\xi_1,\xi_2,\cdots,\xi_k) + g_k(\boldsymbol{x},\xi_1,\xi_2,\cdots,\xi_k)u,
\end{aligned} \tag{4.22}$$

where $x \in \mathbb{R}^n$, $\xi \in \mathbb{R}$, f_i and g_i are smooth nonlinearities.

4.3 ROBUST BACKSTEPPING USING NONLINEAR DAMPING

Backstepping control shares some features with a nonlinear control method called feedback linearization. In feedback linearization a model of the nonlinearity is fed back into the system via the input to cancel the nonlinearity and make the system linear about the equillibrium point. There is a difference between feedback linearization and backstepping. In feedback linearization the nonlinearity is canceled leaving the system linearized. This is not robust as the nonlinearity has to be modelled exactly. In backstepping there is flexibility in the design i.e. only the unwanted components of the nonlinearity may be canceled leaving the useful or good nonlinearities in the system. Bad or unstabilizing nonlinearities are usually dominated using nonlinear damping (Fossen and Strand 1999).

To illustrate the idea a second order system can be considered as shown in Figure 26 modelled by the differential equations (Fossen and Strand 1999)

$$\dot{x}_1 = f(x_1) + x_2, \tag{4.23}$$

$$\dot{x}_2 = u, \tag{4.24}$$

and

$$y = x_1, \tag{4.25}$$

where $x_1 \in \mathbb{R}$, $x_2 \in \mathbb{R}$, $u \in \mathbb{R}$ and $y \in \mathbb{R}$. The purpose of control is to regulate output asymptotically to zero. As the system has two states x_1 and x_2 the recursive backstepping procedure is carried out in two steps. The system represented by equation 4.23 and equation 4.24 is considered as a single cascaded system as shown in Figure 26. In each backstepping step a transformation is used to introduce a new set of variables[2]. The objective is to regulate the output $y = x_1$ to zero. Therefore the first backstepping variable

$$z_1 = x_1, \tag{4.26}$$

is chosen. To stabilize the origin of the system given in equation 4.23, the state

$$x_2 = \alpha_1 + z_2, \tag{4.27}$$

is used as the virtual control input. Where α_1 is the first desired virtual control function and $z_2 = x_2 - \alpha_1$ is the second backstepping error. The derivative of z_1 in equation 4.26 is

$$\dot{z}_1 = \dot{x}_1 = f(x_1) + \alpha_1 + z_2, \tag{4.28}$$

2 $z_i = \phi(x_i)$ where $i = 1, 2, ..$

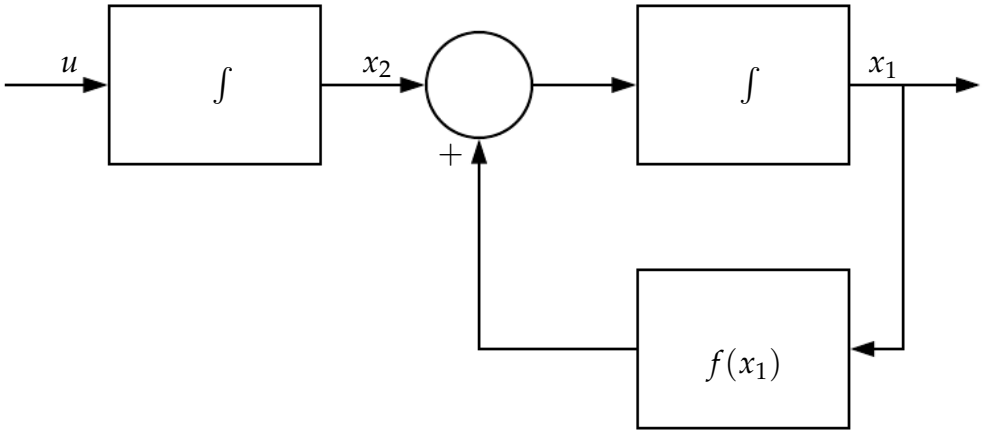

Figure 26: Cascaded system representation.

which describes the error dynamics for the first error system. A Lyapunov function

$$V_1 = \frac{1}{2} z_1^2, \tag{4.29}$$

is chosen to stabilize the origin of the first error system. The derivative of the Lyapunov function in equation 4.29 is

$$\dot{V}_1 = z_1 \dot{z}_1, \tag{4.30}$$

which becomes

$$\dot{V}_1 = z_1 f(x_1) + z_1 \alpha_1 + z_1 z_2, \tag{4.31}$$

after substituting expression for $\dot{z}_1$ from equation 4.28 into equation 4.30. To make the Lyapunov derivative in equation 4.31 negative definite the feedback linearizing control law can be designed with the virtual control function

$$\alpha_1 = -f(x_1) - k_1 z_1. \tag{4.32}$$

After substituting value of α_1 from equation 4.32 into equation 4.28, the error dynamics

$$\dot{z}_1 = -k_1 z_1 + z_2, \tag{4.33}$$

are obtained. Substituting value of $\dot{z}_1$ from equation 4.33 into equation 4.30, the derivative

$$\dot{V}_1 = -k_1 z_1^2 + z_1 z_2, \tag{4.34}$$

is obtained. The first term term of this Lyapunov function is negative definite. The second term namely $z_1 z_2$, is made negative definite in the second backstepping step. Taking derivative of equation 4.27 the second error system

$$\dot{z}_2 = \dot{x}_2 - \dot{\alpha}_1, \tag{4.35}$$

is obtained. Which becomes

$$\dot{z}_2 = u - \dot{\alpha}_1, \tag{4.36}$$

after substituting in equation 4.35 the value of $\dot{x}_2$ from equation 4.24. The augmented Lyapunov candidate function is constructed in the second backstepping step to stabilize the whole system about the origin is

$$V_2 = V_1 + \frac{1}{2} z_2^2. \tag{4.37}$$

The derivative of V_2 is

$$\dot{V}_2 = \dot{V}_1 + z_2 \dot{z}_2. \tag{4.38}$$

After substituting expressions for $\dot{V}_1$ and $\dot{z}_2$ into equation 4.38 the Lyapunov derivative

$$\dot{V}_2 = -k_1 z_1^2 + z_1 z_2 + z_2 \dot{z}_2 = -k_1 z_1^2 + z_2 (u - \dot{\alpha}_1 + z_1), \tag{4.39}$$

is obtained. To make the Lyapunov derivative negative definite and asymptotically stabilize the origin of the system as per Lyapunov's direct method the input

$$u = \dot{\alpha}_1 - z_1 - k_2 z_2, \tag{4.40}$$

is designed, where $k_2 > 0$. This is illustrated in the block diagram of Figure 27. The implementation of this control law is discussed in the next section.

4.3.1 *Derivative implementation in the control law*

In the implementation of control law of equation 4.40 a derivative term $\dot{\alpha}_1$ has to be calculated. For known systems this can be calculated analytically. In the example system presented in the previous section the derivative

$$\dot{\alpha}_1 = \frac{\partial f(x_1)}{\partial x_1} - k_1 \dot{x}_1, \tag{4.41}$$

can be obtained analytically (Fossen and Strand 1999). But there is increase in the number of terms in the derivative at each subsequent backstepping step which makes control design for higher order systems cumbersome. In the next section robustification of backstepping control is discussed.

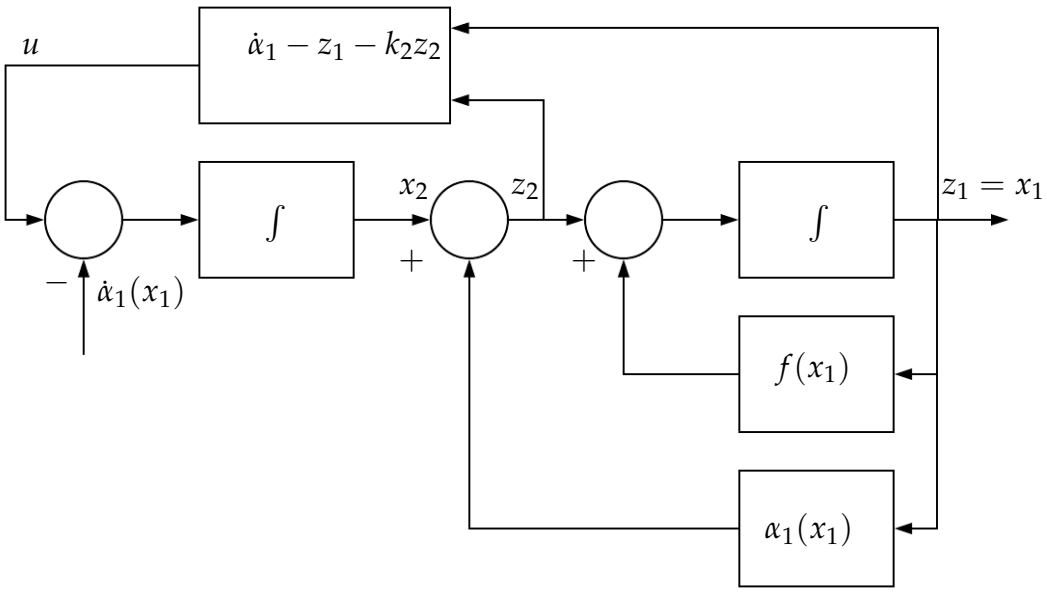

Figure 27: Stabilization of the system using backstepping control law (Fossen and Strand 1999).

4.3.2 *Avoiding cancellations of good nonlinearities*

The backstepping control law of equation 4.40 is a feedback linearizing control law as in the first step of backstepping the virtual control function of equation 4.32 was designed to cancel $f(x_1)$. This required $f(x_1)$ to be known exactly and this approach is not robust against modelling errors. If the nonlinearity

$$f(x_1) = -a_0 x_1 - a_1 x_1^3 + a_2 x_1^2, \tag{4.42}$$

then $-a_0 x_1$ and $-a_1 x_1^3$ are the good nonlinearities because they make the Lyapunov derivative in equation 4.31 negative definite. But $a_2 x_1^2$ is a bad nonlinearity that will cause system instability and introduce a positive definite term in $\dot{V}_1$. This term should be cancelled.

4.3.3 *Stabilization using nonlinear damping*

To explain how the nonlinear damping can be used stabilize an equillibrium point. The nonliner function

$$f(x_1) = \phi(x_1)\Delta(t), \tag{4.43}$$

which is a bounded uncertain function where $\phi(x)$ is a known smooth function and $\Delta(t)$ is a bounded function which describes the bound of $f(x_1)$. In this case the virtual control function of equation 4.32 can be modified to

$$\alpha_1 = -k_1 z_1 - k_2 z_1 \phi(x_1)^2 = -k_1 z_1 - k_2 z_1 \phi(z_1)^2. \tag{4.44}$$

The derivative of the Lyapunov function along the trajectories of equation 4.28 is $\dot{V}_1 = z_1 f(z_1) + z_1\alpha_1 + z_1 z_2$, as given in equation 4.31. The derivative $\dot{V}_1$ for the modified system where $f(z_1) = \phi(z_1)\Delta(t)$ is

$$\dot{V}_1 = z_1\phi(x_1)\Delta(t) + z_1\alpha_1 + z_1 z_2. \tag{4.45}$$

Substituting expression for α_1 in equation 4.45,

$$\dot{V}_1 = z_1\phi(x_1)\Delta(t) - k_1 z_1^2 - k_2 z_1^2\phi(z_1)^2 + z_1 z_2, \tag{4.46}$$

is obtained. The term $z_1 z_2$ is handled in the second backstepping step so only the the first three terms should be negative definite in the first backstepping step. Using the Young's inequality (Krstic, Kanellakopoulos, and Kokotovic 1995: 75)

$$xy \leq k_2 x^2 + \frac{1}{4k_2}y^2,\ k_2 > 0, \tag{4.47}$$

the first term of equation 4.46 can be expressed as

$$z_1\phi(z_1)\Delta(t) \leq k_2 z_1^2\phi(z_1)^2 + \frac{\Delta(t)^2}{4k_2}. \tag{4.48}$$

Substituting equation 4.48 into equation 4.46 it is seen that the first three terms of the derivative $\dot{V}_1$ are negative definite if $|z_1| > \frac{|\Delta(t)|}{2\sqrt{k_1 k_2}}$ (Krstic, Kanellakopoulos, and Kokotovic 1995: 75). This shows how nonlinear damping stabilizes the origin of system in the presence of uncertainty. The remaining backstepping control design steps are the same as in the previous example and are not repeated.

4.4 ROBUST BACKSTEPPING TO REDUCE TORSIONAL OSCILLATIONS IN A DRILL STRING

In this section a full state feedback backstepping control approach is developed and simulated using physical parameters of a full scale drilling rig. Abdulgalil and Siguerdidjane (2005) developed a backstepping approach for drill string torsional oscillation attenuation that uses a lumped parameter model, the backstepping approach uses one of the states as a virtual control function. The state used as virtual control represents the difference in angular displacement between the top drive and drill bit. In three steps the whole system is stabilized in the Lyapunov sense. The nonlinearity in the system is cancelled using the virtual control function and a robust controller is designed and simulated. The nonlinearity is assumed to be known in Abdulgalil and Siguerdidjane (2005) and is cancelled. The control design presented here removes the need for completely cancelling the nonlinearity which if not exactly estimated may lead to errors. Furthermore, nonlinear damping is used to stabilize the system.

The mathematical model is derived assuming a vertical drill string where the mud flow is assumed non turbulent and any lateral or axial vibrations of the drill string

are neglected. The system is modelled using a 2 degree of freedom lumped parameter model. The mathematical model developed in chapter 2 given by equation 2.2 and equation 2.3 can be used. The friction in the top drive is assumed to be dominated by viscous friction so $T_r(x_1)$ in equation 2.2 is neglected. The state space representation of the 2 DOF drill string is

$$\dot{\mathbf{x}} = \begin{bmatrix} -\frac{c_b}{J_2} & \frac{k_t}{J_2} & 0 \\ -1 & 0 & 1 \\ 0 & -\frac{k_t}{J_1} & -\frac{c_r}{J_1} \end{bmatrix} \begin{bmatrix} x_1 \\ x_2 \\ x_3 \end{bmatrix} + \begin{bmatrix} \frac{-T_{fb}(x_1)}{J_2} \\ 0 \\ \frac{T_m}{J_1} \end{bmatrix}, \tag{4.49}$$

with states

$$\mathbf{x} = \begin{bmatrix} x_1 \\ x_2 \\ x_3 \end{bmatrix} = \begin{bmatrix} \dot{\theta}_2 \\ \theta_2 - \theta_1 \\ \dot{\theta}_1 \end{bmatrix}. \tag{4.50}$$

The torque on bit due to friction is modelled using a static dry friction model (Navarro-López and Suárez 2004) given by

$$T_{fb}(x_1) = W_{ob} \cdot R_b \cdot (\mu_{cb} + (\mu_{sb} - \mu_{cb})e^{-\gamma_b |x_1|}) \tanh(\alpha x_1). \tag{4.51}$$

The torque due to friction depends on the velocity of bit x_1, weight on bit W_{ob}, radius of the drill bit R_b. The coulomb friction coefficient is μ_{cb} and the static friction coefficient is μ_{sb}. The term $\tanh \alpha x_1$ approximates the sign function in the dry friction model, where α is a constant, the higher its value the closer the $\tanh(\alpha x_1)$ function will resemble the sign nonlinearity. The positive constant γ_b in the static dry friction model will have a value equal to the reciprocal of the absolute value of Stribeck velocity. To simulate the system the expression for the torque on bit given in equation 4.51 is used.

To apply the backstepping technique, the system described by equation 4.49 has to be written in the strict feedback form

$$\dot{x}_1 = \frac{-T_{fb}(x_1)}{J_2} - \frac{c_b}{J_2} x_1 + \frac{k_t}{J_2} x_2, \tag{4.52}$$

$$\dot{x}_2 = x_3 - x_1, \tag{4.53}$$

and

$$\dot{x}_3 = -\frac{k_t}{J_1} x_2 - \frac{c_r}{J_1} x_3 + \frac{T_m}{J_1}. \tag{4.54}$$

The controller is designed using a recursive backstepping approach. Three error systems are formulated. The first nonlinear error system is stabilized to zero in the sense of Lyapunov since this system does not have any direct control input, a state variable is chosen as a virtual control input for this system. The virtual control function α_1, which is a function of the states, is designed to make the origin of first error system a stable equilibrium point and nonlinear damping is used to dominate the destabilizing nonlinearities in the first system. Similarly, the second error system is also stabilized to make its origin a stable equilibrium point in the sense of Lyapunov using a second virtual control α_2 which is also a function of the system states. The whole design is completed in three steps. The last error system has the real input, which is chosen to make the origin of the whole error system a stable equillibrium point (Ullah, Duarte, and Bohn 2016a). The virtual control α_1 is effectively backstepped through two integrators, whereas virtual control α_2 is backstepped through a single integrator. Since the aim is not to compensate the nonlinearity (torque due to friction) completely, therefore there is no need to have an exact model of the nonlinearity.

The objective is for the drill bit angular velocity x_1 to follow the desired velocity ω_d. Defining the error as

$$z_1 = \omega_d - x_1. \tag{4.55}$$

The derivative of equation 4.55 is

$$\dot{z}_1 = -\dot{x}_1. \tag{4.56}$$

Substituting value of $\dot{x}_1$ from equation 4.52 into equation 4.56 the error dynamics

$$\dot{z}_1 = \frac{T_{fb}(x_1)}{J_2} + \frac{c_b}{J_2}x_1 - \frac{k_t}{J_2}x_2, \tag{4.57}$$

are obtained. The error dynamics becomes

$$\dot{z}_1 = \frac{T_{fb}(\omega_d - z_1)}{J_2} + \frac{c_b}{J_2}(\omega_d - z_1) - \frac{k_t}{J_2}x_2, \tag{4.58}$$

after substituting expression for x_1 from equation 4.55 into equation 4.57. It is assumed that the drill bit never reverses direction which happens very rarely (Jansen and Steen 1995) but can get stuck. If the error is within certain limits the bit torque variation around the set point can be approximated by a quadratic polynomial (Kabziński 2014; Nouailletas, Mendes, and Koenig 2010) shown in Figure 28.

The general form of the polynomial with p_1, p_2 and p_3 as positive coefficients is

$$T_{fb}(\omega_d - z_1) = p_1 - p_2 z_1 + p_3 z_1^2. \tag{4.59}$$

Substituting equation 4.59 into equation 4.58 the error system

$$\dot{z}_1 = \frac{p_1 - p_2 z_1 + p_3 z_1^2}{J_2} + \frac{c_b}{J_2}(\omega_d - z_1) - \frac{k_t}{J_2}x_2, \tag{4.60}$$

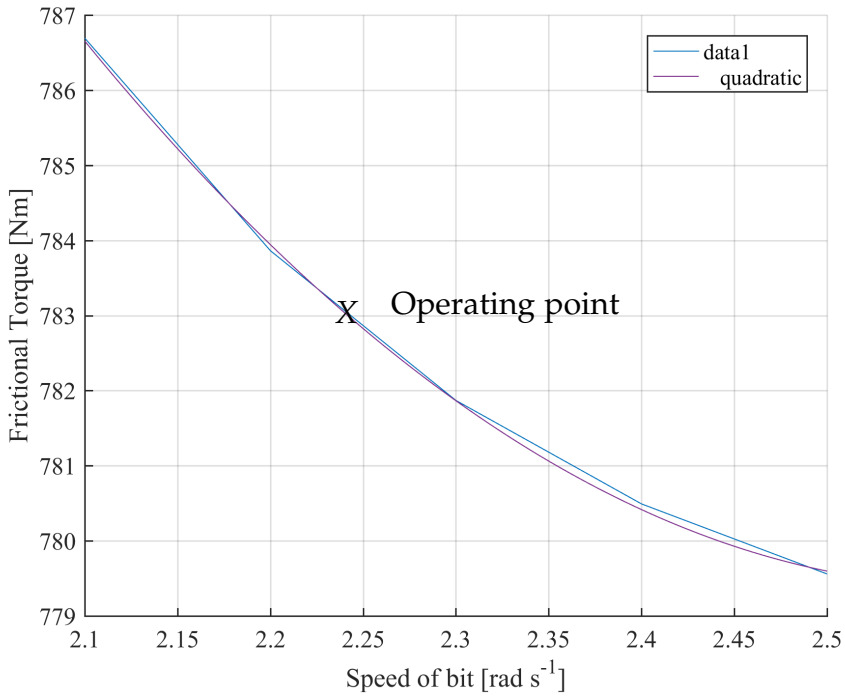

Figure 28: Torque variation approximated about the set point using a quadratic polynomial for parameter values given in Table 6.

is obtained. In the transformed variables the objective in first backstepping step is to regulate the error z_1 to zero, but there is no control input to do this as the system is underactuated. Hence the state x_2 is used as the virtual control input. The objective is to make x_2 follow a desired virtual control function α_1. Hence the second backstepping variable or error variable z_2 is introduced, the virtual input

$$x_2 = z_2 + \alpha_1, \tag{4.61}$$

is used to make the origin of the first error system a stable equilibrium point. The second backstepping variable is

$$z_2 = x_2 - \alpha_1. \tag{4.62}$$

Taking derivative of equation 4.62 the second error system

$$\dot{z}_2 = \dot{x}_2 - \dot{\alpha}_1, \tag{4.63}$$

is obtained. Substituting equation 4.62 in equation 4.60 the first error system

$$\dot{z}_1 = \frac{p_1 - p_2 z_1 + p_3 z_1^2}{J_2} + \frac{c_b}{J_2}(\omega_d - z_1) - \frac{k_t}{J_2}(z_2 + \alpha_1), \tag{4.64}$$

is obtained. To prove stability of the error system of equation 4.64 a candidate Lyapunov function

$$V_1 = \frac{1}{2} z_1^2, \tag{4.65}$$

is considered. The derivative of equation 4.65 is

$$\dot{V}_1 = z_1 \dot{z}_1. \tag{4.66}$$

After substituting expression for $\dot{z}_1$ into equation 4.66

$$\dot{V}_1 = \frac{p_1}{J_2} z_1 - \frac{p_2 z_1^2}{J_2} + \frac{p_3 z_1^3}{J_2} + \frac{c_b \omega_d}{J_2} z_1 - \frac{c_b}{J_2} z_1^2 - \frac{k_t}{J_2} \alpha_1 z_1 - \frac{k_t}{J_2} z_1 z_2, \tag{4.67}$$

the derivative along trajectory of equation 4.64 is obtained. To make $\dot{V}_1$ in equation 4.67 negative definite the virtual control

$$\alpha_1 = \frac{c_b \omega_d}{k_t} + \frac{k_2 J_2}{k_t} \int z_1 dt, \tag{4.68}$$

is designed. Which can be simplified to

$$\alpha_1 = \frac{c_b \omega_d}{k_t} + \frac{p_1}{J_2} + + \frac{k_2 J_2}{2k_t} z_1^2 + \frac{k_2 J_2 c_1}{k_t}, \tag{4.69}$$

where $k_2 > 0$ is a tuning parameter and c_1 a constant. Substitute equation 4.69 in equation 4.67 the Lyapunov derivative becomes

$$\begin{aligned} \dot{V}_1 = & \frac{p_1}{J_2} z_1 - \frac{p_2 z_1^2}{J_2} + \frac{p_3 z_1^3}{J_2} + \frac{c_b \omega_d}{J_2} z_1 - \frac{c_b}{J_2} z_1^2 \\ & - \frac{c_b \omega_d}{J_2} z_1 - \frac{p_1}{J_2} z_1 - \frac{k_2}{2} z_1^3 - k_2 c_1 z_1 - \frac{k_t}{J_2} z_1 z_2. \end{aligned} \tag{4.70}$$

The Lyapunov derivative in equation 4.70 is negative definite if $k_2 = \frac{2p_3}{J_2}$. With this choice of tuning constant the Lyapunov derivative in equation 4.70 can be expressed as

$$\dot{V}_1 \leq -\frac{c_b}{J_2} z_1^2 - k_2 c_1 z_1 - \frac{k_t}{J_2} z_1 z_2. \tag{4.71}$$

Substituting expression for k_2 into the equation above the expression

$$\dot{V}_1 \leq -\frac{c_b}{J_2} z_1^2 - \frac{2p_3}{J_2} c_1 z_1 - \frac{k_t}{J_2} z_1 z_2, \tag{4.72}$$

is obtained. Which can be written as

$$\dot{V}_1 \leq -\frac{c_b}{J_2} (z_1^2 + \frac{2p_3}{c_b} c_1 z_1 + (\frac{2p_3 c_1}{c_b})^2) + \frac{(2p_3 c_1)^2}{c_b J_2} - \frac{k_t}{J_2} z_1 z_2, \tag{4.73}$$

after adding and subtracting the term $\frac{(2p_3 c_1)^2}{c_b J_2}$. The equation 4.73 can be written as

$$\dot{V}_1 \leq -\frac{c_b}{J_2} (z_1 + \frac{2p_3 c_1}{c_b})^2 + \frac{(2p_3 c_1)^2}{c_b J_2} - \frac{k_t}{J_2} z_1 z_2, \tag{4.74}$$

which implies uniform ultimate boundedness. The last term is made negative definite in the second step of backstepping. The second backstepping variable

$$z_2 = x_2 - \alpha_1. \tag{4.75}$$

Taking derivative of equation 4.75 the error dynamics

$$\dot{z}_2 = \dot{x}_2 - \dot{\alpha}_1, \tag{4.76}$$

is obtained. The equation above after substituting expression for $\dot{x}_2$ can be expressed as

$$\dot{z}_2 = x_3 - \omega_d + z_1 - \dot{\alpha}_1. \tag{4.77}$$

Substituting the expression for $\dot{\alpha}_1$ in equation 4.77 the error dynamics become

$$\dot{z}_2 = -\omega_d + z_1 - \frac{k_2 J_2}{k_t} z_1 + x_3. \tag{4.78}$$

The origin of the error system represented by equation 4.78 can be stabilized using the control Lyapunov function

$$V_2 = V_1 + \frac{1}{2} z_2^2. \tag{4.79}$$

For the purpose of simplification all negative definite terms of equation 4.74 are represented by V_n, the derivative of equation 4.79 is expressed as

$$\dot{V}_2 = V_n - \frac{k_t}{J_2} z_1 z_2 + z_2 \dot{z}_2. \tag{4.80}$$

Substituting expression for $\dot{z}_2$ from equation 4.78 into equation 4.80 the Lyapunov derivative can be written as

$$\dot{V}_2 = V_n - \frac{k_t}{J_2} z_1 z_2 - z_2 \omega_d + z_1 z_2 - \frac{k_2 J_2}{k_t} z_1 z_2 + z_2 x_3. \tag{4.81}$$

In the second backstepping step to stabilize the origin of the error system represented by equation 4.78 the state

$$x_3 = z_3 + \alpha_2, \tag{4.82}$$

is used as the virtual input, where α_2 is the second virtual function. The third backstepping variable is

$$z_3 = x_3 - \alpha_2. \tag{4.83}$$

The third error system is

$$\dot{z}_3 = \dot{x}_3 - \dot{\alpha}_2. \tag{4.84}$$

Substituting x_3 from equation 4.82 into equation 4.81

$$\dot{V}_2 = V_n - \frac{k_t}{J_2} z_1 z_2 - z_2 \omega_d + z_1 z_2 - \frac{k_2 J_2}{k_t} z_1 z_2 + z_2 (z_3 + \alpha_3), \tag{4.85}$$

is obtained. The virtual control function

$$\alpha_2 = \frac{k_t}{J_2} z_1 + \omega_d - z_1 + \frac{k_2 J_2}{k_t} z_1, \tag{4.86}$$

is designed to make the Lyapunov derivative in equation 4.85 negative definite. Substituting equation 4.86 into equation 4.85

$$\dot{V}_2 = V_n + z_2 z_3, \tag{4.87}$$

is obtained. The last term of equation 4.87 is made negative definite in the third backstepping step where the real control input torque T_m is used to stabilize the origin of system represented by equation 4.84. Substituting equation 4.54 and equation 4.86 into equation 4.84 the third error dynamics

$$\dot{z}_3 = -\frac{k_t}{J_1} x_2 - \frac{c_r}{J_1} + \frac{T_m}{J_1} - \frac{k_t}{J_2} \dot{z}_1 + \dot{z}_1 - \frac{k_2 J_2}{k_t} \dot{z}_1, \tag{4.88}$$

are obtained. The Lyapunov candidate function to stabilize the origin of the error system of equation 4.88 and hence the whole system is

$$V_3 = V_1 + V_2 + \frac{1}{2} z_3^2. \tag{4.89}$$

The derivative of V_3 along the trajectories of the error systems is

$$\dot{V}_3 = V_n + z_2 z_3 - \frac{k_t}{J_1} x_2 z_3 - \frac{c_r}{J_1} x_3 z_3 + \frac{T_m}{J_1} z_1 - \frac{k_t}{J_2} \dot{z}_1 z_3 + \dot{z}_1 z_3 - \frac{k_t J_2}{k_t} \dot{z}_1 z_3. \tag{4.90}$$

The control input that will make the origin of the whole system stable is thus found to be

$$T_m = -J_1 z_2 + k_2 x_2 + c_r x_3 + \frac{J_1}{J_2} k_t \dot{z}_1 - J_1 \dot{z}_1 + \frac{k_2 J_1 J_2}{k_t} \dot{z}_1. \tag{4.91}$$

4.4.1 *Simulation results and conclusions*

The drill string is simulated using the model represented by equation 4.49 with parameters that represent typical quantities of a full scale drill rig. The parameters used have been used in previous works (Jansen and Steen 1995; Abdulgalil and Siguerdidjane 2005; Navarro-López and Cortés 2007). The parameters used are given in Table 6.

Table 6: Parameters used for simulation of drill string dynamics.

PARAMETER	VALUE
J_1	2122kg m^2
J_2	374kg m^2
k_t	473Nm/rad
c_r	425Nms/rad
c_b	50Nms/rad
μ_{cb}	0.5
μ_{sb}	0.8
γ_b	0.9
α	350
k_2	0.1

The response of the backstepping controller for a desired angular velocity of 6rad/s is shown in Figure 29. The response for a set point angular velocity of 12rad/s is shown in Figure 30. The response for 15rad/s is shown in Figure 31. The input torque is also shown for each set point. It is observed that after initial tuning, the nonlinear controller can work for different operating points without changing the tuning parameter k_2. Thus the presented control design provides a controller that has a large operating envelope.

The controller requires full state feedback. Measurement of top drive velocity, the angular displacement between top drive and drill bit and drill bit velocities is required. Similarly for control design the torque variation about the setpoint should be modelled. The control is robust with respect to estimation errors of the torque as the

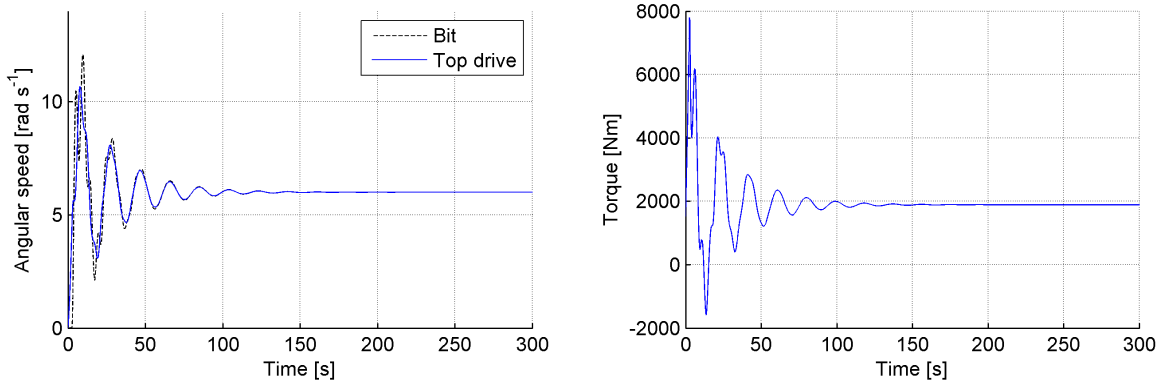

(a) Set point 6rads^{-1}. (b) Input torque for 6rads^{-1} set point.

Figure 29: Response at 6rads^{-1} set point.

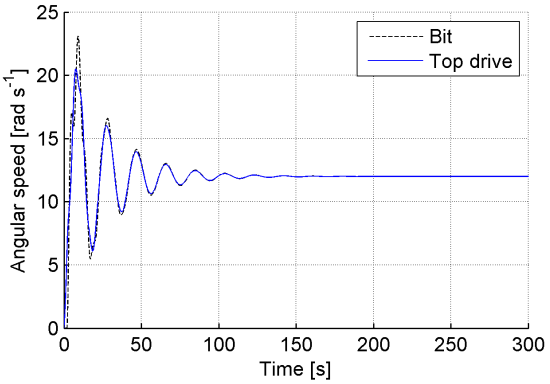

(a) Set point 12rads^{-1}.

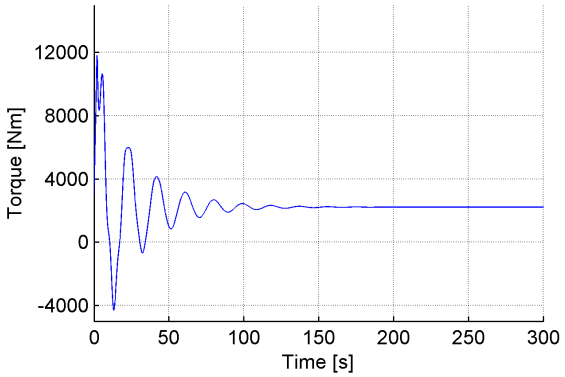

(b) Input torque for 12rads^{-1} set point.

Figure 30: Response at 12 rads^{-1} set point.

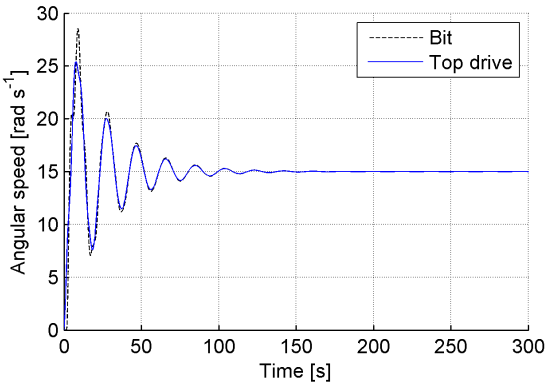

(a) Set point 15rads^{-1}.

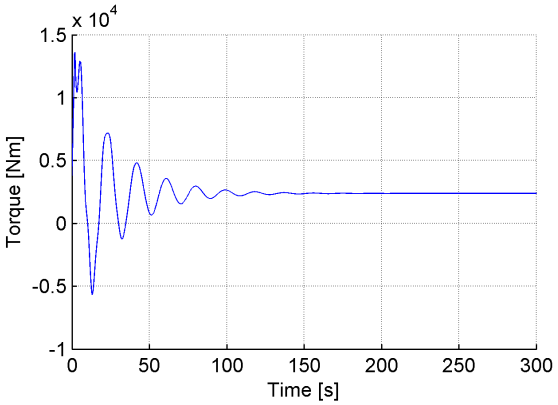

(b) Input torque for 15rads^{-1} set point.

Figure 31: Response at 15rads^{-1} set point.

nonlinear torque is not cancelled completely. The performance of the backstepping controller may be improved using adaptive backstepping which is explored in the next chapter.

In the experimental setup, only angular velocities of the top drive and the bottom assembly are available. Similarly the desire is not to use the torque for feedback because of bandwidth limitations in a real drilling rig. To be implementable observer based control has to be used. The backstepping controller designed in this chapter is a starting point for more complex adaptive backstepping controller designed in chapter 5 and the robust dynamic surface feedback backstepping controller designed in chapter 6.

5

ADAPTIVE BACKSTEPPING USING A TUNING FUNCTION

In chapter 3 it was concluded that friction at the drill bit can not be precisely modeled even for the small scale experimental drill rig. To control the torsional oscillations in the experimental setup adaptive or robust control is needed. In the previous chapter a full state feedback robust backstepping controller was designed and tested in simulations. The focus of this chapter is on adaptive backstepping using tuning function based design. A few simulation studies on adaptive backstepping have been undertaken in previous works. Bu and Dykstra (2014) devised a modular x-swapping based indirect adaptive backstepping approach which used full state feedback to control stick slip torsional vibrations. Ullah, Duarte, and Bohn (2016b) also devised an indirect adaptive approach that required full state feedback. But schemes that rely on full state feedback will be difficult to implement as often sensors are not available to measure all the states in practice. To overcome this shortcoming in this chapter adaptive observer backstepping (Krstic, Kanellakopoulos, and Kokotovic 1995) based designs are evaluated. To the best of the author's knowledge observer based adaptive backstepping control that uses tuning functions based adaptive design has not been reported in the torsional control literature for drill strings.

Observer based control for nonlinear systems is more prone to becoming unstable than observer based control for linear systems because a nonlinear controller can become unstable in finite time even if the observer error is exponentially decreasing. Counterintuitively stability of a nonlinear controlled system in the presence of observer error is ensured by introducing nonlinear damping into the system.

The chapter is organized such that in the first section the adaptive backstepping design is introduced. In the second section issues in observer based control for nonlinear systems are discussed followed by an introduction to observer based adaptive backstepping in the third section. In the fourth section, an observer based adaptive control is designed for the experimental setup.

5.1 ADAPTIVE BACKSTEPPING

To introduce the idea of adaptive backstepping an example system represented by the equations

$$\dot{x}_1 = \boldsymbol{\theta}^T \boldsymbol{\phi}(x_1) + x_2 \tag{5.1}$$

and

$$\dot{x}_2 = u, \tag{5.2}$$

is used, where $\boldsymbol{\theta} \in \mathbb{R}^p$ is a vector of unknown constant parameters, x_1 and x_2 are scalar states of the system. The vector of regressors is given by $\boldsymbol{\phi} \in \mathbb{R}^p$ and u is the control input. The uncertainty $\boldsymbol{\theta}$ is not in the same equation as the input. Such a system is called an unmatched system in control terminology. This system satisfies the extended matching condition i.e. uncertain parameter vector $\boldsymbol{\theta}$ enters the system one integrator before the control input u. If $\boldsymbol{\theta}$ is known then backstepping can be used to control the system. But if $\boldsymbol{\theta}$ is not known adaptive backstepping can be used. Krstić, Kanellakopoulos, and Kokotović (1992) used a Lyapunov based tuning function design for adaptive backstepping that removed overparameterization of previously used adaptive backstepping approaches. An estimate of $\boldsymbol{\theta}$ is $\hat{\boldsymbol{\theta}}$. The constant parameter vector can be written as

$$\boldsymbol{\theta} = \hat{\boldsymbol{\theta}} + \tilde{\boldsymbol{\theta}}, \tag{5.3}$$

where $\tilde{\boldsymbol{\theta}}$ is the estimation error. The derivative of $\boldsymbol{\theta}$ in equation 5.3 is

$$\dot{\boldsymbol{\theta}} = \dot{\hat{\theta}} + \dot{\tilde{\theta}}, \tag{5.4}$$

which can be rearranged into

$$\dot{\hat{\boldsymbol{\theta}}} = \dot{\boldsymbol{\theta}} - \dot{\tilde{\boldsymbol{\theta}}}, \tag{5.5}$$

which implies

$$\dot{\hat{\boldsymbol{\theta}}} = -\dot{\tilde{\boldsymbol{\theta}}}. \tag{5.6}$$

To make the origin of the system given by equation 5.1 and equation 5.2 a stable equillibrium point a two step backstepping procedure is needed. In the first step the backstepping variable is

$$z_1 = x_1. \tag{5.7}$$

The derivative of z_1 in equation 5.7 is

$$\dot{z}_1 = \dot{x}_1 = \boldsymbol{\theta}^T \boldsymbol{\phi}(x_1) + x_2. \tag{5.8}$$

To stabilize the z_1 system dynamics given by equation 5.8 about its origin a Lyapunov function is designed as

$$V_1 = \frac{1}{2} x_1^2 + \frac{1}{2} \tilde{\boldsymbol{\theta}}^T \boldsymbol{\Gamma}^{-1} \tilde{\boldsymbol{\theta}}. \tag{5.9}$$

Taking derivative of the Lyapunov function in equation 5.9

$$\dot{V}_1 = x_1 \dot{x}_1 + \tilde{\boldsymbol{\theta}}^T \boldsymbol{\Gamma}^{-1} \dot{\hat{\boldsymbol{\theta}}}, \tag{5.10}$$

is obtained. Substituting expression for $\dot{x}_1$ in equation 5.10

$$\dot{V}_1 = x_1 (\boldsymbol{\theta}^T \boldsymbol{\phi}(x_1) + x_2) + \tilde{\boldsymbol{\theta}}^T \boldsymbol{\Gamma}^{-1} \dot{\hat{\boldsymbol{\theta}}}, \tag{5.11}$$

is obtained which can be simplified to

$$\dot{V}_1 = x_1\hat{\boldsymbol{\theta}}^T\boldsymbol{\phi}(x_1) + x_1\tilde{\boldsymbol{\theta}}^T\boldsymbol{\phi}(x_1) + x_1x_2 + \tilde{\boldsymbol{\theta}}^T\boldsymbol{\Gamma}^{-1}\dot{\hat{\boldsymbol{\theta}}}. \tag{5.12}$$

The equation above can be factored as

$$\dot{V}_1 = x_1\hat{\boldsymbol{\theta}}^T\boldsymbol{\phi}(x_1) + x_1x_2 + \tilde{\boldsymbol{\theta}}^T\boldsymbol{\Gamma}^{-1}(x_1\boldsymbol{\Gamma}\boldsymbol{\phi}(x_1) + \dot{\hat{\boldsymbol{\theta}}}). \tag{5.13}$$

As $\tilde{\boldsymbol{\theta}}$ is unknown the last term in equation 5.13 is an uncertain term that should be eliminated. In equation 5.13 the uncertain term is made zero by using a tuning function

$$\boldsymbol{\tau}_1 = \dot{\hat{\boldsymbol{\theta}}} = -x_1\boldsymbol{\Gamma}\boldsymbol{\phi}(x_1). \tag{5.14}$$

To avoid overparametrization this tuning function is not implemented in the second step of backstepping in this example problem. In the last backstepping step a single tuning function is designed that has $\boldsymbol{\tau}_1$ as a component (Krstić, Kanellakopoulos, and Kokotović 1992). To stabilize the origin of the error system given in equation 5.8 the tuning function in equation 5.14 together with virtual input x_2 has to be used as there is no real input in the system represented by equation 5.8. The virtual input is designed so that $\dot{V}_1$ given in equation 5.13 becomes negative definite.

The second backstepping variable is

$$z_2 = x_2 - \alpha_1, \tag{5.15}$$

which can be rearranged into

$$x_2 = z_2 + \alpha_1. \tag{5.16}$$

Substituting x_2 from equation 5.16 and τ_1 from equation 5.14 in equation 5.13

$$\dot{V}_1 = x_1\hat{\boldsymbol{\theta}}^T\boldsymbol{\phi}(x_1) + x_1z_2 + x_1\alpha_1 + \tilde{\boldsymbol{\theta}}^T\boldsymbol{\Gamma}^{-1}(x_1\boldsymbol{\Gamma}\boldsymbol{\phi}(x_1) + \boldsymbol{\tau}_1), \tag{5.17}$$

is obtained. To make the terms of $\dot{V}_1$ given in equation 5.17 negative definite except for the terms in brackets and the x_1z_2 term

$$\alpha_1 = -c_1x_1 - \hat{\boldsymbol{\theta}}^T\boldsymbol{\phi}(x_1), \tag{5.18}$$

is designed, where c_1 is a positive constant. The second backstepping system is

$$\dot{z}_2 = \dot{x}_2 - \dot{\alpha_1}. \tag{5.19}$$

Substituting $\dot{x}_2$ from equation 5.2 the equation 5.19 becomes

$$\dot{z}_2 = u - \dot{\alpha_1}. \tag{5.20}$$

Substituting the expression for $\dot{\alpha}_1$ in equation 5.20

$$\dot{z}_2 = u - \frac{\partial\alpha_1}{\partial x_1}\dot{x}_1 - \frac{\partial\alpha_1}{\partial\hat{\boldsymbol{\theta}}^T}\dot{\hat{\boldsymbol{\theta}}}, \tag{5.21}$$

is obtained. To stabilize the error system given in equation 5.21 about the origin a candidate control Lyapunov function

$$V_2 = V_1 + \frac{1}{2}z_2^2 + \frac{1}{2}\tilde{\boldsymbol{\theta}}^T\boldsymbol{\Gamma}^{-1}\tilde{\boldsymbol{\theta}}, \tag{5.22}$$

is used. The derivative of V_2 given by equation 5.22 is

$$\dot{V}_2 = -c_1x_1^2 - x_1z_2 + \tilde{\boldsymbol{\theta}}^T\boldsymbol{\Gamma}^{-1}(\boldsymbol{\Gamma}\boldsymbol{\phi}(x_1) + \boldsymbol{\tau}_1) + z_2\dot{z}_2 + \tilde{\boldsymbol{\theta}}^T\boldsymbol{\Gamma}^{-1}\dot{\hat{\boldsymbol{\theta}}}. \tag{5.23}$$

Substituting $\dot{z}_2$ from equation 5.21 into equation 5.23

$$\dot{V}_2 \leq -x_1z_2 + \tilde{\boldsymbol{\theta}}^T\boldsymbol{\Gamma}^{-1}(\boldsymbol{\Gamma}\boldsymbol{\phi}(x_1) + \boldsymbol{\tau}_1) + z_2(u - \frac{\partial\alpha_1}{\partial x_1}\dot{x}_1 - \frac{\partial\alpha_1}{\partial\hat{\boldsymbol{\theta}}^T}\dot{\hat{\boldsymbol{\theta}}}) + \tilde{\boldsymbol{\theta}}^T\boldsymbol{\Gamma}^{-1}\dot{\hat{\boldsymbol{\theta}}}, \tag{5.24}$$

is obtained. Substituting the function α_1 from equation 5.18 and $\boldsymbol{\theta}$ from equation 5.3 in $\dot{x}_1$ of equation 5.24

$$\begin{aligned}\dot{V}_2 \leq & -x_1z_2 + uz_2 - \frac{\partial\alpha_1}{\partial x_1}\hat{\boldsymbol{\theta}}^T\boldsymbol{\phi}(x_1)z_2 - \frac{\partial\alpha_1}{\partial x_1}z_2^2 \\ & - \frac{\partial\alpha_1}{\partial x_1}\tilde{\boldsymbol{\theta}}^T\boldsymbol{\phi}(x_1)z_2 - \frac{\partial\alpha_1}{\partial\hat{\boldsymbol{\theta}}^T}\dot{\hat{\boldsymbol{\theta}}}z_2 \\ & + \tilde{\boldsymbol{\theta}}^T\boldsymbol{\Gamma}^{-1}(\boldsymbol{\Gamma}\boldsymbol{\phi}(x_1) + \boldsymbol{\tau}_1) + \tilde{\boldsymbol{\theta}}\boldsymbol{\Gamma}^{-1}\dot{\hat{\boldsymbol{\theta}}},\end{aligned} \tag{5.25}$$

is obtained, which can be rearranged by factoring the unknown $\tilde{\boldsymbol{\theta}}$ terms, into

$$\begin{aligned}\dot{V}_2 \leq & -x_1z_2 + uz_2 - \frac{\partial\alpha_1}{\partial x_1}\hat{\boldsymbol{\theta}}^T\boldsymbol{\phi}(x_1)z_2 - \frac{\partial\alpha_1}{\partial x_1}z_2^2 \\ & - \frac{\partial\alpha_1}{\partial\hat{\boldsymbol{\theta}}^T}\dot{\hat{\boldsymbol{\theta}}}z_2 \\ & + \tilde{\boldsymbol{\theta}}^T\boldsymbol{\Gamma}^{-1}(\boldsymbol{\Gamma}\boldsymbol{\phi}(x_1) + \boldsymbol{\tau}_1 - \boldsymbol{\Gamma}\frac{\partial\alpha_1}{\partial x_1}\boldsymbol{\phi}(x_1)z_2 + \dot{\hat{\boldsymbol{\theta}}}).\end{aligned} \tag{5.26}$$

Now the control law can be designed to make the derivative of the Lyapunov function i.e. $\dot{V}_2$ in equation 5.26 negative definite. The real input

$$u = -c_2z_2 + x_1 + \frac{\partial\alpha_1}{\partial x_1}\hat{\boldsymbol{\theta}}^T\boldsymbol{\phi}(x_1) + \frac{\partial\alpha_1}{\partial x_1}z_2 + \frac{\partial\alpha_1}{\partial x_1}\dot{\hat{\boldsymbol{\theta}}}z_2, \tag{5.27}$$

where c_2 is a positive constant and the parameter adaptation law

$$\dot{\hat{\boldsymbol{\theta}}} = -\boldsymbol{\tau}_1 + \boldsymbol{\Gamma}\frac{\partial\alpha_1}{\partial x_1}\boldsymbol{\phi}(x_1)z_2, \tag{5.28}$$

make the Lyapunov derivative given in equation 5.26 negative definite along the trajectory of the given error system and thus stabilizes the error system to zero adaptively.

The discussion above introduced adaptive backstepping for a system where all the states of the system are available for feedback. The next section points out the stability issues that have to be considered when observer based nonlinear control is used.

5.2 OBSERVER BASED CONTROL OF NONLINEAR SYSTEMS

To elaborate issues in observer based backstepping in particular and nonlinear control in general the concept of "finite escape time" has to be understood. Nonlinear systems can become unstable in finite time due to a perturbation or error (Kanellakopoulos, Kokotovic, and Morse 1992). To explain this phenomenon an example of a simple scalar system

$$\dot{x} = x^3 + u + x^2\xi, \tag{5.29}$$

is considered. If the control input

$$u = -x^3 - x - x^2\hat{\xi}, \tag{5.30}$$

where $\hat{\xi}$ is obtained using an estimator is substituted into equation 5.29 the system

$$\dot{x} = -x + x^2\xi - x^2\hat{\xi}, \tag{5.31}$$

is obtained where $\tilde{\xi} = \xi - \hat{\xi}$. Substituting $\tilde{\xi}$ into equation 5.31

$$\dot{x} = -x + x^2\tilde{\xi}, \tag{5.32}$$

is obtained. If it is assumed that the estimation error $\tilde{\xi}$ decreases exponentially i.e. $\tilde{\xi} = ke^{-t}$, then the system

$$\dot{x} = -x + x^2ke^{-t}, \tag{5.33}$$

is obtained. A closed form solution for equation 5.33 is (Kanellakopoulos, Kokotovic, and Morse 1992)

$$x(t) = \frac{2x(0)}{(2 - kx(0))e^t + kx(0)e^{-t}}. \tag{5.34}$$

The denominator of equation 5.34 is zero at $t = \frac{1}{2}\ln(\frac{kx(0)}{kx(0)-2})$. From this it is inferred that whenever $kx(0) > 2$ the solution escapes to infinity in finite time (Kanellakopoulos, Kokotovic, and Morse 1992). This means there always exist initial conditions $x(0)$ from which the system escapes to infinity in finite time even if the estimation error is exponentially convergent.

Using the estimator $\hat{\xi}$ directly in the control law is known as certainty equivalence. In a linear system, an exponentially convergent estimator or observer does not cause any problem for the designed controller due to the separation principle i.e. eigenvalues can be assigned independently. But in nonlinear control in some cases, even an exponentially convergent observer can destabilize the closed loop system for certain initial conditions.

The solution that avoids instability in the presence of observer error is to introduce nonlinear damping in the control law. To explain how the nonlinear damping can be used, an example of a matched nonlinear system

$$\dot{\boldsymbol{x}} = \boldsymbol{f}(\boldsymbol{x}) + \boldsymbol{g}(\boldsymbol{x})u, \tag{5.35}$$

is considered. Where $\boldsymbol{x} \in \mathbb{R}^n$ and $u \in \mathbb{R}$. It is assumed that $u = \alpha(\boldsymbol{x})$ is known such that a Lyapunov candidate function $V(\boldsymbol{x})$ exists with derivative

$$\dot{V} \leq -W(\boldsymbol{x}) \leq 0 \, \forall \boldsymbol{x}, \tag{5.36}$$

along the trajectories of the system represented by equation 5.35. The functions V and W are positive definite and f, g are C^2 [1] on $\mathbb{R}^n$.

The system

$$\dot{\boldsymbol{x}} = \boldsymbol{f}(\boldsymbol{x}) + \boldsymbol{g}(\boldsymbol{x})(u + \boldsymbol{p}^T(\boldsymbol{x})\boldsymbol{d}(\boldsymbol{x}, \boldsymbol{\epsilon})), \tag{5.37}$$

is the system of equation 5.35 with added error or perturbation. It is disturbed or perturbed by a nonlinear damping term given by $\boldsymbol{p}^T(\boldsymbol{x})\boldsymbol{d}(\boldsymbol{x}, \boldsymbol{\epsilon})$ where $\boldsymbol{\epsilon} \in \mathbb{R}^l$, $\boldsymbol{d}(\boldsymbol{x}, \boldsymbol{\epsilon})$ and $\boldsymbol{p}(\boldsymbol{x})$ are continuous and $\boldsymbol{d}(\boldsymbol{x}, 0) = 0$. The estimation error or observer error $\boldsymbol{\epsilon}$ has the error dynamics

$$\dot{\boldsymbol{\epsilon}} = \boldsymbol{q}(\boldsymbol{x}, \boldsymbol{\epsilon}), \tag{5.38}$$

where $\boldsymbol{q}(\boldsymbol{x}, 0) = \boldsymbol{0}$. If there exists a positive definite Lyapunov function $\Omega(\boldsymbol{\epsilon})$, such that its derivative

$$\frac{\partial \Omega}{\partial \boldsymbol{\epsilon}^T}\dot{\boldsymbol{\epsilon}} \leq -||\boldsymbol{d}(\boldsymbol{x}, \boldsymbol{\epsilon})||^2, \tag{5.39}$$

is negative definite along the trajectories of the system described by equation 5.38. Then the feedback control law that stabilizes the system represented by equation 5.37 using nonlinear damping is given by

$$u = \alpha(\boldsymbol{x}) - \frac{\partial V}{\partial \boldsymbol{x}^T}(\boldsymbol{x})\boldsymbol{g}(\boldsymbol{x})||\boldsymbol{p}(\boldsymbol{x})||^2. \tag{5.40}$$

It is proved in Kanellakopoulos, Kokotovic, and Morse (1992) that the Lyapunov function

$$V_2 = V + \Omega, \tag{5.41}$$

has a derivative

$$\dot{V}_2 \leq -W - \frac{3}{4}||\boldsymbol{d}||^2, \tag{5.42}$$

along the trajectories of system represented by equation 5.37 which is negative semidefinite. By LaSalle's invariance principle $\boldsymbol{x}$ and $\boldsymbol{\epsilon}$ are bounded.

1 A function is of class C^2 if the first and second derivatives of the function both exist and are continuous.

The equation 5.42 proves that by adding nonlinear damping in the input stabilizes the origin of the system of equation 5.37. In the absence of nonlinear damping the same system would have become unstable in finite time due to the perturbation. The perturbation can be due to initial parameter variation in an adaptive controller or due to an exponentially decreasing observer error. In the next section nonlinear damping is used to prevent system instability that may occur due to observer error.

5.3 INTRODUCTION TO ADAPTIVE OBSERVER BACKSTEPPING

To better explain the adaptive observer based control approach that is used to control the drill string in Section 5.4 a simple example is used. The adaptive observer based backstepping can be best explained using an example with one unknown parameter θ. The example is described in Krstic, Kanellakopoulos, and Kokotovic (1995: 301). A system

$$\dot{x}_1 = x_2 + \theta\phi_1(y), \tag{5.43}$$

$$\dot{x}_2 = x_3 + \theta\phi_2(y) + u, \tag{5.44}$$

$$\dot{x}_3 = u, \tag{5.45}$$

and with output

$$y = x_1 \tag{5.46}$$

is considered. Only the state x_1 is measured. States x_1 and x_2 are not measured. The system input is represented by u, $\phi_1(y)$ and $\phi_2(y)$ are nonlinear functions and θ is an unknown parameter. The objective is that the output should track a trajectory given by y_r. The observer design is discussed first.

There are a number of complications that arise when designing a backstepping control law for this system. Since x_2 and x_3 are not available for feedback an observer has to be designed to estimate these unmeasured states. But a problem in designing a Luenberger type observer is that θ is unknown.

In Krstic, Kanellakopoulos, and Kokotovic (1995) a so called filtered observer is used. In the filtered observer two filters are designed with state vectors $\boldsymbol{\xi}_0$ and $\boldsymbol{\xi}_1$ such that by definition the equation

$$\boldsymbol{x} = \boldsymbol{\xi}_0 + \theta\boldsymbol{\xi}_1 + \boldsymbol{\epsilon} \tag{5.47}$$

is fulfilled, where $\boldsymbol{\epsilon}$ is the error in estimation of the state vector,

$$\boldsymbol{\xi}_0 = \begin{bmatrix} \xi_{01} \\ \xi_{02} \\ \xi_{03} \end{bmatrix}, \boldsymbol{\xi}_1 = \begin{bmatrix} \xi_{11} \\ \xi_{12} \\ \xi_{13} \end{bmatrix} \text{ and } \boldsymbol{\epsilon} = \begin{bmatrix} \epsilon_1 \\ \epsilon_2 \\ \epsilon_3 \end{bmatrix}.$$

The filter with state vector $\boldsymbol{\xi}_0$ is

$$\dot{\xi}_{01} = k_1(y - \xi_{01}) + \xi_{02}, \tag{5.48}$$

$$\dot{\xi}_{02} = k_2(y - \xi_{01}) + \xi_{03} + u, \tag{5.49}$$

and

$$\dot{\xi}_{03} = k_3(y - \xi_{01}) + u. \tag{5.50}$$

The filter with state vector $\boldsymbol{\xi}_1$ is

$$\dot{\xi}_{11} = -k_1(\xi_{11}) + \xi_{12} + \phi_1(y), \tag{5.51}$$

$$\dot{\xi}_{12} = -k_2(\xi_{11}) + \xi_{13} + \phi_2(y), \tag{5.52}$$

and

$$\dot{\xi}_{13} = -k_3(\xi_{11}). \tag{5.53}$$

The filter equations, i.e, equation 5.48, equation 5.49 and equation 5.50 can be written as

$$\dot{\boldsymbol{\xi}}_0 = \boldsymbol{A}_0\boldsymbol{\xi}_0 + \boldsymbol{k}y + \boldsymbol{b}u. \tag{5.54}$$

Similarly, the filter equations, i.e, equation 5.51, equation 5.52 and equation 5.53 can be written as

$$\dot{\boldsymbol{\xi}}_1 = \boldsymbol{A}_0\boldsymbol{\xi}_1 + \boldsymbol{\phi}(y). \tag{5.55}$$

The plant represented by equation 5.43, equation 5.44 and equation 5.45 can be written in matrix notation as

$$\dot{\boldsymbol{x}} = \boldsymbol{A}_0\boldsymbol{x} + \boldsymbol{k}y + \boldsymbol{b}u + \theta\boldsymbol{\phi}(y), \tag{5.56}$$

where

$$\boldsymbol{k} = \begin{bmatrix} k_1 \\ k_2 \\ k_3 \end{bmatrix}, \boldsymbol{A}_0 = \begin{bmatrix} -k_1 & 1 & 0 \\ -k_2 & 0 & 1 \\ -k_3 & 0 & 0 \end{bmatrix}, \boldsymbol{b} = \begin{bmatrix} 0 \\ 1 \\ 1 \end{bmatrix} \text{ and } \boldsymbol{\phi}(y) = \begin{bmatrix} \phi_1 \\ \phi_2 \\ 0 \end{bmatrix}.$$

The gain vector $\boldsymbol{k}$ is chosen so that $\boldsymbol{A}_0$ is Hurwitz. Taking the derivative of equation 5.47 the filter error dynamics can be expressed as

$$\dot{\boldsymbol{\epsilon}} = \dot{\boldsymbol{x}} - \dot{\boldsymbol{\xi}}_0 - \theta\dot{\boldsymbol{\xi}}_1. \tag{5.57}$$

Substituting in equation 5.57 values of $\dot{\boldsymbol{x}}$ from equation 5.56, $\dot{\boldsymbol{\xi}}_0$ from equation 5.54 and $\dot{\boldsymbol{\xi}}_1$ from equation 5.55

$$\dot{\boldsymbol{\epsilon}} = \boldsymbol{A}_0\boldsymbol{\epsilon}, \tag{5.58}$$

is obtained. The equation 5.58 with $\boldsymbol{A}_0$ Hurwitz implies that the observer error will decrease exponentially. In the following discussion observer based backstepping control design to stabilize the system about the origin is discussed.

Although the filtered observer error decreases exponentially as discussed in section 5.2 the control algorithm has to ensure boundedness of the nonlinear system in presence of this error using nonlinear damping. The adaptive output feedback backstepping control design is similar to normal backstepping as discussed in Chapter 4 but the main difference is that as the state x_2 is not available or not measured its estimate

$$x_2 = \xi_{02} + \theta\xi_{12} + \epsilon_2, \tag{5.59}$$

is used instead. The first backstepping step starts by selecting the first error variable

$$z_1 = y - y_r. \tag{5.60}$$

Taking derivative of equation 5.60 the error system becomes

$$\dot{z}_1 = \dot{y} - \dot{y}_r. \tag{5.61}$$

Substituting $\dot{y} = \dot{x}_1$ in equation 5.61 the error system

$$\dot{z}_1 = \dot{x}_1 - \dot{y}_r, \tag{5.62}$$

is obtained. Substituting equation 5.43 in equation 5.62 the error system

$$\dot{z}_1 = x_2 + \theta\phi_1(y) - \dot{y}_r, \tag{5.63}$$

is derived. The main difference between observer backstepping and full state feedback is that instead of using the actual state x_2 the estimate of x_2 is used as the virtual control. Substituting equation 5.59 into equation 5.63

$$\dot{z}_1 = \xi_{02} + \theta\xi_{12} + \epsilon_2 + \theta\phi_1(y) - \dot{y}_r, \tag{5.64}$$

is derived, which is stabilized despite observer error ϵ_2 using the Lyapunov candidate function

$$V_1 = \frac{1}{2}z_1^2 + \frac{1}{2\gamma}(\theta - \nu_1)^2 + \frac{1}{d_1}\boldsymbol{\epsilon}^T\boldsymbol{P}_0\boldsymbol{\epsilon}, \tag{5.65}$$

where $\gamma > 0$ is adaptation gain and $\boldsymbol{P}_0 = \boldsymbol{P}_0^T > 0$ designed such that $\boldsymbol{P}_0\boldsymbol{A}_0 + \boldsymbol{A}_0^T\boldsymbol{P}_0 = -\mathrm{I}$. The idea is to use adaptive backstepping tools described in section 5.1 to achieve adaptive control and nonlinear damping tools described in section 5.2 to ensure stability in the presence of error ϵ_2. This may be considered as observer and control separation for the nonlinear control system. The derivative of V_1 represented by equation 5.65 along trajectories of the system represented by equation 5.64 is

$$\dot{V}_1 = z_1\dot{z}_1 + \frac{1}{\gamma}(\theta - \nu_1)\dot{\nu} + \frac{1}{d_1}\frac{d}{dt}(\boldsymbol{\epsilon}^T\boldsymbol{P}_0\boldsymbol{\epsilon}). \tag{5.66}$$

Note that in equation 5.66 derivative of the last term can be expressed as

$$\begin{aligned}\frac{1}{d_1}\frac{d}{dt}(\boldsymbol{\epsilon}^T\boldsymbol{P}_0\boldsymbol{\epsilon}) =& \frac{1}{d_1}(\dot{\boldsymbol{\epsilon}}^T\boldsymbol{P}_0\boldsymbol{\epsilon} + \boldsymbol{\epsilon}^T\boldsymbol{P}_0\dot{\boldsymbol{\epsilon}}) \\ =& \frac{1}{d_1}((\boldsymbol{A}_0\boldsymbol{\epsilon})^T\boldsymbol{P}_0\boldsymbol{\epsilon} + \boldsymbol{\epsilon}^T\boldsymbol{P}_0\boldsymbol{A}_0\boldsymbol{\epsilon}) \\ =& \frac{1}{d_1}(\boldsymbol{\epsilon}^T\boldsymbol{A}_0^T\boldsymbol{P}_0\boldsymbol{\epsilon} + \boldsymbol{\epsilon}^T\boldsymbol{P}_0\boldsymbol{A}_0\boldsymbol{\epsilon}) \\ =& \frac{1}{d_1}(\boldsymbol{\epsilon}^T(\boldsymbol{A}_0^T\boldsymbol{P}_0 + \boldsymbol{P}_0\boldsymbol{A}_0)\boldsymbol{\epsilon}) \\ =& \frac{1}{d_1}(\boldsymbol{\epsilon}^T(-\mathrm{I})\boldsymbol{\epsilon}) = -\frac{1}{d_1}(\boldsymbol{\epsilon}^T\boldsymbol{\epsilon}).\end{aligned} \tag{5.67}$$

To stabilize the system represented by equation 5.64 about the origin, ξ_{02} is used as the virtual control input. To do this the second backstepping variable z_2 with the virtual control function α_1 is introduced as

$$z_2 = \xi_{02} - \alpha_1 - \dot{y}_r. \tag{5.68}$$

This implies

$$\xi_{02} = \alpha_1 + \dot{y}_r + z_2. \tag{5.69}$$

Substituting ξ_{02} from equation 5.69 into equation 5.64

$$\dot{z}_1 = z_2 + \alpha_1 + \theta(\xi_{12} + \phi_1(y)) + \epsilon_2, \tag{5.70}$$

is obtained. In equation 5.70 the virtual control function α_1 is designed to make the Lyapunav derivative $\dot{V}_1$ in equation 5.66 along the trajectories of the system given by equation 5.64 negative definite as follows

$$\alpha_1 = -c_1z_1 - d_1z_1 - \nu_1(\xi_{12} + \phi_1(y)). \tag{5.71}$$

Substituting equation 5.70 and equation 5.67 in equation 5.66 the derivative becomes

$$\dot{V}_1 \leq z_1z_2 - c_1z_1^2 + (\theta - \nu_1)(z_1 - \frac{1}{\gamma}\dot{\nu}_1) - \frac{3}{4d_1}\boldsymbol{\epsilon}^T\boldsymbol{\epsilon}. \tag{5.72}$$

The uncertain term $(\theta - \nu_1)$ in equation 5.72 is eliminated by choosing the adaptive tuning function as $\dot{\nu}_1 = \gamma z_1(\xi_{12} + \phi_1(y))$ and the term $z_1 z_2$ is cancelled in the next backstepping step. In the second backstepping step the error system

$$\dot{z}_2 = \dot{\xi}_{02} - \dot{\alpha}_1 - \ddot{y}_r, \tag{5.73}$$

where the term $\dot{\xi}_{02} = k_2(y - \xi_{01}) + \xi_{03} + u$ has real control input u. The control input design procedure from here on is the same as described in the previous sections and is summarized below.

The input

$$\begin{aligned} u = &- c_2 z_2 - z_1 - d_2(\frac{\partial \alpha_1}{\partial y})^2 z_2 - k_2(y - \xi_{01}) - \xi_{03} \\ &+ \frac{\partial \alpha_1}{\partial y}(\xi_{02} + \nu_2(\xi_{12} + \phi_1(y))) + \frac{\partial \alpha_1}{\partial \xi_{12}}(-k_2\xi_{11} + \xi_{13} + \phi_2(y)) \\ &+ \frac{\partial \alpha_1}{\partial y_r}\dot{y}_r + \frac{\partial \alpha_1}{\partial \nu_1}\gamma(\xi_{12} + \phi_1(y))z_1 + \ddot{y}_r, \end{aligned} \tag{5.74}$$

along with the tuning function adaptive law

$$\dot{\nu}_2 = -\gamma \frac{\partial \alpha_1}{\partial y}(\xi_{12} + \phi_1(y))z_2. \tag{5.75}$$

is designed to make the derivative of the Lyapunov function

$$V_2 = V_1 + \frac{1}{2}z_2^2 + \frac{1}{2\gamma}(\theta - \nu_2)^2 + \frac{1}{d_2}\boldsymbol{\epsilon}^T \boldsymbol{P}_0 \boldsymbol{\epsilon}, \tag{5.76}$$

negative semidefinite. The derivative of V using equation 5.75 and equation 5.74 becomes negative semidefinite as follows

$$\dot{V}_2 = -c_1 z_1^2 - c_2 z_2^2 - \frac{3}{4}(\frac{1}{d_1} + \frac{1}{d_2})\boldsymbol{\epsilon}^T \boldsymbol{\epsilon}, \tag{5.77}$$

which according to LaSalle-Yoshizawa theorem given in appendix A1, guarantees boundedness of z_1, z_2, ν_1, ν_2 and $\boldsymbol{\epsilon}$. Therefore the convergence of z_1 and z_2 to zero is also guaranteed.

In the next section an adaptive observer based backstepping controller is designed to attenuate the torsional oscillations of the drill string. It is inspired by the filtered observer based adaptive control explained in the current section. Although there are differences in the observer design, the method used to ensure stability is logically the same.

5.4 ADAPTIVE OBSERVER BACKSTEPPING CONTROL OF EXPERIMENTAL SETUP

An adaptive observer based controller is designed. The mathematical model for the experimental setup given in section 3.3.1 is used. The parameters of the model identified in section 3 given in Table 5 are used for simulation and control design.

It is assumed that the friction at the top end is known and at the drill bit a linear in parameters model can be used to represent the friction torque variation due to bit speed. Furthermore, rotation of drill string of the experimental setup is restricted to positive (clockwise) direction. As state x_2 (the angular displacement between the end of the drill string connected to the topdrive and the end of the drill string connected to the drill bit) is not measured an observer is designed to estimate x_2. The block diagram in Figure 32 represents the structure of control algorithm. In the next section, the observer design is described.

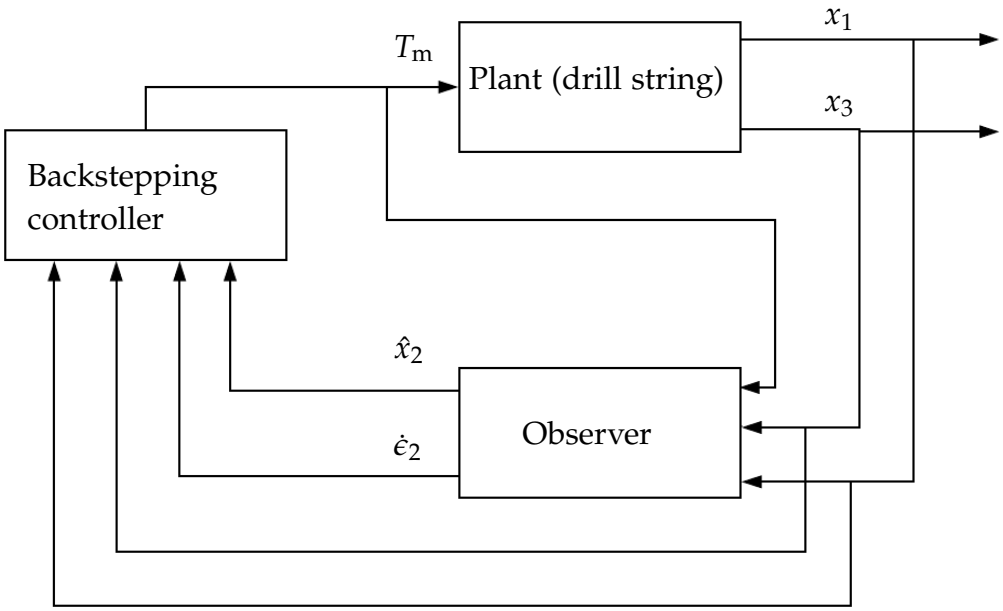

Figure 32: Block diagram for the proposed adaptive controller.

5.4.1 *Observer Design*

The observer for system described by equation 3.15, equation 3.16 and equation 3.17 can be formulated as (Khalil 1996: 612)

$$\dot{\hat{x}}_1 = \frac{c_b}{J_2}\hat{x}_1 + \frac{k_t}{J_2}\hat{x}_2 + \begin{bmatrix} k_{11} & k_{12} \end{bmatrix} \begin{bmatrix} x_1 - \hat{x}_1 \\ x_3 - \hat{x}_3 \end{bmatrix}, \tag{5.78}$$

$$\dot{\hat{x}}_2 = \hat{x}_3 - \hat{x}_1 + \begin{bmatrix} k_{21} & k_{22} \end{bmatrix} \begin{bmatrix} x_1 - \hat{x}_1 \\ x_3 - \hat{x}_3 \end{bmatrix}, \tag{5.79}$$

and

$$\dot{\hat{x}}_3 = -\frac{c_r}{J_1}\hat{x}_3 - \frac{k_t}{J_1}\hat{x}_2 - \frac{T_{fu}}{J_1} + \frac{T_m}{J_1} + \begin{bmatrix} k_{31} & k_{32} \end{bmatrix} \begin{bmatrix} x_1 - \hat{x}_1 \\ x_3 - \hat{x}_3 \end{bmatrix}, \tag{5.80}$$

where $x_1$and x_3 are the measured speeds of the bit and top drive respectively, $\hat{x}_1$, $\hat{x}_2$ and $\hat{x}_3$ are the states estimated by the observer. The variables k_{11}, k_{12}, k_{21}, k_{22}, k_{31} and k_{32} are the observer gains. The observer given by equation 5.78, equation 5.79 and equation 5.80 can be written as

$$\dot{\hat{\boldsymbol{x}}} = \begin{bmatrix} -\frac{c_b}{J_1} - k_{11} & \frac{k_t}{J_2} & -k_{12} \\ 1 - k_{21} & 0 & 1 - k_{22} \\ -k_{31} & -\frac{k_t}{J_1} & -\frac{c_r}{J_1} - k_{32} \end{bmatrix} \begin{bmatrix} \hat{x}_1 \\ \hat{x}_2 \\ \hat{x}_3 \end{bmatrix} + \begin{bmatrix} 0 \\ 0 \\ -\frac{T_{fu}}{J_1} \end{bmatrix} + \begin{bmatrix} 0 \\ 0 \\ \frac{T_m}{J_1} \end{bmatrix}. \tag{5.81}$$

The system matrix is

$$\boldsymbol{A}_0 = \begin{bmatrix} -\frac{c_b}{J_1} - k_{11} & \frac{k_t}{J_2} & -k_{12} \\ 1 - k_{21} & 0 & 1 - k_{22} \\ -k_{31} & -\frac{k_t}{J_1} & -\frac{c_r}{J_1} - k_{32} \end{bmatrix}. \tag{5.82}$$

Subtracting equation 5.78 from equation 3.15, equation 5.79 from equation 3.16 and equation 5.80 from equation 3.17 the error equations

$$\dot{\tilde{x}}_1 = -\frac{c_b}{J_2}\tilde{x}_1 + \frac{k_t}{J_2}\tilde{x}_2 + \delta T_{fb}(x_1) - k_{11}\tilde{x}_1 - k_{12}\tilde{x}_3, \tag{5.83}$$

$$\dot{\tilde{x}}_2 = \tilde{x}_3 - \tilde{x}_1 - k_{21}\tilde{x}_1 - k_{22}\tilde{x}_3, \tag{5.84}$$

and

$$\dot{\tilde{x}}_3 = -\frac{k_t}{J_1}\tilde{x}_2 - \frac{c_r}{J_1}\tilde{x}_3 - k_{31}\tilde{x}_1 - k_{32}\tilde{x}_3, \tag{5.85}$$

for the observer are obtained, where $\tilde{x}_1$, $\tilde{x}_2$ and $\tilde{x}_3$ are the observer estimation errors. The variable δT_{fb} represents the friction modelling error. The error system represented by equation 5.83, equation 5.84 and equation 5.85 can be represented as

$$\dot{\tilde{\boldsymbol{x}}} = \boldsymbol{A}_0\tilde{\boldsymbol{x}} + \boldsymbol{\Delta T}_{fb}, \tag{5.86}$$

and

$$\dot{\tilde{\boldsymbol{y}}} = \boldsymbol{C}\tilde{\boldsymbol{x}}, \tag{5.87}$$

where

$$\tilde{\boldsymbol{x}} = \begin{bmatrix} \tilde{x}_1 \\ \tilde{x}_2 \\ \tilde{x}_3 \end{bmatrix}, \boldsymbol{\Delta T}_{fb} = \begin{bmatrix} \delta T_{fb} \\ 0 \\ 0 \end{bmatrix} \text{ and } \boldsymbol{C} = \begin{bmatrix} 1 & 0 & 1 \end{bmatrix}.$$

As x_1 and x_3 are measured the observer is designed by adjusting the gains so that $\boldsymbol{A}_0$ is Hurwitz and the error system has disturbance rejection properties. If δT_{fb} is considered as the input in equation 5.86 then $\boldsymbol{A}_0$ has to be designed so that effect of of δT_{fb} on $\tilde{x}_2$ is rejected. This can be achieved by using high gains (Khalil 1996: 612) but this leads to noise sensitivity. The gains are chosen by making a compromise between observer noise sensitivity and convergence. The procedure for gain selection is presented in Appendix A.2.

5.4.2 *Control Design*

To design an adaptive backstepping controller, the system described by equation 3.15, equation 3.16, equation 3.17, equation 3.18 and equation 3.19 has to be written in the strict feedback form as

$$\dot{x}_1 = \frac{-T_{\text{fb}}(x_1)}{J_2} - \frac{c_{\text{b}}}{J_2}x_1 + \frac{k_{\text{t}}}{J_2}x_2, \tag{5.88}$$

$$\dot{x}_2 = x_3 - x_1, \tag{5.89}$$

and

$$\dot{x}_3 = -\frac{k_{\text{t}}}{J_1}x_2 - \frac{c_{\text{r}}}{J_1}x_3 - \frac{T_{\text{fu}}(x_3)}{J_1} + \frac{T_{\text{m}}}{J_1}. \tag{5.90}$$

For adaptive control the friction term $\frac{T_{\text{fb}}(x_1)}{J_2}$ in equation 5.88 is modelled using a linear in the parameter representation

$$\frac{T_{\text{fb}}(x_1)}{J_2} = \boldsymbol{\theta}^T \boldsymbol{\phi}(x_1), \tag{5.91}$$

where $\boldsymbol{\theta} \in \mathbb{R}^p$ is the parameter vector and $\boldsymbol{\phi} \in \mathbb{R}^p$ is the regressor. The first error variable for regulation is

$$z_1 = \omega_{\text{d}} - x_1, \tag{5.92}$$

where ω_{d} is the desired angular velocity of drill bit. Taking the derivative of equation 5.92

$$\dot{z}_1 = -\dot{x}_1, \tag{5.93}$$

is obtained. To regulate the error system of equation 5.93 asymptotically to zero a control Lyapunov function is chosen as

$$V_1 = \frac{1}{2}z_1^2 + \frac{1}{2\gamma}\tilde{\boldsymbol{\theta}}^T\tilde{\boldsymbol{\theta}} + \frac{1}{2d_1}\boldsymbol{\epsilon}^T\boldsymbol{P}_0\boldsymbol{\epsilon}. \tag{5.94}$$

The derivative of V_1 in equation 5.94 is

$$\dot{V}_1 = z_1\dot{z}_1 - \frac{1}{\gamma}\tilde{\boldsymbol{\theta}}^T\dot{\hat{\boldsymbol{\theta}}} - \frac{1}{d_1}\boldsymbol{\epsilon}^T\boldsymbol{\epsilon}, \tag{5.95}$$

in which the last term without $\boldsymbol{P}_0$ is derived in the same way as shown in equation 5.67. In equation 5.95

$$\tilde{\boldsymbol{\theta}} = \boldsymbol{\theta} - \hat{\boldsymbol{\theta}}, \tag{5.96}$$

is the parameter estimation error and and its derivative is

$$\dot{\tilde{\theta}} = -\dot{\hat{\theta}}. \tag{5.97}$$

Substituting equation 5.93 , equation 5.88 and equation 5.91 into equation 5.95

$$\dot{V}_1 = \frac{c_b}{J_2} x_1 z_1 - \frac{k_t}{J_2} x_2 z_1 - \boldsymbol{\theta}^T \boldsymbol{\phi}(x_1) z_1 - \frac{1}{\gamma} \tilde{\boldsymbol{\theta}}^T \dot{\hat{\boldsymbol{\theta}}} - \frac{1}{d_1} \boldsymbol{\epsilon}^T \boldsymbol{\epsilon}, \tag{5.98}$$

is obtained. As x_2 is not measured directly but is obtained from the observer it can be represented as

$$x_2 = \hat{x}_2 + \epsilon_2, \tag{5.99}$$

where ϵ_2 is the observer error. The term $\boldsymbol{\theta}^T \boldsymbol{\phi}(x_1)$ can be written as

$$\boldsymbol{\theta}^T \boldsymbol{\phi}(x_1) = \hat{\boldsymbol{\theta}}^T \boldsymbol{\phi}(x_1) + \tilde{\boldsymbol{\theta}}^T \boldsymbol{\phi}(x_1). \tag{5.100}$$

It may be noted that if x_2 were measured it would be used as the virtual control state in the first backstepping step. As this is not the case the observed value $\hat{x}_2$ is used instead i.e. the second backstepping variable is chosen as

$$z_2 = \hat{x}_2 - \alpha_1. \tag{5.101}$$

Substituting equation 5.99, equation 5.100 and equation 5.101 into equation 5.98

$$\begin{aligned} \dot{V}_1 = {} & \frac{c_b}{J_2} \omega_d z_1 - \frac{c_b}{J_2} z_1^2 - \frac{k_t}{J_2} z_2 z_1 - \frac{k_t}{J_2} \alpha_1 z_1 - \frac{k_t}{J_2} \epsilon_2 z_1 \\ & + \hat{\boldsymbol{\theta}}^T \boldsymbol{\phi}(x_1) z_1 + \tilde{\boldsymbol{\theta}}^T \boldsymbol{\phi}(x_1) z_1 - \frac{1}{\gamma} \tilde{\boldsymbol{\theta}}^T \dot{\hat{\boldsymbol{\theta}}} - \frac{1}{d_1} \boldsymbol{\epsilon}^T \boldsymbol{\epsilon}, \end{aligned} \tag{5.102}$$

is obtained which can be made negative semidefinite by designing the virtual function

$$\alpha_1 = \frac{c_b}{k_t} \omega_d - \frac{J_2}{k_t} \hat{\boldsymbol{\theta}}^T \boldsymbol{\phi}(x_1) z_1 - c_1 z_1, \tag{5.103}$$

and the adaptive control law is given by the tuning function

$$\dot{\hat{\boldsymbol{\theta}}} = \gamma \boldsymbol{\phi}(x_1) z_1. \tag{5.104}$$

In the second step of the backstepping control design procedure the error system of equation 5.101 is asymptotically stabilized to zero. Taking the derivative of the second error system given in equation 5.101

$$\dot{z}_2 = \dot{\hat{x}}_2 - \dot{\alpha}_1, \tag{5.105}$$

is obtained. Substituting derivative of x_2 in equation 5.99 into equation 5.105

$$\dot{z}_2 = \dot{x}_2 - \dot{\epsilon}_2 - \dot{\alpha}_1, \tag{5.106}$$

is obtained where $\dot{e}_2 = \dot{\hat{x}}_2$ that can be obtained from the observer. The derivative of the virtual function in equation 5.103

$$\dot{\alpha}_1 = \frac{\partial \alpha_1}{\partial z_1}\dot{z}_1 + (\frac{\partial \alpha_1}{\partial \hat{\boldsymbol{\theta}}^T})\dot{\hat{\boldsymbol{\theta}}}, \tag{5.107}$$

may be calculated analytically or numerically using the partial derivatives

$$\frac{\partial \alpha_1}{\partial z_1} = \frac{J_2}{k_t}\boldsymbol{\theta}^T\boldsymbol{\phi}(x_1) - c_1, \tag{5.108}$$

and

$$\frac{\partial \alpha_1}{\partial \hat{\boldsymbol{\theta}}^T} = \frac{J_2}{k_t}z_1\boldsymbol{\phi}(x_1). \tag{5.109}$$

The derivative $\dot{\alpha}_1$ can be expressed as

$$\dot{\alpha}_1 = f_1(x_1, \hat{\boldsymbol{\theta}})(\frac{c_b}{J_2}x_1 - \frac{k_t}{J_2}x_2) + f_1(x_1, \hat{\boldsymbol{\theta}})\boldsymbol{\theta}^T\boldsymbol{\phi}(x_1) + \frac{J_2}{k_t}z_1\dot{\hat{\boldsymbol{\theta}}}^T\boldsymbol{\phi}(x_1), \tag{5.110}$$

where $f_1(x_1, \hat{\boldsymbol{\theta}}) = \frac{\partial \alpha_1}{\partial z_1}$.

To design a non certainty equivalence controller the way to proceed would be to express $\boldsymbol{\theta}$ as

$$\boldsymbol{\theta} = \hat{\boldsymbol{\theta}} + \tilde{\boldsymbol{\theta}}, \tag{5.111}$$

and regulate z_2 to zero using a Lyapunov candidate function designed as

$$V_2 = V_1 + \frac{1}{2}z_2^2 + \frac{1}{2\gamma_2}\tilde{\boldsymbol{\theta}}^T\tilde{\boldsymbol{\theta}} + \frac{1}{2d_2}\boldsymbol{\epsilon}^T\boldsymbol{P}_0\boldsymbol{\epsilon}, \tag{5.112}$$

where $\boldsymbol{P}_0 = \boldsymbol{P}_0^T > 0$ is such that $\boldsymbol{P}_0\boldsymbol{A}_0 + \boldsymbol{A}_0^T\boldsymbol{P}_0 = -\mathrm{I}$. But this approach failed to control the simulated system. Instead a certainty equivalence approach proved fruitful in which $\hat{\boldsymbol{\theta}}$ estimated in the first step by the first tuning function is used in all proceeding steps hence writing equation 5.110 as

$$\dot{\alpha}_1 = f_1(x_1, \hat{\boldsymbol{\theta}})(\frac{c_b}{J_2}x_1 - \frac{k_t}{J_2}x_2) + f_1(x_1, \hat{\boldsymbol{\theta}})\hat{\boldsymbol{\theta}}^T\boldsymbol{\phi}(x_1) + \frac{J_2}{k_t}z_1\dot{\hat{\boldsymbol{\theta}}}^T\boldsymbol{\phi}(x_1). \tag{5.113}$$

The Lyapunov candidate function of equation 5.112 is simplified to

$$V_2 = V_1 + \frac{1}{2}z_2^2 + \frac{1}{2d_2}\boldsymbol{\epsilon}^T\boldsymbol{P}_0\boldsymbol{\epsilon}. \tag{5.114}$$

The derivative of the Lyapunov function in equation 5.114 is

$$\dot{V}_2 = \dot{V}_1 + z_2\dot{z}_2 - \frac{1}{d_2}\boldsymbol{\epsilon}^T\boldsymbol{\epsilon}. \tag{5.115}$$

Substituting $\dot{z}_2$ from equation 5.106 into equation 5.115

$$\dot{V}_2 = \dot{V}_1 + z_2\dot{x}_2 - z_2\dot{e}_2 - z_2\dot{\alpha}_1 - \frac{1}{d_2}\boldsymbol{\epsilon}^T\boldsymbol{\epsilon}, \tag{5.116}$$

is obtained, where $\dot{e}_2$ is obtained from observer. Substituting value of $\dot{x}_2$ from equation 5.89 into equation 5.116 the derivative becomes

$$\dot{V}_2 = \dot{V}_1 + z_2x_3 - z_2x_1 - z_2\dot{e}_2 - z_2\dot{\alpha}_1 - \frac{1}{d_2}\boldsymbol{\epsilon}^T\boldsymbol{\epsilon}. \tag{5.117}$$

To make $\dot{V}_2$ negative definite x_3 is used as the virtual input , i.e, a backstepping variable z_3 is introduced given by

$$z_3 = x_3 - \alpha_2. \tag{5.118}$$

The equation 5.117 after substituting equation 5.118 becomes

$$\begin{aligned}\dot{V}_2 =& -\frac{k_t}{J_2}z_2z_1 + z_2z_3 + z_2\alpha_2 - z_2x_1 - z_2\dot{e}_2 \\ & - z_2f_1(x_1,\hat{\boldsymbol{\theta}})(\frac{c_b}{J_2}x_1 - \frac{k_t}{J_2}x_2) + z_2f_1(x_1,\hat{\boldsymbol{\theta}})\hat{\boldsymbol{\theta}}^T\boldsymbol{\phi}(x_1) + z_2\frac{J_2}{k_t}z_1\dot{\hat{\boldsymbol{\theta}}}^T\boldsymbol{\phi}(x_1) \\ & - \frac{1}{d_2}\boldsymbol{\epsilon}^T\boldsymbol{\epsilon}.\end{aligned} \tag{5.119}$$

To make $\dot{V}_2$ negative definite the virtual function

$$\begin{aligned}\alpha_2 =& \frac{k_t}{J_2}z_1 + x_1 + \dot{e}_2 + f_1(x_1,\hat{\boldsymbol{\theta}})(\frac{c_b}{J_2}x_1 - \frac{k_t}{J_2}\hat{x}_2) \\ & - f_1(x_1,\hat{\boldsymbol{\theta}})\hat{\boldsymbol{\theta}}^T\boldsymbol{\phi}(x_1) \\ & - \frac{J_2}{k_t}z_1\dot{\hat{\boldsymbol{\theta}}}^T\boldsymbol{\phi}(x_1) - d_2\frac{k_t}{J_2}f_1z_2 - c_2z_2,\end{aligned} \tag{5.120}$$

is designed. The derivative of the third error system represented by equation 5.118

$$\dot{z}_3 = \dot{x}_3 - \dot{\alpha}_2, \tag{5.121}$$

represents the the error dynamics that are stabilized to zero in the third backstepping step. The derivative of α_2 can be expressed as

$$\dot{\alpha}_2 = \frac{\partial\alpha_2}{\partial z_1}\dot{z}_1 + \frac{\partial\alpha_2}{\partial x_1}\dot{x}_1 + \frac{\partial\alpha_2}{\partial\hat{\boldsymbol{\theta}}^T}\dot{\hat{\boldsymbol{\theta}}} + \frac{\partial\alpha_2}{\partial z_2}\dot{z}_2. \tag{5.122}$$

Substituting equation 5.106 into equation 5.122

$$\dot{\alpha}_2 = \frac{\partial\alpha_2}{\partial z_1}\dot{z}_1 + \frac{\partial\alpha_2}{\partial x_1}\dot{x}_1 + \frac{\partial\alpha_2}{\partial\hat{\boldsymbol{\theta}}^T}\dot{\hat{\boldsymbol{\theta}}} + \frac{\partial\alpha_2}{\partial z_2}(\dot{x}_2 - \dot{e}_2 - \dot{\alpha}_1), \tag{5.123}$$

is obtained. Substituting value of $\dot{x}_3$ and $\dot{\alpha}_1$ into equation 5.121 to get

$$\begin{aligned}\dot{z}_3 = &-\frac{k_t}{J_1}x_2 - \frac{c_r}{J_1}x_3 - \frac{T_{fu}(x_3)}{J_1} + \frac{T_m}{J_1} - \frac{\partial\alpha_2}{\partial z_1}\dot{z}_1 - \frac{\partial\alpha_2}{\partial x_1}\dot{x}_1 \\ &- \frac{\partial\alpha_2}{\partial\hat{\boldsymbol{\theta}}^T}\dot{\hat{\boldsymbol{\theta}}} - \frac{\partial\alpha_2}{\partial z_2}(x_3 - x_1 + \dot{\epsilon}_2 - \dot{\alpha}_1).\end{aligned} \tag{5.124}$$

To design a stable control law to stabilize the error system represented by equation 5.124 the Lyapunov function

$$V_3 = V_1 + V_2 + \frac{1}{2}z_3^2 + \frac{1}{2d_3}\boldsymbol{\epsilon}^T\boldsymbol{P}_0\boldsymbol{\epsilon}, \tag{5.125}$$

is used. Taking the derivative of V_3 to obtain

$$\begin{aligned}\dot{V}_3 \leq &z_2z_3 - z_3\frac{k_t}{J_1}\hat{x}_2 - z_3\frac{k_t}{J_1}\epsilon_2 - z_3\frac{c_r}{J_1}x_3 - z_3\frac{T_{fu}(x_3)}{J_1} + z_3\frac{T_m}{J_1} \\ &- z_3\frac{\partial\alpha_2}{\partial z_1}\dot{z}_1 - z_3\frac{\partial\alpha_2}{\partial x_1}\dot{x}_1 \\ &- z_3\frac{\partial\alpha_2}{\partial\hat{\boldsymbol{\theta}}^T}\dot{\hat{\boldsymbol{\theta}}} - z_3\frac{\partial\alpha_2}{\partial z_2}(x_3 - x_1 + \dot{\epsilon}_2 - \dot{\alpha}_1) - \frac{1}{d_3}\boldsymbol{\epsilon}^T\boldsymbol{\epsilon},\end{aligned} \tag{5.126}$$

which can be made negative semidefinite using the control law that uses real input T_m given by

$$\begin{aligned}T_m = J_1(&-z_2 + \frac{k_t}{J_1}\hat{x}_2 - \frac{k_t}{J_1}x_3 - \frac{T_{fu}(x_3)}{J_1} + \quad + \frac{\partial\alpha_2}{\partial z_1}\dot{z}_1 + \frac{\partial\alpha_2}{\partial x_1}\dot{x}_1 \\ &+ \frac{\partial\alpha_2}{\partial\hat{\boldsymbol{\theta}}^T}\dot{\hat{\boldsymbol{\theta}}} + \frac{\partial\alpha_2}{\partial z_2}(x_3 - x_1 + \dot{\epsilon}_2 - \dot{\alpha}_1) \\ &- c_3z_3 - d_3\frac{k_t}{J_1}z_3.\end{aligned} \tag{5.127}$$

The adaptive tuning function based control law is used to control the experimental drill rig mathematical model simulation results are discussed in the next section.

5.4.3 *Simulation results and conclusions*

It is determined from simulations that for the purpose of controlling the simulated plant a simple first order polynomial model of friction can achieve acceptable control performance. Plots in Figure 33 show the performance of adaptive backstepping control for a set point of 10rad/s. The friction is parametrized as $\boldsymbol{\theta}\boldsymbol{\phi}(x_1) = a_1x_1$. The tuning constants used during simulation are given in Table 7. Similarly plots in Figure 34 show the performance for a set point of 5rad/sec. The performance of observer is shown in Figure 35, the observer error is bounded. The torsional oscillations are attenuated and transient response is remarkably improved as compared to the nonadaptive control in chapter 4. Most of the adaptive control algorithms reported

in the literature as discussed in chapter 1 exhibit improved performance over non-adaptive controllers. But most of the studies do not report the effect of measurement noise on control performance. It is observed if noise is added to the system, the performance of the adaptive backstepping controller deteriorates as shown in Figure 36. The adaptive control was not robust to measurement noise and tuning proved difficult in the drill string setup. Furthermore, analytically finding the derivatives of the virtual functions is difficult because the number of terms increase in each consecutive backstepping step. This is the so called parameter explosion problem. This makes the control design intractable for a system with higher degrees of freedom. Thus the approach is not convenient for a drill string that may have to be modelled using more than two DOF's.

Methods that are robust to measurement noise and that avoid the parameter explosion problem are presented in the next chapter. But the mathematical framework developed for the adaptive control design serves as a foundation for the more robust control method.

Table 7: Tuning parameters used for simulation.

PARAMETER	VALUE
c_1	3
c_2	3
c_3	5
d_1	0.01
d_2	0.001
d_3	0.000001
γ_1	0.9

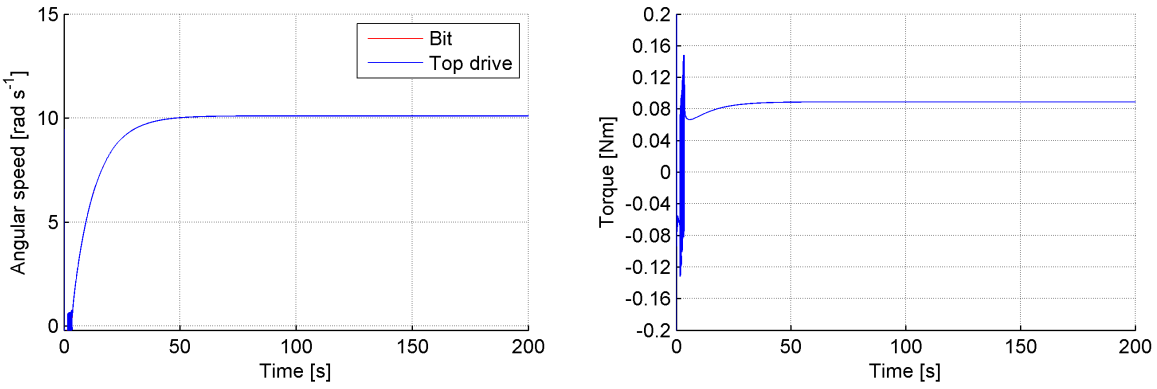

(a) Angular velocity set point 10rads^{-1}.

(b) Input torque for 10rads^{-1} set point.

Figure 33: Response at 10rads^{-1} set point.

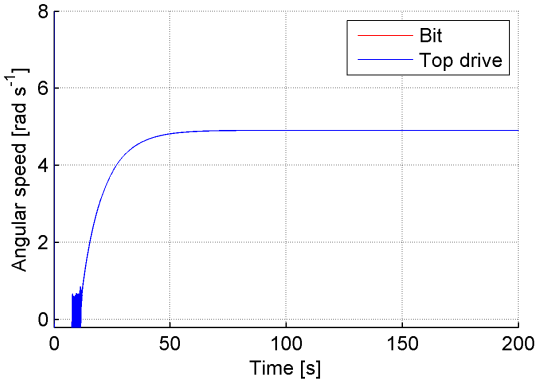

(a) Angular velocity set point 5rads^{-1}.

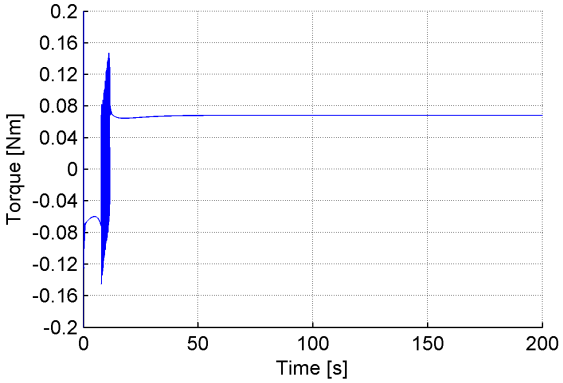

(b) Input torque for 5rads^{-1} set point.

Figure 34: Response at 5 rads^{-1} set point.

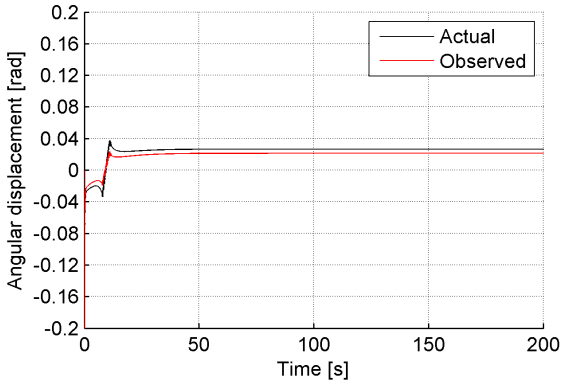

(a) Deflection at angular velocity of 5rads^{-1}.

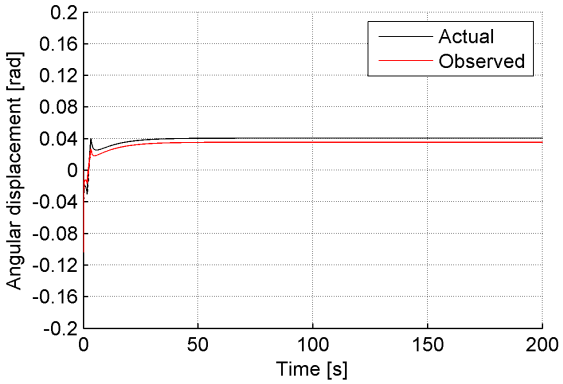

(b) Deflection at angular velocity of 10rads^{-1}.

Figure 35: Comparison between real value and observed value of deflection.

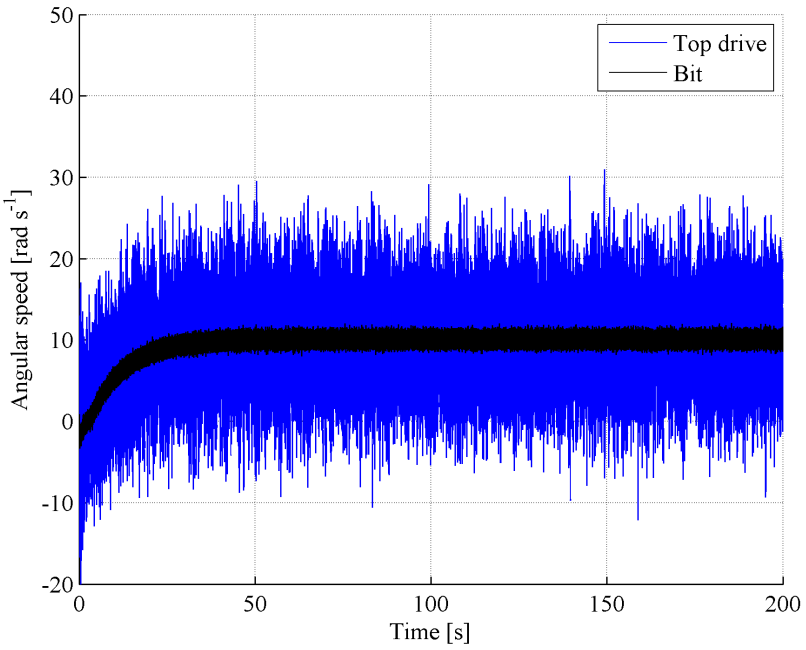

Figure 36: Control performance in the presence of measurement noise for set point 10rads^{-1}.

6

DYNAMIC SURFACE CONTROL FOR THE ATTENUATION OF TORSIONAL OSCILLATIONS

The adaptive backstepping control described in the previous chapter was not robust to noise. Furthermore, in each backstepping step analytical derivatives are needed that are cumbersome to derive and lead to a problem that has been named the explosion of terms in the control literature. Even if the tuning function based approach were robust to measurement noise the explosion of terms would make control design for a system with more than two degrees of freedom complex.

A method that is robust to friction modelling errors and measurement noise has to be used. The assumptions that the friction can be modelled using a linear in parameter polynomial friction model have to be discarded. An approach that allows robust control of the drill string experimental setup that has shown promising results in experiments is dynamic surface control (DSC).

The chapter is organized such that in the first Section 6.1 the dynamic surface control design is explained. In Section 6.2 the main contribution of this chapter is presented which is an observer based dynamic surface control design approach to attenuate the torsional oscillations in the experimental setup. To the best of the author's knowledge the observer based DSC algorithm has previously not been reported in the drill string control literature.

6.1 INTRODUCTION

The adaptive backstepping control design for the drill string was not robust. The friction is modelled using a linear in parameter model and the approach becomes increasingly cumbersome as the number of terms needed to calculate the derivatives $\dot{\alpha}_i$ where $i = 1, 2, 3, ...$ analytically increases with increase in the relative degree of the system. This is known as the explosion of terms (Hedrick and Yip 2000).

To make the control robust the uncertainty in bit friction has to be considered. Thus the problem of nonlinear control with an unmatched uncertainty has to be tackled. Robust control approaches, for example sliding mode control are applicable to systems where the uncertainty satisfies the matching condition.

Green and Hedrick (1990) developed the multiple sliding surface (MSS) control approach which extended the sliding mode control approach to systems with unmatched uncertainty. The dynamic surface control is an extension of MSS control. Therefore in the next section, the MSS control approach is explained first.

6.1.1 *Multiple Sliding Surface Control*

The MSS control approach has been applied to speed control problems in automotive applications (Green and Hedrick 1990; Alt et al. 2009), twin rotor aerial vehicle systems (Nguyen and Hyun 2014) but to the best of the authors knowledge the approach has not been applied to drilling applications.

To illustrate the MSS control approach consider the nonlinear system (Hedrick and Yip 2000)

$$\dot{x}_1 = f_1(x_1) + x_2 + \Delta f_1(x_1), \tag{6.1}$$

and

$$\dot{x}_2 = u, \tag{6.2}$$

is considered where Δf_1 is an unmatched uncertainty. It is required that Δf_1 be bounded by a known nonlinear function $\rho_1(x_1)$. The objective is to track the desired trajectory represented by ω_d . The first error variable called the first sliding surface defined as

$$S_1 = x_1 - \omega_\mathrm{d}. \tag{6.3}$$

The derivative of S_1 in equation 6.3 is

$$\dot{S}_1 = f_1(x_1) + x_2 + \Delta f_1(x_1) - \dot{\omega}_\mathrm{d}. \tag{6.4}$$

The first Lyapunov function candidate is chosen as

$$V_1 = \frac{1}{2} S_1^2. \tag{6.5}$$

The derivative of V_1 in equation 6.5 is given by

$$\dot{V}_1 = S_1 \dot{S}_1. \tag{6.6}$$

To make $\dot{V}_1$ in equation 6.6 negative definite x_2 is used as the virtual control input and the second backstepping variable or sliding surface is defined as

$$S_2 = x_2 - x_{2\mathrm{d}}. \tag{6.7}$$

A suitable choice for $x_{2\mathrm{d}}$ to make $\dot{V}_1$ negative definite is

$$x_{2\mathrm{d}} = \dot{\omega}_\mathrm{d} - f_1(x_1) - k_1 S_1 - \rho_1 \mathrm{sgn}(S_1). \tag{6.8}$$

The second error surface or sliding surface dynamics

$$\dot{S}_2 = \dot{x}_2 - \dot{x}_{2\mathrm{d}}, \tag{6.9}$$

are obtained by taking the derivative of equation 6.7. Substituting $\dot{x}_2$ from equation 6.2 into equation 6.9

$$\dot{S}_2 = u - \dot{x}_{2d}, \tag{6.10}$$

the dynamics of the second sliding surface are obtained. In the MSS control approach of Green and Hedrick (1990) the derivative $\dot{x}_{2d}$ is calculated in an ad hoc manner by numerical differentiation to avoid explosion of terms and avoid calculating the analytical derivative of the uncertain term Δf_1 which cannot be computed. The numerical derivative is calculated as

$$\dot{x}_{2d} \simeq \frac{x_{2d}[n] - x_{2d}[n-1]}{\Delta T}, \tag{6.11}$$

where ΔT is the sample time. The second Lyapunov function V_2 to stabilize the origin of the dynamics of error surface in equation 6.10 is

$$V_2 = V_1 + \frac{1}{2} S_2^2. \tag{6.12}$$

To make the derivative of V_2 from equation 6.12 negative definite and regulate S_2 to zero, the input

$$u = \dot{x}_{2d} - k_2 S_2, \tag{6.13}$$

is used. In the next section the dynamic surface control algorithm is described.

6.1.2 *Dynamic surface control*

An observer based dynamic surface control approach is used to attenuate the friction induced torsional oscillations in the experimental setup. This section will explain the full state feedback dynamic surface control approach. The dynamic surface control developed by Swaroop et al. (1997) modified the MSS control by making the following two modifications:

1. Bounded uncertainty is dominated using smooth nonlinear damping.
2. First order filters are introduced to calculate the derivatives.

The first modification ensures robustness of the system in the presence of the nonlinear unmatched uncertainty, for example, Δf_1 as discussed in the previous section 6.1.1. The DSC approach replaces the discontinuous sign function used in equation 6.8 by a smooth Lipschitz function. The system trajectory converges to a bounded region about the origin which implies ultimate uniform boundedness.

To further elaborate the differences between DSC and MSS control the second order system that was analyzed in Section 6.1.1 is revisited. In the following discussion, the DSC control approach for a system with full state feedback is presented. The first modification is made by replacing the virtual control of equation 6.8 with

$$\overline{x_{2d}} = \dot{\omega}_d - f_1(x_1) - k_1 S_1 - \frac{\rho_1^2 S_1}{2\epsilon}. \tag{6.14}$$

The second modification involves introducing a first order filter designed as

$$\tau \dot{x}_{2d} + x_{2d} = \dot{\omega}_d - f_1(x_1) - k_1 S_1 - \frac{\rho_1^2 S_1}{2\epsilon}, \tag{6.15}$$

which can be written as

$$\tau \dot{x}_{2d} + x_{2d} = \overline{x_{2d}}, \tag{6.16}$$

where $x_{2d}(0) = \overline{x_{2d}}(0)$. Introduction of the low-pass filter removes the problem of explosion of terms that is a drawback of backstepping. Even though the addition of a filter increases the dynamic order of the closed loop system complicating the stability analysis, the DSC method is more convenient to implement because higher order systems can easily be handled as analytical derivatives in each backstepping step are not required. As in the MSS control described in Section 6.1.1 the control input that stabilizes the whole system is given by

$$u = \dot{x}_{2d} - k_2 S_2. \tag{6.17}$$

Using equation 6.16, $\dot{x}_{2d}$ in equation 6.17 is implemented as

$$u = \frac{\overline{x_{2d}} - x_{2d}}{\tau} - k_2 S_2. \tag{6.18}$$

The filter error is

$$\eta_2 = x_{2d} - \overline{x_{2d}}. \tag{6.19}$$

The error system is given by the three equations for dynamics of S_1, S_2 and η_2 which will be derived next. If x_{2d} and $\overline{x_{2d}}$ are added and subtracted in equation 6.1

$$\dot{x}_1 = x_2 - x_{2d} + x_{2d} - \overline{x_{2d}} + \overline{x_{2d}} + f_1 + \Delta f_1, \tag{6.20}$$

is obtained. Substituting $\overline{x_{2d}}$ from equation 6.14 in equation 6.20

$$\dot{x}_1 = S_2 + \eta_2 + \dot{\omega}_d + \overline{x_{2d}} + f_1 + \Delta f_1, \tag{6.21}$$

is derived. The derivative of the first sliding surface in equation 6.3 becomes

$$\dot{S}_1 = S_2 + \xi_2 - k_1 S_1 + \Delta f_1 - \frac{S_1 \rho_1^2}{2\epsilon}. \tag{6.22}$$

Substituting value of u from equation 6.18 into equation 6.2

$$\dot{S}_2 = -k_2 S_2, \tag{6.23}$$

is obtained. The filter error dynamics

$$\dot{\xi}_2 = -\frac{\xi_2}{\tau} + \frac{d}{dt}(f_1 + S_1\frac{\rho_1^2}{2\epsilon} + k_1 S_1), \tag{6.24}$$

are obtained by taking the derivative of equation 6.19. The filter error dynamics in equation 6.24 can be written in terms of a general function η with arguments S_1, S_2 and ξ_2 as

$$\dot{\xi}_2 = -\frac{\xi_2}{\tau} + \eta(S_1, S_2, \xi_2, k, \epsilon), \tag{6.25}$$

where η is bounded if the error surfaces are constrained in a compact subset, i.e., a compact and convex set $\mathbb{B} = \{z \in \mathbb{R}^3 | S_1^2 + S_2^2 + \xi_2^2 \leq 2p, p > 0, z = [S_1 S_2 \xi_2]^T\}$ exists for $\eta < M$, where $M > 0$ (Song and Hedrick 2011; Swaroop et al. 1997). The Lyapunov function for the error system is chosen as

$$V = \frac{S_1^2 + S_2^2 + \xi_2^2}{2}. \tag{6.26}$$

The derivative of V is given as

$$\dot{V} = S_1\dot{S}_1 + S_2\dot{S}_2 + \xi_2\dot{\xi}_2. \tag{6.27}$$

Substituting equation 6.25, equation 6.23 and equation 6.22 into equation 6.27

$$\begin{aligned}\dot{V} = {} & S_1(S_2 + \xi_2 - k_1 S_1 + \Delta f_1 - \\ & \frac{S_1\rho_1^2}{2\epsilon}) + S_2(-k_2 S_2) + \xi_2(-\frac{\xi_2}{\tau} + \eta(S_1, S_2, \xi_2, k, \epsilon)),\end{aligned} \tag{6.28}$$

is obtained. As $\Delta f_1 < \rho$ and $\eta < M$ equation 6.28 can be written as

$$\dot{V} \leq S_1(S_2 + \xi_2 - k_1 S_1 + \rho - \frac{S_1\rho_1^2}{2\epsilon}) + S_2(-k_2 S_2) - \frac{\xi_2^2}{\tau} + \xi_2 M. \tag{6.29}$$

Simplifying equation 6.29

$$\dot{V} \leq (S_1 S_2 + S_1\xi_2 - k_1 S_1^2 + S_1\rho - \frac{S_1^2\rho_1^2}{2\epsilon}) - k_2 S_2^2 - \frac{\xi_2^2}{\tau} + \xi_2 M, \tag{6.30}$$

is obtained.

To prove that the system is uniformly bounded stable with a bound ϵ which can be chosen arbitrarily Young's inequality is used (Song and Hedrick 2011 ; Swaroop et al. 1997). Young's inequality can generally be stated as

$$ab \leq \frac{k^p}{p}|a|^p + \frac{1}{qk^q}|b|^q, \tag{6.31}$$

where $p > 1$, $q > 1$, such that $(p-1)(q-1) = 1$. Substituting $a = 1$, $b = S_1\rho$, $p = q = 2$ and $\epsilon = k^2$ into equation 6.31 the following inequality is obtained

$$S_1\rho \leq \frac{\epsilon}{2} + \frac{S_1^2\rho^2}{2\epsilon}. \tag{6.32}$$

Similarly,

$$\xi_2 M \leq \frac{\epsilon}{2} + \frac{\xi_2^2 M^2}{2\epsilon}. \tag{6.33}$$

Substituting $a = S_1$, $b = S_2$, $p = q = 2$ and $k = 1$ into equation 6.31 the following inequality is obtained

$$S_1S_2 \leq \frac{S_1^2}{2} + \frac{S_2^2}{2}. \tag{6.34}$$

Similarly,

$$S_1\xi_2 \leq \frac{S_1^2}{2} + \frac{\xi_2^2}{2}. \tag{6.35}$$

Substituting equation 6.32, equation 6.33, equation 6.34, equation 6.35 into equation 6.29 the derivative of Lyapunov function V can be expressed as

$$\dot{V} \leq (\frac{S_1^2 + S_2^2}{2} + \frac{S_1^2 + \xi_2^2}{2} - k_1S_1^2 + \frac{\epsilon}{2}) - k_2S_2^2 - \frac{\xi_2^2}{\tau} + \frac{\xi_2^2M^2}{2\epsilon} + \frac{\epsilon}{2}. \tag{6.36}$$

To make this negative definite choose the time constant $1/\tau$ as follows (Swaroop et al.1997)

$$\frac{1}{\tau} = 1 + \frac{M^2}{2\epsilon} + \alpha_0, \tag{6.37}$$

where α_0 is a constant that may be tuned. Substituting this into equation 6.36

$$\dot{V} \leq \frac{2S_1^2 + S_2^2 + \xi_2^2}{2} - k_1S_1^2 - k_2S_2^2 - \xi_2^2 - \alpha_0\frac{\xi_2^2}{2} + \epsilon, \tag{6.38}$$

is obtained. The constants k_1, k_2 and α_0 can be tuned so the Lyapunov derivative becomes

$$\dot{V} \leq \epsilon, \tag{6.39}$$

which shows uniform ultimate boundedness with arbitrary bound ϵ. To further explain the dynamic surface control approach a simple example is given in the next section

6.1.3 *Example*

To illustrate the design procedure an example (Swaroop et al. 1997) of control design is simulated. The plant to be controlled is modelled by

$$\dot{x}_1 = x_2 + \Delta f_1(x_1), \tag{6.40}$$

$$\dot{x}_2 = x_3, \tag{6.41}$$

and

$$\dot{x}_3 = u. \tag{6.42}$$

The output is given by

$$y = x_1. \tag{6.43}$$

The uncertainty is simulated using the function $\Delta f_1(x_1) = x_1^2 \sin x_1$, which is designed to be bounded by x_1^2. The objective is for y to track the reference $r(t)$ The first error surface is

$$S_1 = x_1 - r(t). \tag{6.44}$$

Taking the derivative of equation 6.45

$$\dot{S}_1 = x_2 + \Delta f_1(x_1) - \dot{r}(t), \tag{6.45}$$

is derived. The desired virtual state to make the first error surface dynamics stable is designed as

$$\overline{x_{2d}} = \dot{r}(t) - k_1 S_1 - S_1 \frac{x_1^4}{2\epsilon}. \tag{6.46}$$

The first low-pass filter

$$\tau_2 \dot{x}_{2d} + x_{2d} = \overline{x_{2d}}, \tag{6.47}$$

is designed, where $x_{2d}(0) = \overline{x_{2d}}(0)$. The second error surface is given by

$$S_2 = x_2 - x_{2d}. \tag{6.48}$$

Taking the derivative of equation 6.48

$$\dot{S}_2 = \dot{x}_2 - \dot{x}_{2d}, \tag{6.49}$$

is obtained. The derivative of the virtual function $\dot{x}_{2d}$ is conveniently obtained from the first filter without introducing the problem of explosion of terms. The equation 6.49 can be written as

$$\dot{S}_2 = x_3 - \dot{x}_{2d}. \tag{6.50}$$

To make the augmented Lyapunov function derivative negative definite x_3 will be used as a virtual input using the third backstepping variable $S_3 = x_3 - x_{3d}$ and setting $x_{3d} = \dot{x}_{2d} - k_2 S_2$ will make the Lyapunov function negative definite but to generate $\dot{x}_{3d}$ a filter

$$\tau_3 \dot{x}_{3d} + x_{3d} = \overline{x_{3d}}, \tag{6.51}$$

is used, where $x_{3d}(0) = \overline{x_{3d}}(0)$ and

$$\overline{x_{3d}} = \dot{x}_{2d} - k_2 S_2. \tag{6.52}$$

The third error surface is given by

$$S_3 = x_3 - x_{3d}. \tag{6.53}$$

The derivative of S_3 in equation 6.53 is

$$\dot{S}_3 = \dot{x}_3 - \dot{x}_{3d}, \tag{6.54}$$

which after substituting $\dot{x}_3$ from equation 6.42 becomes

$$\dot{S}_3 = u - \dot{x}_{3d}. \tag{6.55}$$

The third error surface is stabilized about the origin using input

$$u = \dot{x}_{3d} - k_3 S_3. \tag{6.56}$$

The system was simulated using controller tuning parameters given in Table 8. The simulation results given in Figure 37 show that the control algorithm tracks the reference well even in the presence of unmatched modelling uncertainty.

Table 8: Tuning parameters used for simulation.

PARAMETER	VALUE
τ_2	0.01
τ_3	0.01
k_1	40
k_2	60
k_3	60
ϵ	0.01

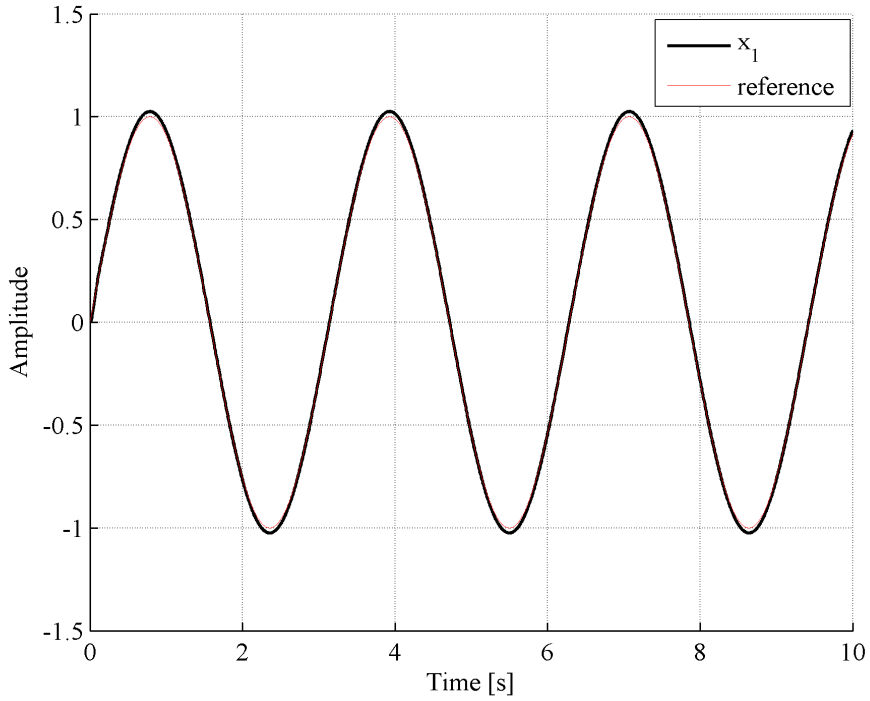

Figure 37: Simulated output of the plant and generated reference.

6.2 DSC FOR THE REDUCTION OF TORSIONAL OSCILLATIONS IN THE EXPERIMENTAL SETUP

The dynamic surface control approach is investigated in a scaled experimental drill string setup. As one of the states i.e. x_2 is not available for feedback, an observer is designed to estimate the unmeasured state. The Welch power spectral density analysis of the measured signals show a reduction in low frequency torsional oscillations as well as high frequency torsional oscillations. The attenuation of high frequency torsional oscillations is important because as discussed in chapter 1 such oscillations have been measured in real drill strings where they are localized to the bottom hole assembly. High frequency torsional oscillations have been found responsible for fatigue damage of the drill collars of the bottom hole assembly.

The DSC approach does not require an exact friction model, only a bounded Lipschitz function to model the uncertainty must be known which is an advantage of this approach because friction is difficult to model in practice and changes with the change in drilling conditions such as the type of rock or soil. Even in controlled laboratory conditions, the friction showed considerable variation between different experiments performed on the same experimental setup.

The mathematical model for the experimental setup given in Section 3.3.3 is used. The parameters of the model identified in section 3 given in Table 4 are used for simulation and control design.

It is assumed that the friction at the top end is known and at the drill bit the friction uncertainty is modelled by a function δT_{fb}. The function δT_{fb} is assumed to be bounded by a known Lipschitz function. Furthermore, rotation of drill string of the experimental setup is restricted to positive (clockwise) direction. The next section explain in detail the observer based control design. To the best of the author's knowledge the presented observer along with the dynamic surface control and stability analysis of the closed loop has not been reported in the literature to date.

6.2.1 *Control Design*

In the experimental setup shown in Figure 7 the top drive speed x_3 and drill bit speed x_1 are measured the state x_2 is not measured so a full order observer is designed based on the identified model. The desired property is that in absence of drill bit friction modelling error the observer error should be asymptotically convergent and in the presence of friction model uncertainty it may reject the effect of the uncertainty on $\tilde{x}_2$ where $\tilde{x}_2$ is the state estimation error. Assuming the model uncertainty is due to modelling error of the drill bit friction an observer with the error equations

$$\dot{\tilde{\boldsymbol{x}}} = \boldsymbol{A}_0\tilde{\boldsymbol{x}} + \boldsymbol{\Delta T}_{\text{fb}}, \tag{6.57}$$

and

$$\dot{\tilde{\boldsymbol{y}}} = \boldsymbol{C}\tilde{\boldsymbol{x}}, \tag{6.58}$$

is designed where

$$\tilde{\boldsymbol{x}} = \begin{bmatrix} \tilde{x}_1 \\ \tilde{x}_2 \\ \tilde{x}_3 \end{bmatrix}, \boldsymbol{\Delta T}_{\text{fb}} = \begin{bmatrix} \delta T_{\text{fb}} \\ 0 \\ 0 \end{bmatrix} \text{ and } \boldsymbol{C} = \begin{bmatrix} 1 & 0 & 1 \end{bmatrix}.$$

As x_1 and x_3 are measured the observer is designed by adjusting the gains so that $\boldsymbol{A}_0$ is Hurwitz and the error system has disturbance rejection properties. If δT_{fb} is considered as the input in equation 6.57 then $\boldsymbol{A}_0$ has to be designed so that effect of of δT_{fb} on $\tilde{x}_2$ is rejected. Note that the observer is the same as that designed in section 5.4.1 and appendix A1, therefore detailed derivation is not repeated.

The control objective is that the drill bit velocity x_1 should track a desired reference velocity ω_{d}. Therefore the first error surface is defined as

$$S_1 = x_1 - \omega_{\text{d}}. \tag{6.59}$$

The derivative of equation 6.59 is

$$\dot{S}_1 = \dot{x}_1 - \dot{\omega}_{\text{d}}. \tag{6.60}$$

Substituting equation 3.15 into equation equation 6.60 and treating bit friction as an uncertainty

$$\dot{S}_1 = -\frac{c_b}{J_2}x_1 + \frac{k_t}{J_2}x_2 + \frac{\delta T_{fb}}{J_2} - \dot{\omega}_d, \tag{6.61}$$

is obtained. The state x_2 is not measured so it cannot be used directly as a virtual control input. Instead the state estimated by the observer $\hat{x}_2$ is used. The state x_2 can be represented as the sum of the estimated value $\hat{x}_2$ and the estimation error $\tilde{x}_2$ as

$$x_2 = \hat{x}_2 + \tilde{x}_2. \tag{6.62}$$

Substituting equation 6.62 into equation 6.61 the surface dynamics

$$\dot{S}_1 = -\frac{c_b}{J_2}x_1 + \frac{k_t}{J_2}\hat{x}_2 + \frac{k_t}{J_2}\tilde{x}_2 + \frac{\delta T_{fb}}{J_2} - \dot{\omega}_d, \tag{6.63}$$

are derived. The desired value of $\hat{x}_2$ is x_{2d} and it is obtained by implementing a first order filter

$$\tau_1 \dot{x}_{2d} + x_{2d} = \overline{\hat{x}_2}, \tag{6.64}$$

with time constant τ_1 and where $x_{2d}(0) = \overline{\hat{x}_2}(0)$. The $\overline{\hat{x}_2}$ is designed as

$$\overline{\hat{x}_2} = \frac{c_b}{J_2}x_1 - \frac{1}{k_t}\frac{S_1\rho_1^2}{2\epsilon} - c_1 S_1 + \dot{\omega}_d\frac{J_2}{k_t} - d_1(\frac{k_t}{J_2})^2 S_1, \tag{6.65}$$

where c_1 and d_1 are positive tuning parameters to introduce damping into the system and ϵ is a small positive constant also used as a tuning parameter. The function ρ_1 is a locally Lipschitz function bounding the uncertainty δT_{fb} such that $|\delta T_{fb}| \leq \rho_1(x_1)$. For the experimental setup the bounding function $\rho_1(x_1)$ is given by

$$\rho_1(x_1) = \frac{5}{1 - 0.2x_1 e^{-20x_1}}. \tag{6.66}$$

The second error surface is

$$S_2 = \hat{x}_2 - x_{2d}. \tag{6.67}$$

Taking derivative of equation 6.67

$$\dot{S}_2 = \dot{\hat{x}}_2 - \dot{x}_{2d}, \tag{6.68}$$

is obtained. The error in estimated x_2 is

$$\tilde{x}_2 = x_2 - \hat{x}_2. \tag{6.69}$$

Taking the derivative of equation 6.69

$$\dot{\hat{x}}_2 = \dot{x}_2 - \dot{\tilde{x}}_2, \tag{6.70}$$

is obtained. The term $\dot{x}_2$ in equation 6.70 is measured as its difference between the measured top and bit speeds. Similarly $\dot{\tilde{x}}_2$ is obtained from the full order observer, hence $\dot{\hat{x}}_2$ is available. Substituting equation 6.70 into equation 6.68

$$\dot{S}_2 = \dot{x}_2 - \dot{\tilde{x}}_2 - \dot{x}_{2d}, \tag{6.71}$$

is derived. Substituting into equation 6.71 the value of $\dot{x}_2$ from equation 3.16

$$\dot{S}_2 = x_3 - x_1 - \dot{\tilde{x}}_2 - \dot{x}_{2d}, \tag{6.72}$$

is derived. The error system equation 6.72 is regulated about the origin by using x_3 as the virtual input with desired value x_{3d} which can be generated using a second filter

$$\tau_2 \dot{x}_{3d} + x_{3d} = \overline{x_3}, \tag{6.73}$$

where $x_{3d}(0) = \overline{x_3}(0)$. To stabilize the second error surface dynamics represented by equation 6.72, $\overline{x_3}$ is designed as

$$\overline{x_3} = -\frac{k_t}{J_2} S_1 + x_1 + \dot{\tilde{x}}_2 + \dot{x}_{2d} - c_2 S_2. \tag{6.74}$$

The third error surface is defined as

$$S_3 = x_3 - x_{3d}. \tag{6.75}$$

Taking derivative of equation 6.75 the dynamics of the third error surface are obtained as

$$\dot{S}_3 = \dot{x}_3 - \dot{x}_{3d}. \tag{6.76}$$

Substituting equation 3.17 into equation 6.76

$$\dot{S}_3 = -\frac{k_t}{J_1}\hat{x}_2 - \frac{k_t}{J_1}\tilde{x}_2 - \frac{c_r}{J_1}x_3 - \frac{T_r}{J_1} + \frac{T_m}{J_1} - \dot{x}_{3d}, \tag{6.77}$$

that represents the dynamics of the third error system is derived. Any uncertainty in top drive friction modelling is ignored to simplify control design. As T_m is the actual torque exerted by the top drive motor, the control law to stabilize the whole system is designed as follows

$$T_m = -J_1 c_1 S_2 + k_2 \hat{x}_2 + c_r x_3 + \frac{T_r}{J_1} - d_2 \frac{k_t}{J_1} S_3 - \frac{c_3 S_3}{J_1} - J_1 \dot{x}_{3d}. \tag{6.78}$$

To prove stability the closed loop error dynamics of the control system have to be analysed. As two filters are used the filter dynamics have to be considered during stability analysis too. To obtain the expressions for the filter dynamics define the filter errors for filters represented by equation 6.64 as

$$\eta_2 = x_{2d} - \overline{\hat{x}_2}, \tag{6.79}$$

and similarly filter error for the filter given by equation 6.73 is

$$\eta_3 = x_{3d} - \overline{x_3}. \tag{6.80}$$

Substituting equation 6.79 into equation 6.64

$$\dot{x}_{2d} = -\frac{\eta_2}{\tau_1}, \tag{6.81}$$

is derived. Substituting equation 6.80 in equation 6.73

$$\dot{x}_{3d} = -\frac{\eta_3}{\tau_2}, \tag{6.82}$$

is obtained. Taking derivative of equation 6.79 and substituting in the resulting derivative $\dot{x}_{2d}$ from equation 6.81, the following dynamic equation for the first filter is obtained

$$\dot{\eta}_2 = -\frac{\eta_2}{\tau_1} - \dot{\overline{\hat{x}_2}}. \tag{6.83}$$

Similarly, taking derivative of equation 6.80 and substituting in the resulting derivative $\dot{x}_{3d}$ from equation 6.82, the dynamic equation for the second filter is

$$\dot{\eta}_3 = -\frac{\eta_3}{\tau_2} - \dot{\overline{x_3}}. \tag{6.84}$$

The derivative of equation 6.65 and equation 6.74 are denoted by $\dot{\overline{\hat{x}_2}}$ and $\dot{\overline{x_3}}$ respectively. Both can be expressed as functions $g_1(S_1)$ and $g_2(S_1, S_2)$ respectively. So the error dynamics of the filters can be expressed by the equations

$$\dot{\eta}_2 = -\frac{\eta_2}{\tau_1} - g_1(S_1), \tag{6.85}$$

and

$$\dot{\eta}_3 = -\frac{\eta_3}{\tau_2} - g_2(S_1, S_2). \tag{6.86}$$

The functions g_1 and g_2 are bounded if the error surfaces are constrained in a compact subset i.e A compact and convex set
$\mathbb{B} = \{z \in \mathbb{R}^4 | S_1^2 + S_2^2 + \eta_2^2 + \eta_3^2 \leq 2p, p > 0, z = \begin{bmatrix} S_1 & S_2 & S_3 & \eta_2 & \eta_3 \end{bmatrix}^T\}$
exists then $g_1 < M_1$ and $g_2 < M_2$ where $M_1 > 0$ and $M_2 > 0$ (Song and Hedrick 2011; Swaroop et al. 1997).

In order to analyse the stability of the closed loop the expressions for $\dot{S}_1$ given by equation 6.63, $\dot{S}_2$ given by equation 6.72 and $\dot{S}_3$ given by equation 6.77 have to be manipulated further to obtain a form suitable for stability analsis (Song and Hedrick 2011). The first manipulation is undertaken by adding $\frac{k_t}{J_2}\overline{\hat{x}_2}$ and $\frac{k_t}{J_2}x_{2d}$ to equation 6.63

and subtracting $\frac{k_t}{J_2}\overline{\hat{x}_2}$ and $\frac{k_t}{J_2}x_{2d}$ from equation 6.63. After this manipulation the expression for the dynamics of the first surface becomes

$$\dot{S}_1 = -\frac{c_b}{J_2}x_1 + \frac{k_t}{J_2}(\hat{x}_2 - x_{2d}) + \frac{k_t}{J_2}(x_{2d} - \overline{\hat{x}_2}) + \frac{k_t}{J_2}\overline{\hat{x}_2} - \frac{\delta T_{fb}}{J_2} + \tilde{x}_2 - \dot{\omega}_d. \tag{6.87}$$

Substituting values of $(\hat{x}_2 - x_{2d})$ and $(x_{2d} - \overline{\hat{x}_2})$ from equation 6.67 and equation 6.79 respectively

$$\dot{S}_1 = -\frac{c_b}{J_2}x_1 + \frac{k_t}{J_2}(\hat{x}_2 - x_{2d}) + \frac{k_t}{J_2}(x_{2d} - \overline{\hat{x}_2}) + \frac{k_t}{J_2}\overline{\hat{x}_2} - \frac{\delta T_{fb}}{J_2} + \tilde{x}_2 - \dot{\omega}_d, \tag{6.88}$$

is derived. Inserting the expression for $\overline{\hat{x}_2}$ from equation 6.65 into equation 6.88

$$\dot{S}_1 = +\frac{k_t}{J_2}S_2 + \frac{k_t}{J_2}\eta_2 - \frac{1}{J_2}\frac{S_1\rho_1^2}{2\epsilon} - \frac{k_t}{J_2}c_1S_1 - d_1(\frac{k_t}{J_2})^2S_1 - \frac{\delta T_{fb}}{J_2} + \tilde{x}_2, \tag{6.89}$$

is obtained. Adding and subtracting both $\overline{x_3}$ and x_{3d} to equation 6.72 the expression for the dynamics of the second error surface become

$$\dot{S}_2 = (x_3 - x_{3d}) + (x_{3d} - \overline{x_3}) + \overline{x_3} - x_1 - \dot{\tilde{x}}_2 - \dot{x}_{2d}. \tag{6.90}$$

Substituting $(x_3 - x_{3d})$ and $(x_{3d} - \overline{x_3})$ from equation 6.75 and equation 6.80 respectively into equation 6.90

$$\dot{S}_2 = S_3 + \eta_3 + \overline{x_3} - x_1 - \dot{\tilde{x}}_2 - \dot{x}_{2d}. \tag{6.91}$$

is derived. Simplifying further substitute value of $\overline{x_3}$ from equation 6.74 into equation 6.91 to obtain

$$\dot{S}_2 = S_3 + \eta_3 - \frac{k_t}{J_2}S_1 - c_2S_2. \tag{6.92}$$

The expression for the dynamics of the third error surface given by equation 6.77 is manipulated by substituting T_m from equation 6.78 into equation 6.77 to get

$$\dot{S}_3 = -\frac{k_t}{J_2}\tilde{x} - d_2(\frac{k_t}{J_1})S_3 - S_2 - c_3S_3. \tag{6.93}$$

The closed loop error dynamics are represented by equation 6.85, equation 6.86, equation 6.89, equation 6.92 and equation 6.93. Consider a Lyapunov function candidate

$$V = \frac{S_1^2}{2} + \frac{1}{d_1}\tilde{\boldsymbol{x}}^T\boldsymbol{P}_0\tilde{\boldsymbol{x}} + \frac{S_2^2}{2} + \frac{S_3^2}{2} + \frac{1}{d_2}\tilde{\boldsymbol{x}}^T\boldsymbol{P}_0\tilde{\boldsymbol{x}} + \frac{\eta_2^2}{2} + \frac{\eta_3^2}{2}, \tag{6.94}$$

for the closed loop error dynamics, where $\boldsymbol{P}_0$ is a symmetric matrix such that $\boldsymbol{P}_0\boldsymbol{A}_0 + \boldsymbol{A}_0^T\boldsymbol{P}_0 = -\mathrm{I}$. The derivative of equation 6.94 is given by

$$\dot{V} = S_1\dot{S}_1 - \frac{1}{d_1}\tilde{\boldsymbol{x}}^T\tilde{\boldsymbol{x}} + S_2\dot{S}_2 + S_3\dot{S}_3 + \frac{1}{d_2}\tilde{\boldsymbol{x}}^T\tilde{\boldsymbol{x}} + \eta_2\dot{\eta}_2 + \eta_3\dot{\eta}_3. \tag{6.95}$$

Substituting values of $\dot{S}_1$, $\dot{S}_2$, $\dot{S}_3$, $\dot{\eta}_2$ and $\dot{\eta}_3$ from equation 6.89, equation 6.92, equation 6.93, equation 6.86 and equation 6.85 respectively to get

$$\begin{aligned}\dot{V} =& \frac{k_t}{J_2}S_1S_2 + \frac{k_t}{J_2}S_1\eta_2 - \frac{1}{J_2}\frac{\rho_1^2 S_1^2}{2\epsilon} \\ & - c_1\frac{k_t}{J_2}S_1^2 - d_1\left(\frac{k_t}{J_2}\right)^2 S_1^2 + \frac{\delta T_{fb}}{J_2}S_1 \\ & + \tilde{x}_2 S_1 - \frac{1}{d_1}\tilde{\boldsymbol{x}}^T\tilde{\boldsymbol{x}} + \eta_3 S_2 \\ & - \frac{k_t}{J_2}S_1S_2 - c_2S_2^2 - \frac{k_t}{J_1}\tilde{x}_2S_3 \\ & - d_2\left(\frac{k_t}{J_1}\right)^2 S_3^2 - c_3S_3^2 - \frac{1}{d_2}\tilde{\boldsymbol{x}}^T\tilde{\boldsymbol{x}} \\ & - \frac{\eta_2^2}{\tau_1} + \eta_2 g_1 - \frac{\eta_3^2}{\tau_2} + \eta_3 g_2.\end{aligned} \tag{6.96}$$

In equation 6.96 the fifth and seventh terms that contain the observer error are manipulated and proven to be negative definite by completing square, similarly the twelfth and thirteenth terms containing observer error are combined and by completing square are made negative definite. From Young's inequality the following inequalities are derived

$$S_1\delta T_{fb} \leq \frac{S_1^2\rho_1^2}{2\epsilon} + \frac{\epsilon}{2}, \tag{6.97}$$

$$S_1\eta_2 \leq \frac{S_1^2 + \eta_2^2}{2}, \tag{6.98}$$

$$S_2\eta_3 \leq \frac{S_2^2 + \eta_3^2}{2}, \tag{6.99}$$

$$\eta_2 g_1 \leq \frac{\eta_2^2 g_1^2}{2\epsilon} + \frac{\epsilon}{2}, \tag{6.100}$$

and

$$\eta_3 g_2 \leq \frac{\eta_3^2 g_2^2}{2\epsilon} + \frac{\epsilon}{2}. \tag{6.101}$$

Substituting equation 6.97, equation 6.98, equation 6.99, equation 6.100 and equation 6.101 in equation 6.96 the Lyapunov derivative becomes

$$\begin{aligned}\dot{V} \leq & \frac{1}{2}\left(\frac{k_t}{J_2}S_1^2 + \eta_2^2 + S_2^2 + \eta_3^2\right) - \frac{1}{2}\left(c_1\frac{k_t}{J_2}S_1^2 + c_2S_2^2 + c_3S_3^2 + \frac{2\eta_2^2}{\tau_1} + S_2^2 + \frac{2\eta_3^2}{\tau_2}\right) \\ & + \frac{\epsilon(1+2J_2)}{2J_2}.\end{aligned} \tag{6.102}$$

By tuning c_1, c_2, c_3, τ_1 and τ_2 ultimate uniform bounded stabilization can be achieved.

6.2.2 *Simulation results*

The drill string model with adaptive control is simulated for the plant parameters given in Table 5 that are identified for the experimental setup in Chapter 3. The values of the tuning parameters that are used are given in Table 9. The tuning parameters given in Table 9 are found to insure stable performance. The constants c_1 , d_1 and c_2, d_2 are taken equal to single parameters c_1' and c_2' respectively. Simulation of the control algorithm can be seen in Figure 38. The simulations show good performance even when measurement noise is added to the output.

Table 9: Tuning parameters used for simulation and experiments.

PARAMETER	VALUE
τ_1	1
τ_2	0.0001
c_1'	10
c_2'	5
c_3	400
ϵ	0.1

6.3 EXPERIMENTAL RESULTS

The control algorithm is then implemented in a Ds 1104 rapid prototyping system and the control algorithm is executed at a sampling rate of 10KHz. The tuning parameters given in Table 9 are used.

Similarly, a PID controller is manually tuned for the same setup. The PID controller also executes at 10KHz. The PID controller is used during parameter estimation of the experimental setup as the system cannot be operated in open loop at the required angular velocities. The PID controller is also implemented in the Ds 1104 prototyping system. The PID controller only gets feedback from the top drive velocity. This is how most of the current drill rigs are configured such that only the top drive is controlled and no feedback from the bit is employed. The PID controller makes the top drive of the experimental setup stiff. It is found that a controller that maintains the top drive velocity without taking in to consideration the bit velocity can excite high frequency torsional oscillations in the drill string.

Comparing control algorithms is not the aim of this work but as a reference, the PID control is used to highlight why a properly designed controller is needed during

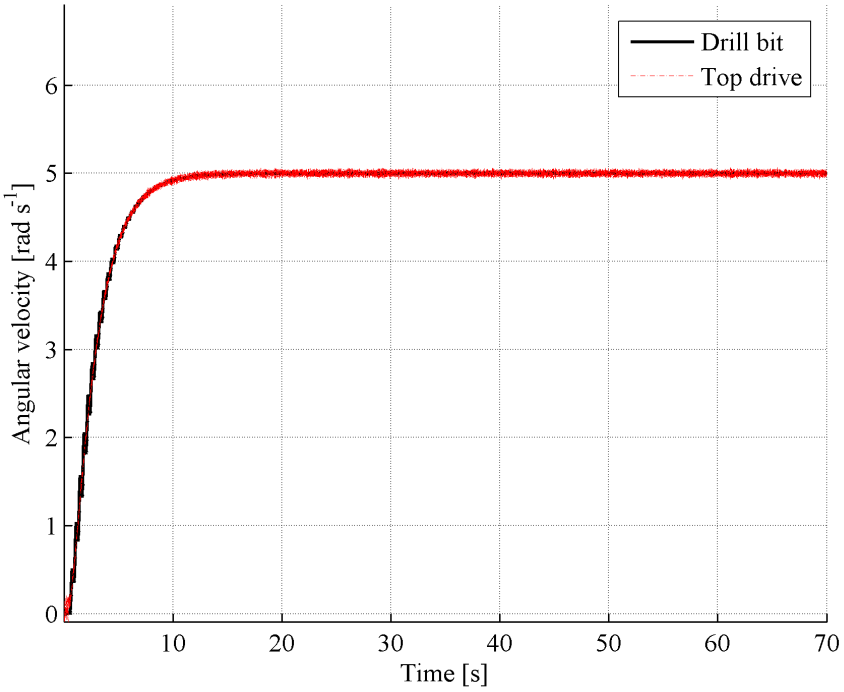

Figure 38: Simulated performance of the dynamic surface control.

drilling. If the controller is not properly tuned the actuator introduces high frequency torsional oscillations. In practice such control solutions are difficult to tune and may need retuning for each drill rig (Runia, Dwars, and Stulemeijer 2013).

In Figure 39 the experimental setup is commanded to track a reference speed of 6rad/sec . As shown in Figure 39 the transient response of the dynamic surface controller is damped. The top drive speed closely follows the drill bit speed for the dynamic surface control. A close up of steady state response in Figure 40 shows that the top drive speed closely follows the drill bit speed for dynamic surface control.

A Welch power spectral density (PSD) estimate (Kodakadath Premachandran et al. 2017) of the observed deflection between drill bit and top drive is shown in Figure 41. To calculate the PSD only the steady state response is considered during analysis. The transient response part is removed from the measured data before estimation of the PSD. A sampling frequency of 1KHz is used for data acquisition. A Hanning window is used and 3000 point FFT at 50% overlap is used. The DSC controller attenuates both high frequency torsional oscillations and low frequency torsional oscillations. For the PID controller a pronounced vibration at 241.7Hz is observed which can cause drill collar fatigue in real drill rigs.

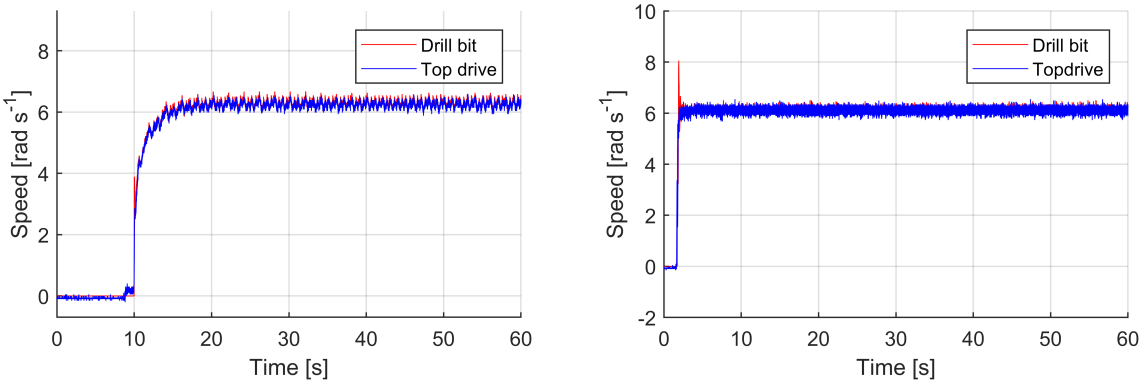

(a) Performance of dynamic surface control.

(b) Performance of PID control.

Figure 39: Comparison of the performance of dynamic surface control with a stiff PID controller (measurement from the experimental setup are shown).

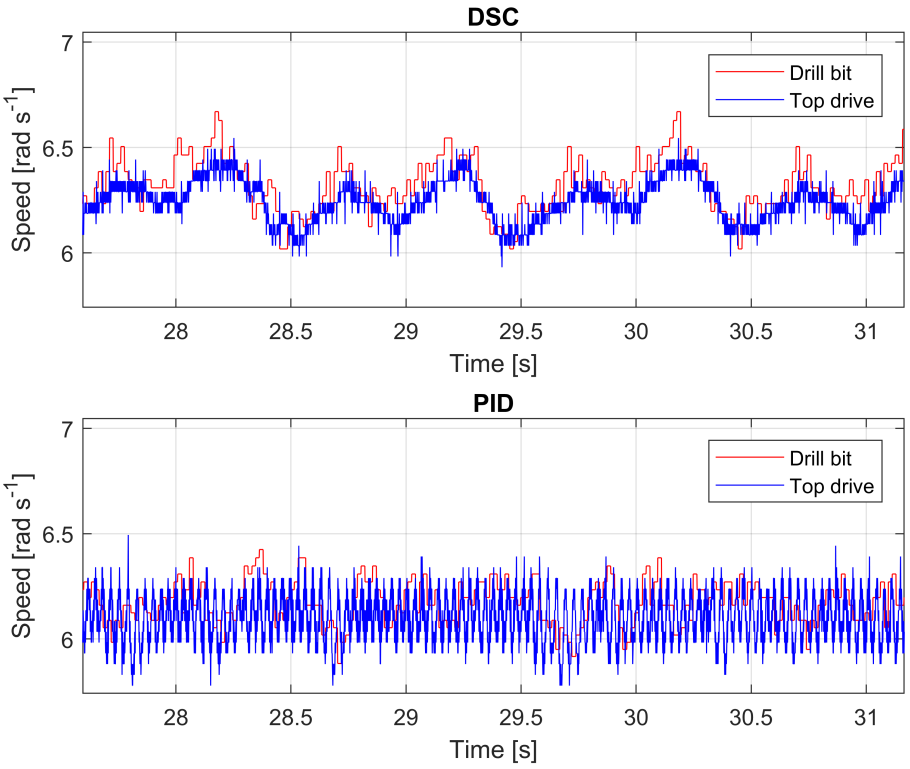

Figure 40: Closeup of dynamic surface control and stiff PID controller performance (experimental results are shown).

6.4 CONCLUSION

Simulation studies ignore the effects of measurement noise which may lead to instability when the control algorithm is applied to a real system. Robustness of adaptive control algorithms needs to be studied in experimental setups.

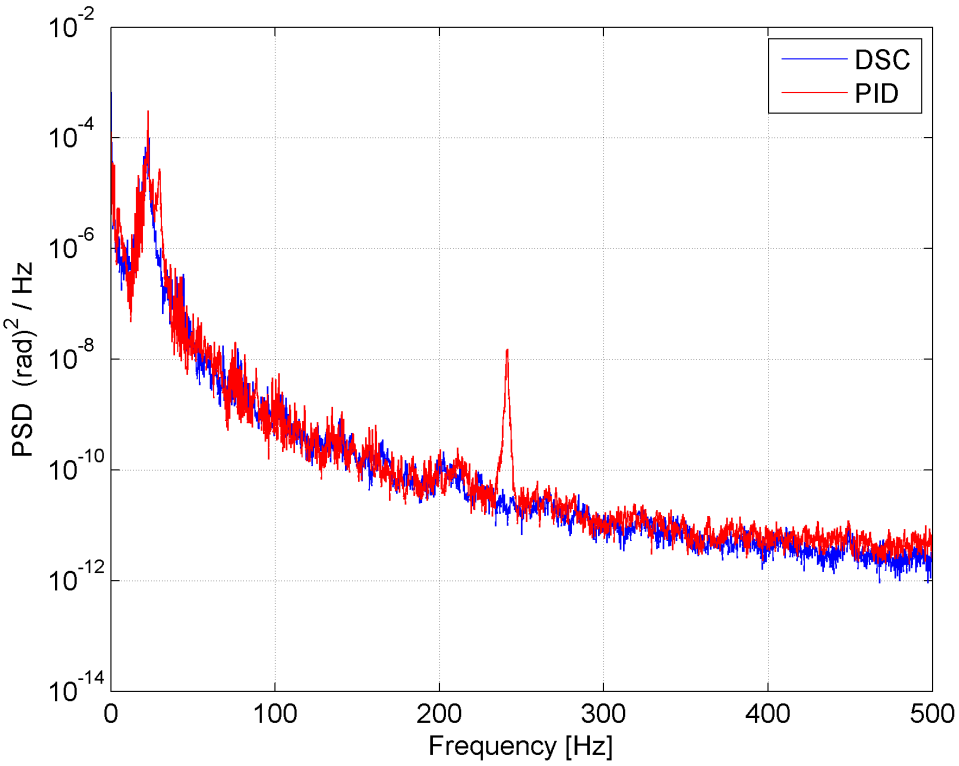

Figure 41: Power spectral density of $\hat{x}_2$.

Dynamic surface control can be applied to a higher degree of freedom system and does not suffer from the explosion of terms issue faced in adaptive backstepping control.

A drawback that may hinder implementation of the controller designed in this work is that it requires feedback of measured bit speed. Which require wired drill string to be used. Vromen (2015) developed algorithms that used only surface data (measurements from the top drive) and developed an observer based torsional oscillation control algorithms that worked well in simulations but the algorithms that utilized only surface measurements failed to perform in an experimental setup as reported in Vromen (2015) . Observers that may be robust to modelling errors and use only surface data are a potential area of future research.

Even when the data from down hole is available the data rate constraints prohibit the closing of the control loop. To implement feedback control algorithms that work on conventional drill strings, that utilize mud pulse telemetry, the data rate constraints will have to be overcome. Control algorithms that may work under data rate limitation have to be developed.

7

SUMMARY AND CONCLUSIONS

Torsional oscillations can lead to fatigue due to cyclic stresses, connection failure due to unwinding, damage to measurement while drilling (MWD) tools, impact damage to PDC bits and in extreme cases drill pipe breakage (Fear and Abbasian 1994) hence a lot of effort to identify optimal operating regions for drilling that avoid torsional oscillations is being made. Similarly efforts to develop control systems for torsional oscillation attenuation are currently underway. At present no simple solution to the stick-slip mitigation problem that works in all circumstances exists. Using down hole measurements to provide feedback using wired drill strings has been identified by a special IADC committee as the next frontier in torsional vibration attenuation (Womer et al. 2011).

The focus of this work was on active control of torsional oscillations in drill strings. The literature on active control of torsional oscillations in drill strings was reviewed. From the review of the state of the art it was noticed that most of the control oriented literature is limited to simulation studies. Particularly to the best of the author's knowledge no experimental evaluation of backstepping control have been reported in the literature on drill string torsional oscillation attenuation.

To fill this gap in the literature an experimental drill string setup was designed and built. The parameters of the experimental drill rig were identified using the nonlinear least squares trust region reflective algorithm. Validation experiments showed that the friction even in a laboratory setup shows considerable variations. This meant that control algorithms have to be robust to model uncertainties. It was also found that system identification of experimental drill string setups has not been sufficiently addressed in the current literature.

A common assumption in control design for the drill string is that all the states of the system should be measured so full state feedback could be used to control the drill string. In a real drill string this is not possible. Similarly, in the experimental setup used in this work only the top drive velocity and drill bit velocity is measured. The designed control algorithms require a third state which is the of angular deflection between the top and bottom of the drill string. The unmeasured state had to be estimated using an observer. The use of an observer complicates the nonlinear control design as stability of the closed loop has to be proved.

To overcome the challenge of uncertain friction the control algorithm either has to be adaptive or it has to be robust to the uncertain friction. First a tuning function based adaptive observer backstepping controller was designed. Simulation studies

showed good performance in attenuating torsional oscillations. But experimental results and further simulation studies showed that the adaptive control was not robust to measurement noise. This presented a new challenge. Furthermore, it became clear that the adaptive backstepping control design becomes too complicated for higher order systems.

From the findings described above it is apparent that the control algorithm for the drill string experimental setup has to be observer based. The control algorithm has to be robust to uncertainty in the friction and robust to measurement noise. The algorithm should ensure closed loop stability in the presence of observer errors and the control algorithm complexity should not make it prohibitive to design controllers for higher order systems. An observer based dynamic surface control algorithm was designed that fulfilled the requirements. The observer and dynamic surface control algorithms are proven to be closed loop stable. Experiments show that the dynamic surface control algorithm can eliminate stick slip torsional oscillations and also does not excite high frequency modes of the drill string experimental setup.

Experimentation using an experimental scaled drill rig can be used to test the working of the control algorithm in the presence of unmodelled dynamics and noise but the conditions in which real drilling takes place are harsher than the conditions in the laboratory. A control design that performs well in the laboratory may not perform well during actual drilling. It also has to be pointed out that a control algorithm that fails to perform in the experimental scaled drill rig will have little chances of working in the full scale drill rig, so experiments using an experimental scaled drill rigs are useful. The control algorithm was implemented using a sampling frequency of 10KHz, whereas the data rate of current mud pulse telemetric devices is 3 to 10bits/s. Feedback control that utilizes the drill bit speed may be feasible for wired drill strings that have a faster data rate. The current limitation of the experimental setup is that the length of the drill string does not change during operation in contrast the length of a real drill string does not remain fixed. As the length changes the stiffness and other parameters of the drill rig will change. These parameter variations can be modelled as bounded uncertain functions and a dynamic surface control algorithm can be designed that takes these uncertainties into consideration. It would require experimentation to determine whether the torsional oscillation attenuation performance stays the same or changes. Another solution is to adjust the parameters of the controller during the time when new drill string sections are added.

A possible extension of the work is to devise the dynamic surface control algorithm for a drill string setup with more than two degrees of freedom. A linear matrix equality (LMI) based approach to extend the dynamic surface control approach to higher order systems can be found in Song and Hedrick (2011). It may be used to extend the approach to higher order systems.

Another possible future research direction is the design and evaluation of observer based quantized output feedback. One of the main hurdles in feedback control implementation for drill strings is the data rate limitation. Conceptual frameworks that deal with data rate constrained feedback control such as the one presented in Liberzon (2007) should be investigated.

Part III

APPENDIX

A

APPENDIX

A.1 LASALLE-YOSHIZAWA THEOREM

Let $V(x,t)$ be a continuously differentiable function such that

$$\gamma_1(|x| \leq V(x,t) \leq \gamma_2(|x|), \tag{A.1}$$

and

$$\dot{V}(x,t) \leq -W(x) \leq 0 \tag{A.2}$$

$\forall\, t \geq 0$, $x \in \mathbb{R}^n$, where γ_1 and γ_2 are K_∞ functions and W is a continuous function. Then all trajectories of the solution are globally uniformly bounded and satisfy $\lim_{x\to\infty} W(x(t)) = 0$. In addition if $W(x)$ is positive definite then the equilibrium $x = 0$ is globally uniformly asymptotically stable.

A.2 OBSERVER DESIGN

The error system represented by equation 5.83, equation 5.84 and equation 5.85 can be represented in state space form as

$$\dot{\tilde{\boldsymbol{x}}} = \boldsymbol{A}_0\tilde{\boldsymbol{x}} + \boldsymbol{\Delta T}_{\text{fb}}, \tag{A.3}$$

and

$$\dot{\tilde{\boldsymbol{y}}} = \boldsymbol{C}\tilde{\boldsymbol{x}}, \tag{A.4}$$

where

$$\tilde{\boldsymbol{x}} = \begin{bmatrix} \tilde{x}_1 \\ \tilde{x}_2 \\ \tilde{x}_3 \end{bmatrix}, \boldsymbol{\Delta T}_{\text{fb}} = \begin{bmatrix} \delta T_{\text{fb}} \\ 0 \\ 0 \end{bmatrix} \text{ and } \boldsymbol{C} = \begin{bmatrix} 1 & 0 & 1 \end{bmatrix}.$$

As x_1 and x_3 are measured the observer is designed by adjusting the gains so that $\boldsymbol{A}_0$ is Hurwitz.

To determine the stability the state space system has to be converted in to its equivalent transfer function. Any state space system in the general form

$$\dot{\boldsymbol{q}} = \boldsymbol{A}\boldsymbol{q} + \boldsymbol{B}u, \tag{A.5}$$

and

$$y = \boldsymbol{C}\boldsymbol{q} + \boldsymbol{D}u, \tag{A.6}$$

can be converted in to an equivalent transfer function matrix

$$\boldsymbol{H}(s) = \frac{\boldsymbol{Y}(s)}{\boldsymbol{U}(s)} = \boldsymbol{C}(s\boldsymbol{I} - \boldsymbol{A})^{-1}\boldsymbol{B} + \boldsymbol{D}. \tag{A.7}$$

For the error system is represented by equation A.3 and equation A.4 the transfer function from ΔT_{fl} to $\tilde{x}_2$ can be found using

$$\boldsymbol{H}_1(s) = \begin{bmatrix} 0 & 1 & 0 \end{bmatrix} (s\boldsymbol{I} - \boldsymbol{A}_0)^{-1} \begin{bmatrix} 1 \\ 0 \\ 0 \end{bmatrix}. \tag{A.8}$$

In equation A.8 the gains k_{11}, k_{21} and k_{31} are set equal to k_1. Similarly the gains k_1, k_{22} and k_{32} are set equal to k_2. This is done to simplify the observer gain assignment design. A Routh table is used as a design tool (Nise 2007).
The equation A.8 becomes

$$\boldsymbol{H}_1(s) = \frac{35 \times (4 + 4k_1)s + 35 \times (29k_1 + 4k_2 + 25)}{140s^3 + (140k_1 + 140_{k_2} + 991)s^2 + (410732 + 42927k_1 - 367839k_2)s + k_3}, \tag{A.9}$$

where $k_3 = (672832k_1 + 105130k_2 + 567702)$. Using the Routh table as explained in Appendix A.3 the stability of $\boldsymbol{H}_1(s)$ is insured by choosing $k_1 = 10$ and $k_2 = -5$. The magnitude of the transfer function $\boldsymbol{H}_1(s)$ is low as shown in Figure 42 which implies good rejection properties. The transfer function

$$\boldsymbol{H}_1(s) = \frac{1540s + 10325}{140s^3 + 1691s^2 + 2.679 \times 10^6 s + 6.77 \times 10^6}, \tag{A.10}$$

has been calculated in Matlab using the identified parameters for the experimental setup and the code is given in Listing 1.

A.3 ROUTH TABLE

A Routh table can be used as a design tool that indicates the number of left hand poles and right hand poles for a closed loop transfer function. Consider the transfer function

$$\boldsymbol{G}(s) = \frac{N(s)}{a_4 s^4 + a_3 s^3 + a_2 s^2 + a_1 s + a_0}. \tag{A.11}$$

Using the Routh- Hurwitz stability criterion the routh table can be used to determine stability of the transfer function (Nise 2007). The routh table is constructed for equation A.11 is given in Table 10. The Routh-Hurwitz criterion states that the number of sign changes in the first column i.e column containing a_4, a_3, b_1, c_1 and d_1, is equal

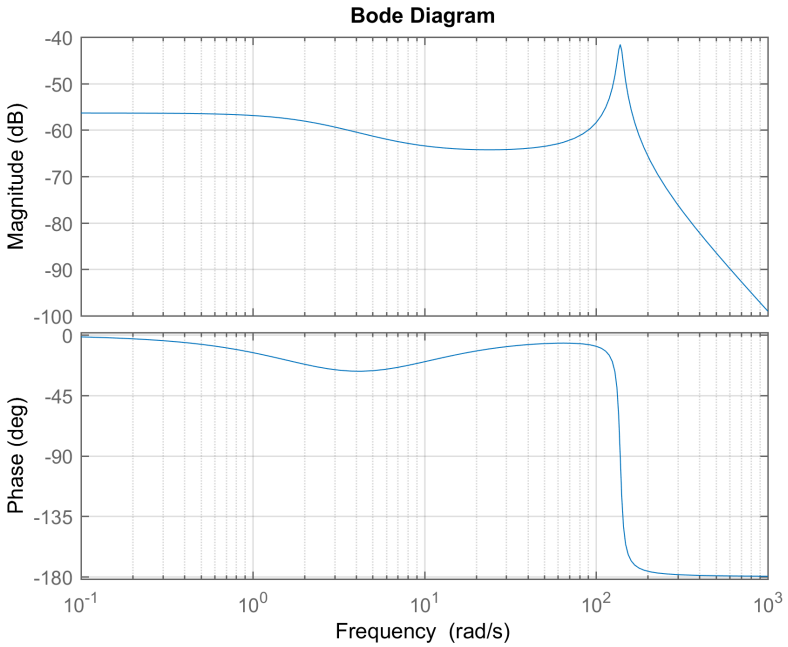

Figure 42: Bode diagram of $\boldsymbol{H}_1(s)$

.

Table 10: Routh table for system of equation A.11

s^4	a_4	a_2	a_0	
s^3	a_3	a_1	0	
s^2	$b_1 = \frac{-\begin{vmatrix} a_4 & a_2 \\ a_3 & a_1 \end{vmatrix}}{a_3}$	$b_2 = \frac{-\begin{vmatrix} a_4 & a_0 \\ a_3 & 0 \end{vmatrix}}{a_3}$	$b_3 = \frac{-\begin{vmatrix} a_4 & 0 \\ a_3 & 0 \end{vmatrix}}{a_3} = 0$	
s^1	$c_1 = \frac{-\begin{vmatrix} a_3 & a_1 \\ b_1 & b_2 \end{vmatrix}}{b_1}$	$c_2 = \frac{-\begin{vmatrix} a_3 & 0 \\ b_1 & 0 \end{vmatrix}}{b_1} = 0$	$c_3 = \frac{-\begin{vmatrix} a_3 & 0 \\ b_1 & 0 \end{vmatrix}}{b_1}$=o	
s^0	$d_1 = \frac{-\begin{vmatrix} b_1 & b_2 \\ c_1 & 0 \end{vmatrix}}{c_1}$	$d_2 = \frac{-\begin{vmatrix} b_1 & 0 \\ c_1 & 0 \end{vmatrix}}{c_1} = 0$	$d_3 = \frac{-\begin{vmatrix} b_1 & 0 \\ c_1 & 0 \end{vmatrix}}{c_1} = 0$	

to the right hand poles. A stable system with all the roots in left half plane will have no sign changes. The gains k_1 and k_2 are selected to ensure this for the system of equation A.9. This is done by using the Routh table given in Table 11.

Table 11: Routh table for system of equation A.9.

s^3	$a_3 = 140$	$a_1 = 410732 + 42927k_1 - 367839k_2$	0
s^2	$a_2 = 140k_1 + 140k_2 + 991$	$a_0 = 672832k_1 + 105130k_2 + 567702$	0
s^1	$b_1 = -\begin{vmatrix} a_3 & a_1 \\ a_2 & a_0 \end{vmatrix} \frac{1}{a_2}$	$b_2 = -\begin{vmatrix} a_3 & 0 \\ a_2 & 0 \end{vmatrix} \frac{1}{a_2} = 0$	0
s^0	$c_1 = -\begin{vmatrix} a_2 & a_0 \\ b_1 & b_2 \end{vmatrix} \frac{1}{b_1}$	$c_2 = -\begin{vmatrix} a_2 & 0 \\ b_1 & 0 \end{vmatrix} \frac{1}{b_1} = 0$	0

Listing 1: Matlab code to calculate the transfer function

```
Cr=0.0025;
Cb=.0029;
kt=1.0513
j1=0.0004;
j2=0.0035;
 syms s k1 k2 k3;
  a=s*diag([1,1,1])
  A1=[-(Cb/j2)-k1 kt/j2 -k2;-1-k1 0 +1-k2;-k1 -kt/j1 -Cr/j1-k2];
  phi=a-A1;
  inv(phi);
  H=[0,1,0]*inv(phi)*[1;0;0];
  pretty(H)
```

REFRENCES

Aarsnes, U. J. F and N. van de Wouw (2018). "Dynamics of a distributed drill string system: Characteristic parameters and stability maps." *Journal of Sound and Vibration* 417, pp. 376–412.

Abdulgalil, F. and H. Siguerdidjane (2005). "Backstepping design for controlling rotary drilling system." *Proceedings of IEEE Conference on Control Applications. Toronto, August 2005.* Pp. 120–124.

Alt, B., J. P. Blath, F. Svaricek, and M. Schultalbers (2009). "Multiple sliding surface control of idle engine speed and torque reserve with dead start assist control." *IEEE transactions on industrial electronics* 56.9, pp. 3580–3592.

Armstrong-Hélouvry, B., P. Dupont, and C. Canudas De Wit (1994). "A survey of models, analysis tools and compensation methods for the control of machines with friction." *Automatica* 30.7, pp. 1083–1138.

Astrom, K. J. and C. Canudas-De-Wit (2008). "Revisiting the LuGre friction model." *IEEE control Systems* 28.6, pp. 101–114.

Åström, K. J. and P. Eykhoff (1971). "System identification—a survey." *Automatica* 7.2, pp. 123–162.

Bekiaris-Liberis, N. and M. Krstic (2013). "Oil drilling inspired compensation of wave actuator dynamics for nonlinear systems." *Proceedings of IEEE 52nd Annual Conference on Decision and Control. Florence, December 2013.* Pp. 3032–3037.

Belokobyl'skii, S. V. and V. K. Prokopov (Dec. 1982). "Friction-induced self-excited vibrations of drill rig with exponential drag law." *Soviet Applied Mechanics* 18, pp. 1134–1138. DOI: 10.1007/BF00882226.

Brandt, A. R. (2007). "Testing Hubbert." *Energy Policy* 35.5, pp. 3074 –3088.

Bresch-Pietri, D. and M. Krstic (2014). "Adaptive output-feedback for wave PDE with anti-damping-Application to surface-based control of oil drilling stick-slip instability." *Proceedings of IEEE 53rd Annual Conference on Decision and Control. Los Angeles, December 2014*, pp. 1295–1300.

Brett, J. F, T. M. Warren, and S. M. Behr (1989). "Bit whirl: A new theory of PDC bit failure." *Society of Petroleum Engineers* 5.4, pp. 275–281.

Bu, F. and J. Dykstra (2014). "Indirect adaptive robust controller design for drilling rotary motion control." *Proceeding of the 2014 American Society of Mechanical Engineers Dynamic Systems and Control Conference. San Antonio, Texas, October 2014.* DOI: 10.1115/DSCC2014-5926.

Chen, D. C. K., B. C. Comeaux, G. M. Gillespie, G. T. Irvine, and B. Wiecek (2006). "Real-time downhole torsional vibration monitor for improving tool performance and bit design." *Proceedings of the Society of Petroleum Engineers Drilling Conference. Miami, February 2006.* DOI: 10.2118/99193-MS.

Coleman, T. F. and Y. Li (1996). "A reflective Newton method for minimizing a quadratic function subject to bounds on some of the variables." *SIAM Journal on Optimization* 6.4, pp. 1040–1058.

De Bruin, J. C. A., A. Doris, N. van de Wouw, W. P. M. H. Heemels, and H. Nijmeijer (2009). "Control of mechanical motion systems with non-collocation of actuation and friction: A Popov criterion approach for input-to-state stability and set-valued nonlinearities." *Automatica* 45.2, pp. 405–415.

Dong, Guangjian and Ping Chen (2016). "A review of the evaluation, control, and application technologies for drill string vibrations and shocks in oil and gas well." *Shock and Vibration* 2016.

Doris, A. (2007). "Output-feedback design for non-smooth mechanical systems: Control synthesis and experiments." PhD thesis. Eindhoven Institute of Technology.

Emmerich, W., A. Greten, I. B. Brahim, and O. Akimov (2016). "Evolution in Reliability of High-Speed Mud Pulse Telemetry." *In proceeding of the Offshore Technology Conference. Houston, May 2016.* DOI: 10.4043/26886-MS.

Fear, M. J. and F. Abbassian (1994). "Experience in the detection and suppression of torsional vibration from mud logging data." *Proceedings of Society of Petroleum Engineers European Petroleum Conference. London, October 1994.* DOI: 10.2118/28908-MS.

Fossen, T. I. and J. P. Strand (1999). "Tutorial on nonlinear backstepping: Applications to ship control." *Modeling Identification and Control* 20.2, pp. 83–134.

Germay, C., N. Van de Wouw, H. Nijmeijer, and R. Sepulchre (2009). "Nonlinear drillstring dynamics analysis." *SIAM Journal on Applied Dynamical Systems* 8.2, pp. 527–553.

Ghasemi, M. and X. Song (2017). "Control of a vertical drilling system using a cascade sliding mode controller." *Proceedings of the American Control Conference. Seattle, July 2017.* Pp. 5830–5835.

Ghasemloonia, A., D. G. Rideout, and S. D. Butt (2015). "A review of drillstring vibration modeling and suppression methods." *Journal of Petroleum Science and Engineering* 131, pp. 150–164.

Green, J. H. and J. K. Hedrick (1990). "Nonlinear speed control for automotive engines." *Proceedings of the IEEE American Control Conference*, pp. 2891–2897.

Halsey, G. W., A. Kyllingstad, and A. Kylling (1988). "Torque feedback used to cure slip-stick motion." *Proceedings of the Society of Petroleum Engineers Annual Technical Conference and Exhibition*. DOI: 10.2118/18049-MS.

Harris, Matthew W, Behçet Açıkmese, and Eric van Oort (2014). "LMI Based Control of Stick-Slip Oscillations in Drilling." *ASME 2014 Dynamic Systems and Control Conference*. American Society of Mechanical Engineers, V001T09A004–V001T09A004.

Hedrick, J. K. and A. Girard (2005). *Control of nonlinear dynamic systems: Theory and applications*. URL: https://www.researchgate.net/publication/290128700_Control_of_nonlinear_dynamic_systems_theory_and_applications.

Hedrick, J. K. and P. P. Yip (2000). "Multiple sliding surface control: theory and application." *Journal of dynamic systems, measurement, and control* 122.4, pp. 586–593.

Horacio, M. J. (2003). "Nonlinear control systems: Analysis and design." *Departament of electrical and computer engineering, Editorial Wiley Interscience, cap* 2, pp. 65–80.

I. Finnie and J. J. Bailey (1960). "An experimental study of drill-string vibration." *Journal of Engineering for Industry* 82.2, pp. 129–135.

Jain, J. R., H. Oueslati, A. Hohl, H. Reckmann, L. W. Ledgerwood III, M. Tergeist, and G. P. Ostermeyer (2014). "High-Frequency Torsional Dynamics of Drilling Systems: An Analysis of the Bit-System Interaction." *Proceedings of the Society of Petroleum Engineers Drilling Conference and Exhibition. Fort Worth, March 2014.* DOI: 10.2118/167968-MS.

Jansen, J. D (1991). "Non-linear rotor dynamics as applied to oilwell drillstring vibrations." *Journal of Sound and Vibration* 147.1, pp. 115 –135.

Jansen, J. D. and L Van den Steen (1995). "Active damping of self-excited torsional vibrations in oil well drillstrings." *Journal of sound and vibration* 179.4, pp. 647–668.

Kabziński, J. (2014). "Adaptive servo control with polynomial approximation of stribeck curve." *Przegląd Elektrotechniczny* 90.5, pp. 20–24.

— (2017). "Adaptive Control of Drillstring Torsional Oscillations." *IFAC-PapersOnLine* 50.1, pp. 13360–13365.

Kamooly (2012). URL: https://commons.wikimedia.org/wiki/File%3A%D8%AC%D9%87%D8%A7%D8%B2_%D8%AD%D9%81%D8%B1_%D8%A2%D8%A8%D8%A7%D8%B1.jpg.

Kanellakopoulos, I., P. V. Kokotovic, and A. S. Morse (1992). "A toolkit for nonlinear feedback design." *Systems & Control Letters* 18.2, pp. 83–92.

Karkoub, M., M. Zribi, L. Elchaar, and L. Lamont (2010). "Robust μ-synthesis controllers for suppressing stick-slip induced vibrations in oil well drill strings." *Multibody System Dynamics* 23.2, pp. 191–207.

Khalil, H. K. (1996). *Nonlinear control*. Prentice Hall, New Jersey.

Kirkup, Les and Robert B Frenkel (2006). *An introduction to uncertainty in measurement: using the GUM (guide to the expression of uncertainty in measurement)*. Cambridge University Press.

Kodakadath Premachandran, R., A. Linderholt, L. Håkansson, and M. Gothberg (2017). "An initial investigation of the correlation between a number of drilling related quantities measured during down the hole drilling." *In proceedings of the 24th International Congress on Sound and Vibration. London, July 2017.*

Kokotović, P. and M. Arcak (2001). "Constructive nonlinear control: A historical perspective." *Automatica* 37.5, pp. 637 –662.

Kreyszig, E. and E. J. Norminton (1993). *Advanced engineering mathematics*. Vol. 4. Wiley New York.

Krstić, M., I. Kanellakopoulos, and P. V. Kokotović (1992). "Adaptive nonlinear control without overparametrization." *Systems & Control Letters* 19.3, pp. 177–185.

Krstic, M., I. Kanellakopoulos, and P. V. Kokotovic (1995). *Nonlinear and adaptive control design*. Wiley.

Leine, R. I. (1997). *Literature survey on torsional drill string vibrations*. Tech. rep. Division of Computational and Experimental Mechanics, Department of Mechanical Engineering, Eindhoven university of Technology.

Leine, R. I. (2000). "Bifurcations in discontinuous mechanical systems of Filippov-type." *The Universiteitsdrukkerij TU Eindoven, The Netherlands*.

Liberzon, D. (2007). "Observer-based quantized output feedback control of nonlinear systems." *Proceedings of the Mediterranean Conference on Control & Automation. Athens, June 2007.* Pp. 1–5.

Liu, Y. (2014). "Suppressing stick-slip oscillations in underactuated multibody drill-strings with parametric uncertainties using sliding-mode control." *IET Control Theory & Applications* 9.1, pp. 91–102.

Liu, Y., J. P. Chávez, R. De Sa, and S. Walker (2017). "Numerical and experimental studies of stick–slip oscillations in drill-strings." *Nonlinear dynamics* 90.4, pp. 2959–2978.

Lu, H., J. Dumon, and C. Canudas-de Wit (2009). "Experimental study of the D-OSKIL mechanism for controlling the stick-slip oscillations in a drilling laboratory testbed." *Proceedings of the Control Applications & Intelligent Control. Saint Peterbergs, Russia, July 2009.* Pp. 1551–1556.

Majeed, F. A., H. Karki, M. Karkoub, and Y. L. A. Magid (2013). "Experimental verification of drill string vibration suppression using an adaptive self-tuning controller." *International Journal of Acoustics and Vibration* 18.1, pp. 20–26.

Mihajlovic, N. (2005). "Torsional and lateral vibrations in flexible rotor systems with friction." PhD thesis. Eindhoven Institute of Technology.

Navarro-López, E. M. (2009). "Hybrid modelling of a discontinuous dynamical system including switching control." *IFAC Proceedings Volumes* 42.7, pp. 87–92.

Navarro-López, E. M. and R. Carter (2011). "Hybrid automata: an insight into the discrete abstraction of discontinuous systems." *International Journal of Systems Science* 42.11, pp. 1883–1898.

Navarro-López, E. M. and D. Cortés (2007). "Sliding-mode control of a multi-DOF oilwell drillstring with stick-slip oscillations." *Proceedings of the American Control Conference. New York City, USA, July 2007.* Pp. 3837–3842.

Navarro-López, E. M. and E. Licéaga-Castro (2009). "Non-desired transitions and sliding-mode control of a multi-DOF mechanical system with stick-slip oscillations." *Chaos, Solitons & Fractals* 41.4, pp. 2035–2044.

Navarro-López, E. M. and R. Suárez (2004). "Practical approach to modelling and controlling stick-slip oscillations in oilwell drillstrings." *Proceedings of the International Conference on Control Applications. Taipei, September 2004.* Pp. 1454–1460.

Nessjoen, Pal Jacob, Age Kyllingstad, Pedro Dambrosio, Isaac Samuel Fonseca, Alexis Garcia, Bruno Levy, et al. (2011). "Field experience with an active stick-slip prevention system." *Proceedings of Society of Petroleum Engineers Drilling Conference and Exhibition. Amsterdam, March 2011.*

Nguyen, Q. V. and C. Hyun (2014). "Multiple sliding surface sontrol approach to twin rotor MIMO systems." *International Journal of Fuzzy Logic and Intelligent Systems* 14, pp. 171–180.

Nise, N. S. (2007). *Control systems engineering*. John Wiley & Sons.

Nouailletas, R., E. Mendes, and D. Koenig (2010). "Hybrid modeling and identification of dry friction systems, application to a clutch actuator." *Control Engineering Practice* 18.8, pp. 904–917.

Olsson, H., K. J. Åström, C. Canudas De Wit, M. Gäfvert, and P. Lischinsky (1998). "Friction models and friction compensation." *European journal of control* 4.3, pp. 176–195.

Oueslati, H., J. R. Jain, H. Reckmann, L. W. Ledgerwood III, R. Pessier, and S. Chandrasekaran (2013). "New insights into drilling dynamics through high-frequency vibration measurement and modeling." *Proceedings of the Society of Petroleum Engineers Annual Technical Conference and Exhibition. New Orleans, October 2013.* DOI: 10.2118/166212-MS.

Patil, P. A. (2013). "Investigation of torsional vibration in a drillstring using modelling and laboratory experimentation." PhD thesis. Institute of Petroleum engineering, TU Clausthal.

Patil, P. A. and C. Teodoriu (2013). "A comparative review of modelling and controlling torsional vibrations and experimentation using laboratory setups." *Journal of Petroleum Science and Engineering* 112, pp. 227–238.

Pavković, D., J. Deur, and A. Lisac (2011). "A torque estimator-based control strategy for oil-well drill-string torsional vibrations active damping including an autotuning algorithm." *Control engineering practice* 19.8, pp. 836–850.

Pehlivantürk, C., D. Chen, and E. van Oort (2017). "Torsional drillstring vibration modelling and mitigation with feedback control." *Proceedings of the Society of Petroleum Engineers Drilling Conference and Exhibition. The Hague, March 2017.* DOI: 10.2118/184697-MS.

Petrella, R., M. Tursini, L. Peretti, and M. Zigliotto (2007). "Speed measurement algorithms for low-resolution incremental encoder equipped drives: a comparative analysis." *Electrical Machines and Power Electronics, 2007. ACEMP'07. International Aegean Conference on*. IEEE, pp. 780–787.

Rao, G.P. and H. Unbehauen (2006). "Identification of continuous-time systems." *IEE Proceedings-Control theory and applications* 153.2, pp. 185–220.

Reeves, M. E., M. L. Payne, A. G. Ismayilov, and M. J. Jellison (2005). "Intelligent drill string field trials demonstrate technology functionality." *Proceedings of Society of Petroleum Engineers Drilling Conference. Amsterdam, February 2005.* DOI: 10.2118/92477-MS.

Richard, T., C. Germay, and E. Detournay (2007). "A simplified model to explore the root cause of stick–slip vibrations in drilling systems with drag bits." *Journal of sound and vibration* 305.3, pp. 432–456.

Runia, D. J., S. Dwars, and I. P. J. M. Stulemeijer (2013). "A brief history of the Shell "Soft Torque Rotary System" and some recent case studies." *Proceedings of the Society of Petroleum Engineers Drilling Conference and Exhibition. Amsterdam, March 2013*. DOI: 10.2118/163548-MS.

Saldivar, B., S. Mondié, J. J. Loiseau, and V. Rasvan (2011). "Stick-slip oscillations in oillwell drilstrings: distributed parameter and neutral type retarded model approaches." *IFAC Proceedings Volumes* 44.1, pp. 284–289.

Saldivar, B., S. Mondié, S. I. Niculescu, H. Mounier, and I. Boussaada (2016). "A control oriented guided tour in oilwell drilling vibration modeling." *Annual Reviews in Control* 42, pp. 100–113.

Serrarens, A. F. A., M. J. G. Van de Molengraft, J. J. Kok, and L. Van den Steen (1998). "H_∞ control for suppressing stick-slip in oil well drillstrings." *IEEE Control systems* 18.2, pp. 19–30.

Shor, R. J., M. Pryor, and E. Van Oort (2014). "Drillstring vibration observation, modeling and prevention in the oil and gas industry." *Proceedings of the American Society of Mechanical Engineers 2014 Dynamic Systems and Control Conference. San Antonio, Texas, October 2014.* DOI: 10.1115/DSCC2014-6147.

Slotine, J. and W. Li (1991). *Applied nonlinear control*. Vol. 199. 1. Prentice hall Englewood Cliffs, NJ.

Song, B. and J. K. Hedrick (2011). *Dynamic surface control of uncertain nonlinear systems: an LMI approach*. Springer Science & Business Media.

Spanos, P. D., A. M. Chevallier, N. P. Politis, and M. L. Payne (2003). "Oil and gas well drilling: a vibrations perspective." *The Shock and Vibration Digest* 35.2, pp. 85–103.

Swaroop, D. V. A. H. G., J. C. Gerdes, P. P. Yip, and J. K. Hedrick (1997). "Dynamic surface control of nonlinear systems." *Proceedings of the American Control Conference. Albuquerque, June 1997.* Pp. 3028–3034.

Ullah, F. K., F. Duarte, and C. Bohn (2016a). "A novel backstepping approach for the attenuation of torsional oscillations in drill strings." *Solid State Phenomena* 248, pp. 85–92.

— (2016b). "Adaptive control of torsional oscillations in drill strings using a continuous-discrete extended Kalman filter." *Proceedings of 21st International Conference on Methods and Models in Automation and Robotics. Miedzyzdroje, Poland, September 2016.* Pp. 1022–1026.

Vaziri, V., M. Kapitaniak, and M. Wiercigroch (2018). "Suppression of drill-string stick–slip vibration by sliding mode control: Numerical and experimental studies." *European Journal of Applied Mathematics*, pp. 1–21.

Viguié, R., G. Kerschen, J. C. Golinval, D. M. McFarland, L. A. Bergman, A. F. Vakakis, and N. Van de Wouw (2009). "Using passive nonlinear targeted energy transfer to stabilize drill-string systems." *Mechanical Systems and Signal Processing* 23.1, pp. 148–169.

Vromen, T. G. M. T. (2015). "Control of stick-slip vibrations in drilling systems." PhD thesis. Technische Universiteit Eindhoven.

Warren, T. M. and J. H. Oster (1998). "Torsional resonance of drill collars with PDC bits in hard rock." *Proceedings of Society of Petroleum Engineers Annual Technical Conference and Exhibition. New Orleans, September 1998.* DOI: 10.2118/49204-MS.

Wiercigroch, M., K. Nandakumar, P. Lijun, M. Kapitaniak, and V. Vaziri (2017). "State dependent delayed drill-string vibration: Theory, experiments and new model." *Procedia IUTAM* 22, pp. 39–50.

Wit, C. Canudas de, M. A. Corchero, F. R. Rubio, and E. M. Navarro-López (2005). "D-OSKIL: A new mechanism for suppressing stick-slip in oil well drillstrings."

Proceedings of the Conference on Decision and Control, and European Control Conference. Seville, December 2005. Pp. 8260–8265.

Womer, K. A., D. R. Torkay, G. Villanueva, T. Geehan, J. Brakel, D. Pirovolou, D. Reid, and M. Killalea (2011). "Results of the July 15, 2010 IADC stick-slip mitigation workshop." *Proceedings of the Society of Petroleum Engineers Drilling Conference and Exhibition. Amsterdam, March 2011.* DOI: 10.2118/140044-MS.

Zhang, Z., Y. Shen, W. Chen, J. Shi, W. Bonstaff, K. Tang, D. L. Smith, Y. I Arevalo, and B. Jeffryes. (2017). "Continuous high frequency measurement improves understanding of high frequency torsional oscillation in north America land drilling." *Proceedings of the Society of Petroleum Engineers Annual Technical Conference and Exhibition. San Antonio, October 2017.* DOI: 10.2118/187173-MS.

Zhao, Y. (2017). "Torsional vibration control in oilwell drilling." *IFAC-PapersOnLine* 50.1, pp. 6035–6042.

Zhu, X., L. Tang, and Q. Yang (2014). "A literature review of approaches for stick-slip vibration suppression in oilwell drillstring." *Advances in Mechanical Engineering* 6, pp. 967–952.